ABSTRACT

Title of Dissertation: ADVANCED ADHESION STRENGTH TESTING METHODS OF THIN FILM MULTILAYERS IN ELECTRONIC PACKAGING SYSTEMS

Kenneth Howard Mahan, Doctor of Philosophy, 2016

Dissertation directed by: Professor Bongtae Han, Mechanical Engineering

With the continued miniaturization and increasing performance of electronic devices, new technical challenges have arisen. One such issue is delamination occurring at critical interfaces inside the device. This major reliability issue can occur during the manufacturing process or during normal use of the device. Proper evaluation of the adhesion strength of critical interfaces early in the product development cycle can help reduce reliability issues and time-to-market of the product. However, conventional adhesion strength testing is inherently limited in the face of package miniaturization, which brings about further technical challenges to quantify design integrity and reliability.

Although there are many different interfaces in today's advanced electronic packages, they can be generalized into two main categories:

1) rigid to rigid connections with a thin flexible polymeric layer in between, or

2) a thin film membrane on a rigid structure.

Knowing that every technique has its own advantages and disadvantages, multiple testing methods must be enhanced and developed to be able to accommodate all the interfaces encountered for emerging electronic packaging technologies.

For evaluating the adhesion strength of high adhesion strength interfaces in thin multilayer structures a novel adhesion test configuration called "single cantilever adhesion test (SCAT)" is proposed and implemented for an epoxy molding compound (EMC) and photo solder resist (PSR) interface. The test method is then shown to be capable of comparing and selecting the stronger of two potential EMC/PSR material sets. Additionally, a theoretical approach for establishing the applicable testing domain for a four-point bending test method was presented.

For evaluating polymeric films on rigid substrates, major testing challenges are encountered for reducing testing scatter and for factoring in the potentially degrading effect of environmental conditioning on the material properties of the film. An advanced blister test with predefined area test method was developed that considers an elasto-plastic analytical solution and implemented for a conformal coating used to prevent tin whisker growth. The advanced blister testing with predefined area test method was then extended by employing a numerical method for evaluating the adhesion strength when the polymer's film properties are unknown.

ADVANCED ADHESION STRENGTH TESTING METHODS OF THIN FILM MULTILAYERS IN ELECTRONIC PACKAGING SYSTEMS

By

Kenneth Howard Mahan

Dissertation submitted to the Faculty of the Graduate School of the
University of Maryland, College Park, in partial fulfillment
of the requirements for the degree of
Doctor of Philosophy
2016

Advisory Committee:
Professor Bongtae Han, Chair/Advisor
Professor Abhijit Dasgupta
Professor Sung Lee
Professor Teng Li
Professor Patrick McCluskey

© Copyright by

Kenneth Howard Mahan

2016

Acknowledgement

I would like to acknowledge my family, friends, labmates, and advisor who helped to guide and support me through this process. Without them I would not have been able to achieve this feat.

Thank you to my parents, Howard and Jeanne, who have always loved, guided, and supported me along whatever path I choose to take. My two sisters, Lauren and Samantha, and lovely nieces and nephews who have always been no more than a phone call away to spread joy and laughter.

Thank you to my friends from back home in Alabama, new friends in DC, and my friends who have moved all over the globe. No matter when our paths crossed throughout my time in Alabama and DC, I cherish the time each and every one of us spent together. Your friendships have only enhanced and broadened the insight, knowledge, and experiences I have discovered during my time in academia.

Thank you to my LOMSS labmates: CJ, Michelle, Yong, Dae-Suk, Bulong, Sean, Dr. Oh, Byung, Hyeun-Seop, David, Stephen, and Brian who have been there in the trenches with me as we all progressed towards higher degrees.

Finally, thank you to my advisor, Professor Bongtae Han, who has challenged me every single day to further develop my logical thought process to enhance my ability as a future engineer. You have imparted upon me many valuable lessons that I will not soon forget.

Table of Contents

Acknowledgement ii

Table of Contents iii

List of Tables vii

List of Figures viii

Chapter 1: Introduction 1

1.1. Motivation 1

1.2. Objective 3

1.3. Organization of Dissertation 4

Part I: Adhesion Strength Testing of Thin Rigid/Flexible/Rigid Multilayer Structures 7

Chapter 2: Background and Literature Review of Adhesion Strength Testing Methods of Thin Rigid/Flexible/Rigid Multilayer Structures 8

2.1. Background 8

2.2. Quantifying Reliability Parameters 9

2.2.1. Numerical Methods to Evaluate Reliability Properties. 14

2.3. Literature Review of Adhesion Testing in Rigid/Flexible/Rigid Multilayer Structures 17

2.3.1. Double Cantilever Beam (DCB) Testing Method 18

2.3.2. Four-Point Bending (4PB) with Symmetric Side Cracks 20

2.3.3. Four-Point Bending with Vertical Central Crack 21

Chapter 3: Applicable Testing Domain of Four-Point Bending Adhesion Test Method for Assessing Critical Interfaces in Thin Multilayer Microelectronic Systems 34

Abstract 34

3.1. Introduction ... 35
3.2. Crack competition in an interface ... 36
3.3. Approach ... 38
3.3.1. Numerical model for a thin multilayer 4PB specimen ... 38
3.3.2. Evaluation of $G_{kink}(\omega)$ at various kinking angles ... 39
3.3.3. Establishing an applicable testing domain ... 42
3.4. Implementation of the Applicable Testing Domain for EMC/PSR Interface ... 43
3.5. Conclusion ... 50

Chapter 4: Single Cantilever Adhesion Test for Interfaces in Thin Multilayer Semiconductor Packages 51

Abstract ... 51
4.1. Introduction ... 52
4.2. Background ... 55
4.2.1. J-integral Approach ... 55
4.2.2. Virtual Crack Closure Technique ... 56
4.2.3. Crack Tip Mode Mixity ... 58
4.3. Single Cantilever Adhesion Test (SCAT) Method ... 59
4.3.1. Physical Description ... 59
4.3.2. Numerical Analysis ... 61
4.3.3. Mode Mixity in SCAT Method ... 61
4.4. Test preparation ... 64
4.4.1. Specimen Design ... 64
4.4.2. Specimen Preparation ... 66
4.5. Experiment and Results ... 70
4.5.1. Testing ... 70
4.5.2. Evaluation of Adhesion Strength ... 74
4.6. Discussions ... 78
4.6.1. Validity of LEFM ... 78
4.6.2. Uncertainty Analysis: Effect of Moment Arm on G in SCAT ... 82
4.7. Conclusion ... 85

Part II Adhesion Strength Testing of Flexible Membranes on Rigid Substrates 86

Chapter 5: Background and Literature Review of Adhesion Strength Testing Methods of Flexible Membranes on Rigid Substrates 87

5.1. Background ... 87

5.2. Literature review of adhesion testing in flexible membranes on rigid substrates systems ... 87

5.2.1. Peel test ... 87

5.2.2. Blister test ... 88

5.2.3. Constrained blister test (CBT) ... 89

Chapter 6: Adhesion and Puncture Strength of Polyurethane Coating Used to Mitigate Tin Whisker Growth 92

Abstract ... 92

6.1. Introduction ... 92

6.2. Test Method ... 94

6.2.1. Adhesion Strength Test: Modified Blister Test ... 94

6.2.2. Puncture Strength Test ... 96

6.3. Experimental Procedure ... 97

6.3.1. Modified Blister Test ... 97

6.3.1.1 Experimental Setup and Test Procedure ... 101

6.3.2. Puncture Test ... 103

6.3.2.1 Experimental Setup and Test Procedure ... 103

6.4. Experimental Results ... 104

6.4.1. Adhesion Strength ... 105

6.4.1.1 Accelerated Testing Results ... 107

6.4.2. Puncture Strength ... 109

6.5. Discussions: Failure Modes ... 111

6.6. Conclusion ... 115

Chapter 7: Blister Testing for Adhesion Strength Measurement of Polymer Films Subjected to Environmental Conditions **117**
7.1. Introduction 118
7.2. Background: review of analytical solutions 120
7.3. Numerical Procedure to Calculate Energy Release Rate 122
7.3.1. FEA Model Setup 122
7.3.2. Energy Release Rate Calculation 123
7.4. Energy Release Rate with Pseudo-Properties 128
7.5. Application 131
7.5.1. Sample Preparation 131
7.5.2. Experimental Setup and Testing Procedure 136
7.5.3. Results of Environmental Testing 139
7.6. Conclusion 142

Chapter 8: Contributions and Future Works **144**
8.1. Dissertation Contributions 144
8.2. Future Work 146

References 151

List of Tables

Table 1. Specimen configuration for EMC/PSR specimen tested in 4PB. 45

Table 2. Material properties for the EMC/PSR specimen. 64

Table 3. Energy release rate results for EMC/PSR1 material set. 78

Table 4. Energy release rate results for EMC/PSR2 material set. 78

Table 5. Puncture strength with different probe radii. 109

Table 6. Consequence of ad-hoc Poisson's ratio selection. 130

Table 7. Comparison of testing results. 140

List of Figures

Figure 1. Schematic highlighting potential interfaces in semiconductor packages. 8

Figure 2. Schematic of an interfacial crack in a bimaterial body. 10

Figure 3. Schematic of three loading modes in fracture mechanics. 12

Figure 4. Schematic of relationship between G and Ψ. 13

Figure 5. Schematic diagram of crack tip mesh. 17

Figure 6. Schematic of bimaterial double cantilever beam test. 19

Figure 7. Schematic of typical load vs. displacement curve in DCB testing. 19

Figure 8. Schematic of symmetric side crack 4PB testing. 21

Figure 9. Schematic of a 4PB setup for a vertical center crack. 22

Figure 10. Schematic of typical load vs. displacement curve in 4PB test method with a vertical center crack 22

Figure 11. Schematic of a 4PB setup with a thin film stack sandwiched between two much larger substrates. 25

Figure 12. (a) Thin film stack sandwiched in Dauskardt's implementation, and (b) the load vs. displacement graph for 4PB testing of SiO_2/TiN interface [17]. 26

Figure 13. Schematic of a 4PB setup with a thin adhesive layer between two much larger substrates. 27

Figure 14. Second configuration for 4PB testing of CDO/SiN interface (a) schematic of multilayer stack sandwiched between two much larger substrates with epoxy below the interface of interest and (b) typical load vs. displacement curve of 4PB [18]. 27

Figure 15. Second configuration for 4PB testing of CDO/SiN interface (a) schematic of multilayer stack sandwiched between two much larger substrates with epoxy above the interface of interest and (b) typical load vs. displacement curve of 4PB [18]. 29

Figure 16. Schematic of copper-copper bonding samples created on larger silicon substrates [41]. 30

Figure 17. Load vs. displacement curve for Cu-Cu direct bond 4PB adhesion testing [41]. 31

Figure 18. Cross section image of typical microelectronic package with EMC/copper leadframe interface [19]. 32

Figure 19. Schematic of crack trapped in the interface with two outcomes. 37

Figure 20. Schematic of bimaterial 4PB sample. 39

Figure 21. Singular crack tip elements used for evaluating $G_{kink}(\omega)$ (a) before and (b) after crack closure [7]. 40

Figure 22. Several $G_{Kink}(\omega)/G_0$ vs. kink angle curves for different material combinations. 41

Figure 23. Applicable testing domains over several test configurations for a bimaterial 4PB specimen. 43

Figure 24. SEM image of EMC/PSR specimen tested. 44

Figure 25. Large deflection in 4PB samples prior to testing thin multilayer structure. 44

Figure 26. Reinforcement system for EMC/PSR specimen shown a) schematically, and b) during testing. 46

Figure 27. Example of evaluating preferred crack kinking direction when establishing the applicable testing domain for a EMC/PSR interface. 47

Figure 28. Establishing applicable testing domain over several test configurations. 48

Figure 29. Load vs. displacement curve for reinforced EMC/PSR interface sample. 49

Figure 30. Initial and final states of EMC/PSR sample testing 49

Figure 31. Close up SEM image of thin multilayer stacks consisting of EMC, PSR, and PCB. 53

Figure 32. Schematic diagram of crack tip mesh for VCCT method. 58

Figure 33. Schematic of (a) test configuration for SCAT specimen with a precrack and (b) load vs. displacement graph for a SCAT test. 60

Figure 34. Mode mixity vs. upper layer thickness for several material combinations in SCAT test configuration. 62

Figure 35. Mode mixity vs. moment arm length for $E_1/E_2 = 5$ and $h_1 = 2$ mm in SCAT test configuration. 63

Figure 36. Plot of 3D energy release rate normalized by plane strain energy release rate vs. specimen width for a EMC/PSR SCAT sample. 66

Figure 37. Sample preparation steps: a) schematic of board layout with dicing markers and planned predefined area, b) masked area on top of PSR/PCB layers for predefined area, and c) finished silicon oil/aluminum sputtered predefined area on PSR surface. 67

Figure 38. Cross-sectional schematic view of predefined area creation for EMC/PSR SCAT specimens along with an inset of a zoomed in SEM image of silicon oil and aluminum sputtered layers of predefined area. 69

Figure 39. Schematics of typical (a) two SCAT specimen with predefined area prior to dicing, and (b) test configuration for a SCAT test. 70

Figure 40. SCAT a) test setup with EMC/PSR specimen, test stand, loading fixture, and camera used to monitor delamination; and b) in-situ camera image of delamination occurring at EMC/PSR interface during testing. 71

Figure 41. Determining the moment arm in a SCAT test a) cross-sectional schematic used to determine the offset distance, b) schematic of delaminated EMC side of specimen, and c) inset from b) highlighting a delaminated specimen used to verify the extent of the predefined area. 73

Figure 42. Comparison of load vs. normalized displacement curves for both EMC/PSR material. 75

Figure 43. Delaminated surfaces from SCAT tested specimens with crack propagation corresponding to load drops during testing for the a) EMC/PSR1 and b) EMC/PSR2 material sets. 76

Figure 44. Comparison of adhesion strength results for both EMC/PSR material sets. 77

Figure 45. Moiré fringe patterns on EMC/PSR specimen after delamination along interface for a) u_x displacement field and b) u_y displacement field. 80

Figure 46. Near crack tip moiré images before and after applying load for a EMC/PSR SCAT specimen for a) u_x displacement field and b) u_y displacement field. 81

Figure 47. Uncertainty in G as a function of moment arm for several levels of moment arm length uncertainty in the EMC/PSR SCAT configuration. 83

Figure 48. Uncertainty in G vs. normalized moment arm length per moment arm deviation. 84

Figure 49. Schematic of the 180° peel test. 88

Figure 50. Schematic of a traditional blister test. 89

Figure 51. Schematic of a constrained blister test. 91

Figure 52. Schematic illustration of a modified blister test specimen. 96

Figure 53. 3D view of (a) copper substrate and (b) copper plug mold. 98

Figure 54. Copper substrate with epoxy plugs. 99

Figure 55. Schematic cross sectional view of sample preparation process: a) tin plated substrate and plug mold; b) temporary mask and release agent application; c) temporary shim for conformal coating curing; and d) final blister test specimen. 100

Figure 56. Schematic diagram of the blister test setup. 102

Figure 57. Blister test setup. 102

Figure 58. Schematic diagram of the puncture test setup. 103

Figure 59. Puncture test setup. 104

Figure 60. Typical pressure vs. blister height results for the blister test of a polyurethane conformal coating before aging. 105

Figure 61. Nonlinear regression results of the elasto-plastic curve to determine the hardening constant and yield strength of the coating. 107

Figure 62. Adhesion strength versus hours in a T/H chamber. 108

Figure 63. Adhesion strength versus cycles in a T/C chamber. 109

Figure 64. Typical load vs. deflection results for the puncture test of a polyurethane conformal coating. 110

Figure 65. Puncture strength versus hours in a T/H chamber. 111

Figure 66. Schematic of tin whisker nucleating on tin coated substrate. 112

Figure 67. Puncture force and buckling force versus whisker length. 113

Figure 68. Critical whisker length for buckling versus whisker diameter. 114

Figure 69. Schematic illustration of a blister test. 120

Figure 70. Schematic of boundary conditions applied in axisymmetric 2D model of blister test. 123

Figure 71. Deflection v. pressure curve for ideal (a) bending and (b) stretching specimens; FEM results and analytical solutions are compared. 125

Figure 72. Blister profile before and after a delamination of Δa = 75 μm obtained from the FEA analysis: the case of Figure 71b with P_{crit} = 10 psi. 126

Figure 73. G vs. Δa plot for numerically determined energy release rate for the case shown in Figure 72. 128

Figure 74. Deflection vs. pressure curve for a blister test specimen with an intermediate thickness. 129

Figure 75. Deflection vs. pressure curve for intermediate case with several pseudo material property pairs to fit experimental curve. 130

Figure 76. Copper substrates for blister test samples (a) before and (b) after attaching the stencil. 132

Figure 77. Schematic of sample preparation procedure: a) creating temporary plug, b) creating the predefined area, c) curing the adhesive, and d) the final sample ready for testing. 134

Figure 78. Schematic diagram of the blister test setup. 136

Figure 79. Representative deflection vs. pressure curves for an epoxy/coper interface at as-is testing conditions. 137

Figure 80. A typical blister sample a) before and b) after critical delamination event. 138

Figure 81. Representative deflection vs. pressure curves for an epoxy/copper sample at three conditions: a) as-is, b) after thermal aging, and c) after moisture degradation. 140

Figure 82. Energy release rate comparison of three conditions: a) as-is, b) after thermal aging, and c) after moisture degradation. 141

Figure 83. Moduli comparison of three conditions: a) as-is, b) after thermal aging, and c) after moisture degradation. 141

Figure 84. A schematic of the ACBT setup. 149

Chapter 1: Introduction

1.1. Motivation

In today's ultra-connected world, electronic devices are more prevalent than ever. High consumer demand has driven the industry to continuously evolve in order to deliver the smaller and high functioning portable electronics that consumers crave. Advances in electronic packaging have played a tremendous role in this evolution. Effective electronic packaging systems must integrate discrete components while balancing the mechanical, electrical, and thermal design criterion of the system. Contributions such as new chip designs, advanced materials, and improved manufacturing methods are responsible for the persistence of new and ground-breaking electronics every year.

However, with continued miniaturization and increasing performance of electronic devices, new technical challenges have arisen. One such issue is delamination occurring at critical interfaces inside the device. With advancing thin-profile designs and closer line spacing, delamination is not only a mechanical durability issue, but also a functionality issue. Additionally, due to the quick time-to-market requirements within industry, it is important that design feasibility and reliability are assessed at early stages of the product development cycle. Not only must the design be feasible, but the reliability of the design must be quantified and assured sufficient over the product's lifetime to withstand the harsh environmental conditions that portable electronics will undergo during normal use.

To assess the reliability of an interface, adhesion strength testing can be employed to quantitatively characterize the integrity of the interface. However, conventional

adhesion strength testing is inherently limited in the face of package miniaturization, which brings about further technical challenges to quantify design integrity and reliability.

While there are many different interfaces in today's advanced electronic packages, they can be generalized into two main categories:

1) Rigid to rigid connections with a thin flexible polymeric layer in between, or
2) A thin film membrane on a rigid structure.

Knowing that every technique has its own advantages and disadvantages, multiple testing methods must be enhanced and developed to be able to accommodate all the interfaces encountered in the emerging electronic packaging technologies. Conventional adhesion strength testing is most effective at evaluating interfaces with low adhesion strength and simple bimaterial structures. However, in typical electronic packages, the interface-of-interest has much larger adhesion strength and is found in more complex thin multilayer structures. Another consideration is for when high adhesion strengths must be evaluated with compliant and/or low fracture toughness adherends, considerations must be made to possible crack kinking into adjacent layers. This will involve a thorough investigation of the mode mixity at the crack tip and an evaluation of new testing configurations to best induce interfacial delamination for assessing the adhesion strength.

Additionally, for evaluating polymeric films on rigid substrates, major testing challenges are encountered for reducing testing scatter and for factoring in the potentially degrading effect of environmental conditioning on the material properties of the film. Consequently, conventional ideas and testing methods are not directly applicable requiring both enhancements of current methods and the introduction of novel test methods to effectively evaluate all interface types.

The proposed approaches and test methods in this dissertation will enable the industry to quantitatively test any interface in an electronic package early in the product development cycle to assess reliability and design feasibility. This ability to quantitatively assess product reliability early on will enable packaging engineers to make cost-effective design decisions that will greatly reduce the time-to-market of the product.

1.2. Objective

The objective of this dissertation is, thus, to enhance and develop specific adhesion strength testing techniques to quantitatively assess the reliability of the interfaces found in electronic packaging devices. Achieving this objective entails the following:

1. Rigid/Flexible/Rigid Interfaces
    a. Establish a theoretical approach for determining an applicable testing domain for where the four-point bending (4PB) test method can be employed to evaluate the adhesion strength of a given material set based on mode mixity and crack kinking considerations;
    b. Create a Single Cantilever Adhesion Strength Test (SCAT) method for quantitative adhesion strength measurements; and
    c. Characterize the adhesion strength of multiple material sets for an EMC/PSR interface using the SCAT method
2. Thin Membrane on Rigid Substrate Interfaces
    a. Develop an advanced blister test with predefined area test method that considers an elasto-plastic analytical solution;

b. Extend the advanced blister testing with predefined area test method with a numerical method for evaluating the adhesion strength when the polymer's film properties are unknown; and
c. Demonstrate the ability to characterize the adhesion strength of between film/substrates using the above methods before and after subjecting samples to environmental conditions.

1.3. Organization of Dissertation

This first chapter introduces the reader to the motivation behind this work and describes the objectives sought to be accomplished by it. The remainder of the dissertation is divided into two parts to address the two main types of interfaces seen in electronic packaging systems: I) rigid/flexible/rigid interfaces and II) thin membrane on rigid substrate interfaces.

Chapter 2 reviews background information of the specific rigid/flexible/rigid interfaces of interest found in electronic packaging systems and how the reliability of the interfaces can be quantified through the energy release rate and mode mixity concepts. Specific numerical methods used to evaluate the reliability parameters, such as the J-integral and Virtual Crack Closures (VCCT) methods are then discussed. A literature review of conventional experimental adhesion test methods is then presented.

Chapter 3 presents a theoretical approach for determining if the adhesion strength of a potential material combination in a thin multilayer stack can be evaluated under the four-point bending test method. The approach takes into account the fracture toughness and structural material properties of the interface materials, global loading configurations,

and the potential adhesion strength of the interface to analyze the crack kinking competition at the interface of interest. Through a numerical approach it is shown an applicable testing domain for the given test configuration and material set can be established to clearly indicate the limits of the test configuration.

Chapter 4 introduces a novel adhesion strength testing method, the Single Cantilever Adhesion Test (SCAT) for evaluating the reliability of critical interfaces in thin multilayer stacks. Motivation for this test method and an experimental/numerical test procedure are presented. The method is then implemented for an EMC/PSR interface that is known to have very large adhesion strength. In addition, the test method is used to evaluate the adhesion strength of two separate EMC/PSR material sets. This chapter has been submitted to the *Journal of Microelectronics Reliability* and is currently under a review process.

Chapter 5 reviews typical thin membrane on rigid substrate interfaces found in electronic packaging systems. A literature review of conventional experimental adhesion test methods is then presented.

Chapter 6 presents a reliability analysis for a conformal coating used to mitigate tin whisker migration. Methods for evaluating the adhesion strength and puncture strength are presented. For the adhesion strength evaluation, the development of an advanced blister test with predefined area test method that considers an elasto-plastic analytical solution is presented. A puncture strength test is also presented and a discussion on factors associated with tin whisker mitigation is discussed. This chapter was published in the *Journal of Electronic Packaging*.

Chapter 7 presents an extension to the capabilities of the typical blister test when the material properties of the film are unknown or subject to change during environmental conditioning. To cope with the problem, the concept of pseudo properties is introduced that can be determined from an experimental deflection vs. pressure curve and a typical numerical model of the blister specimen. From here, a classical energy balance approach is employed to evaluate the energy release rate from the critical pressure and "pseudo" material properties. This approach was carried out for an epoxy/copper interface after subjecting samples to both full moisture saturation and a high temperature storage condition. Adhesion strength and pseudo-modulus results of an epoxy/copper interface for each condition are presented which underline the importance of this consideration. This chapter has been submitted to *Journal of Electronic Packaging* and is currently under a review process.

Chapter 8 contains a summary of the contributions made by this study and a discussion for future studies that can be extended from the present study.

Part I: Adhesion Strength Testing of Thin Rigid/Flexible/Rigid Multilayer Structures

Chapter 2: Background and Literature Review of Adhesion Strength Testing Methods of Thin Rigid/Flexible/Rigid Multilayer Structures

2.1. Background

There are many critical interfaces throughout a semiconductor packages that poses a reliability concern. The schematic in Figure 1 highlights a few of the possible interfaces. Interfaces can stem from connecting discrete chips and components to the printed circuit board (PCB), as well as interfaces due to protecting plastic encapsulation of packages using epoxy molding compounds (EMC). Even within silicon chips, the introduction of through-silicon-vias introduces additional potential failure locations.

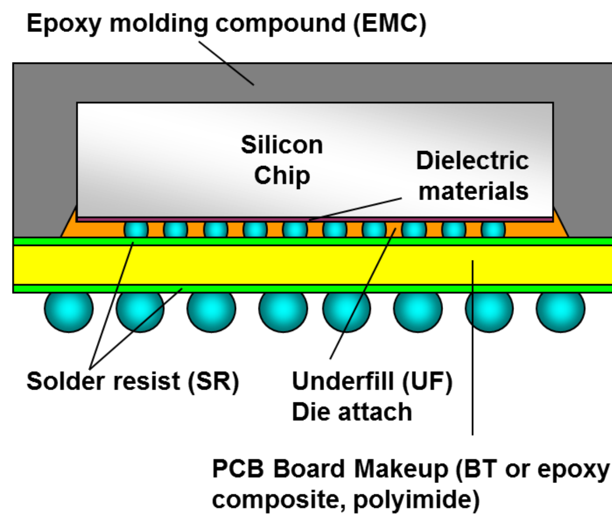

Figure 1. Schematic highlighting potential interfaces in semiconductor packages.

Quantitatively assessing the reliability of critical interfaces in electronic packages is of utmost importance for total device reliability. Testing must be performed in a straightforward manner that allows for evaluation of the as-manufactured product and must have the capability of evaluating the potential degradation of the interface over the lifetime of the product. The reliability of the interface is assessed through two key parameters: the adhesion strength and the mode mixity. The adhesion strength represents the interfaces resistance to delamination, whereas the mode mixity indicates the ratio of shear-to-opening loading the interface is under.

In this section fundamental concepts are introduced, such as, adhesion strength, the energy release rate, fracture toughness, and mode mixity. Complexities of adhesion strength testing due to the nature of the material mismatch at the interface are also explored. Finally some conventional adhesion strength testing methods for rigid/flexible/rigid multilayer structures is presented.

2.2. Quantifying Reliability Parameters

To determine if an interface will be resistant to delamination, a bimaterial property called the interfacial fracture toughness, Γ, is often used. The interfacial fracture toughness is an indication of the adhesion strength of the interface, or in other words how well the interface resists delamination. Several factors affect Γ including the material properties of each layer, the moisture absorbed by the specimen, and the temperature. One way to assess this bimaterial property is to determine the energy release rate, G, which is a measure of the energy available for an increment of crack extension [1].

$$G = -\frac{dU}{dA} \tag{1}$$

where U is the energy in the body and A is the new surface area created due to crack extension. For testing consider a bimaterial body that has an interfacial crack and is experiencing monotonic loading (Figure 2). As the load increases, so does the stress around the crack tip until finally a critical loading condition is reached and the crack delaminates. When the crack delaminates two key events happen: new surface area is created, and some of the stored energy in the body is released. This release of stored energy to create new surface area is defined as the critical energy release rate, G_c [1]. Under linear elastic conditions, the critical energy release is equivalent to the interfacial fracture toughness.

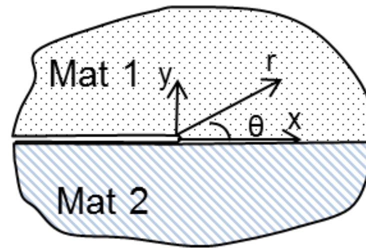

Figure 2. Schematic of an interfacial crack in a bimaterial body.

Interfacial fracture properties are more complicated to describe because of the addition of a material discontinuity at the interface. Williams found that the stress and displacement fields oscillate very close to an interfacial crack tip [2]. Because of this material mismatch at the interface, even under a global pure tensile loading, three will be a mixed mode loading condition at the crack tip due to the material discontinuity. To describe the material mismatch at the interface the Dundars introduced two nondimensional parameters [3]. A parameter to characterize the elastic mismatch, α:

$$\alpha = \frac{\overline{E_1} - \overline{E_2}}{\overline{E_1} + \overline{E_2}} \tag{2}$$

where $\overline{E_j}$ represents the Young's modulus for each material. Under plane strain conditions $\overline{E_j} = \frac{E_j}{\left(1-\nu_j^2\right)}$, and under plane stress conditions, $\overline{E_j} = E_j$, where ν is the Poisson's ratio of the material. The second Dundars' parameter characterizes the bulk modulus mismatch, β:

$$\beta = \frac{\mu_1\left(\vartheta_2 - 1\right) - \mu_2\left(\vartheta_1 - 1\right)}{\mu_1\left(\vartheta_2 + 1\right) + \mu_2\left(\vartheta_1 + 1\right)} \quad (3)$$

where μ_i represents the shear modulus and θ_i accounts for either plane strain, $\vartheta_j = \left(3 - 4\nu_j\right)$, or plane stress, $\vartheta_j = \frac{\left(3-\nu_j\right)}{\left(1+\nu_j\right)}$, conditions at the crack front. When there is no material mismatch, i.e. a homogeneous material, both parameters vanish. However if the materials are switched, then the sign of the parameter also changes. By using these parameters, an idea of the crack tip stress and strain field can be determined.

Depending on bimaterial properties and the global loading conditions, the stress field near the crack tip will behave differently due to the ratio of shear to opening load. Three loading modes are used to describe the type of loading at the interface. Mode I represents tensile or opening loading, mode II represents in-plane shear loading, and mode III represents out-of-plane shear or tearing loading. The individual loading modes are schematically shown in Figure 3.

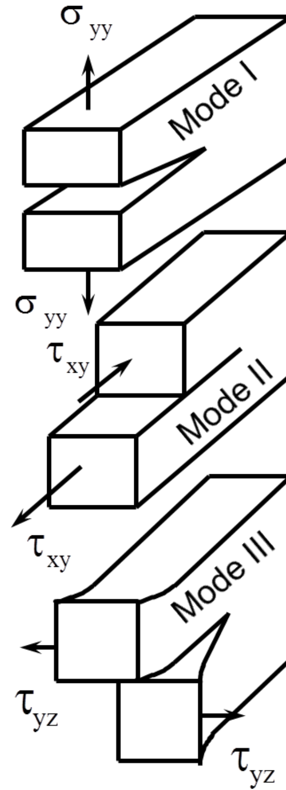

Figure 3. Schematic of three loading modes in fracture mechanics.

Due to the material mismatch at the interface a mixture of the different loading modes at the interface is unavoidable when assessing the adhesion strength. A parameter known as the mode mixity, Ψ, is used to quantify the ratio of shear-to-opening loading at the crack front [4-8]:

$$\tan\psi = \sqrt{\frac{G_{II}}{G_I}} \tag{4}$$

where G_I and G_{II} represent the mode I and mode II energy release rate components. The mode mixity ranges from 0° for pure mode I loading to 90° for pure mode II loading. As the amount of shear loading at the interface increases so does the energy required to

delaminate new surface area. This relationship results in G increasing as a function of the mode mixity. This relationship is shown schematically in Figure 4. To fully describe the strength of an interface, both G and Ψ should be determined and reported. Both parameters can be evaluated through either analytical or numerical methods.

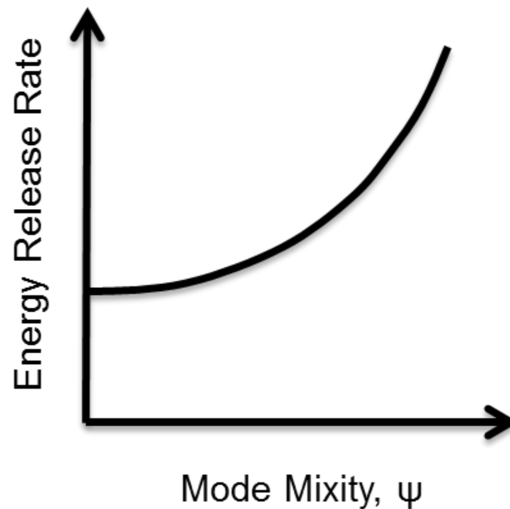

Figure 4. Schematic of relationship between G and Ψ.

Common multilayer rigid/flexible/rigid adhesion strength test methods include double cantilever beam (DCB) [9-15], four-point bending (4PB) with a central notch [10, 16-20] and. 4PB with side cracks testing method [20]. Each method and their analytical solutions – when applicable – will be explored further in the following sections. However when dealing with more advanced structures, like the ones found in semiconductor packages, numerical methods must be applied. Two useful numerical methods for evaluating the energy release rate include the J-integral method proposed by Rice [21, 22] and the Virtual Crack Closure Technique (VCCT) [4, 5, 7, 8, 23, 24]. Numerical methods are also available to evaluate the mode mixity at the crack tip, namely the crack tip opening

displacement method [16, 25-27], and the VCCT method. Numerical methods will be further discussed before introducing the specific multilayer rigid/flexible/rigid adhesion strength test methods.

2.2.1. Numerical Methods to Evaluate Reliability Properties.

2.2.1.1. J-integral Method

When analytical solutions are not directly applicable to a certain specimen and testing configuration, a numerical modeling approach, which employs the J integral, can be used to evaluate the energy release rate when the material behavior remains linear elastic. This approach is especially useful for determining the interfacial energy release rate for cracks that lie on the interface of two materials in multilayer structures.

The energy release rate, *G*, was proposed by Irwin as a measure of the energy available for crack extension when materials remain linear elastic [28]. Rice later went on to expand upon Irwin's approach by idealizing elastic-plastic deformation as nonlinear elastic. This allowed for the extension of fracture mechanics beyond the linear elastic deformation by use of the J integral [21]. The J integral considers an arbitrary path going counter-clockwise around a crack tip:

$$G = J = \int_c \left(w n_i - T_i \frac{du_i}{dx} \right) ds \tag{5}$$

where *w* is strain energy density:

$$w = \int_0^{\varepsilon} \sigma_{ij} d\varepsilon_{ij} \tag{6}$$

n_i is the normal vector to *c*, and T_i is the traction vector:

$$T_i = \sigma_{ij} n_j \quad (7)$$

c is an arbitrary contour around the tip of the crack; σ , ε, and u are the stress, strain, and displacement field, respectively [21]. The J-integral remains equivalent to the energy release rate as long as the sample is under small scale yielding. This can be readily shown in other source material [1, 21, 22]. Another key criterion is that the J-integral is path independent. This derivation can also be found in source material [1, 29] and holds true for a crack in a multilayer structure as long as the structure is under small scale yielding and the crack is parallel to the layered structures.

The J-integral can be analyzed numerically after experimental testing of a specimen. Once the critical condition of the specimen is modeled using a commercial FEA method, the critical stress and displacement fields can be assessed on the contour around the crack tip. The J-integral can then be performed in post processing steps to evaluate the energy release rate.

2.2.1.2. Virtual Crack Closure Method

The VCCT method is a numerical method for evaluating the energy release rate and mode mixity in a single step. According to Irwin, the work required to close a crack by an infinitesimal crack length, Δa, is equal to the work required to close the crack to its original length [28]. For homogeneous, isotropic materials, this interpretation allows for the mode I and mode II components of the energy release rate to be expressed as [4, 7]:

$$G_I = \lim_{\Delta \to 0} \frac{1}{2\Delta} \int_0^{\Delta} \sigma_{yy}(\Delta - r)\delta_y(r)\,dr \quad (8)$$

$$G_{II} = \lim_{\Delta \to 0} \frac{1}{2\Delta} \int_0^{\Delta} \sigma_{xy}(\Delta - r)\delta_x(r)\,dr \quad (9)$$

$$G = G_I + G_{II} \tag{10}$$

where Δ is an infinitesimal crack extension, σ_{yy} and σ_{xy} are the normal and shear tractions at a distance r ahead of the crack tip, and δ_x and δ_y are the displacement jumps at a distance, *r*, behind the crack tip along the x- (sliding mode) and y- (opening mode) directions.

This theoretical interpretation can be extended to a numerical finite element model. Considering the crack tip mesh in Figure 5, the energy release rate can be expressed in terms of the nodal forces and displacements as [7]:

$$G_I = -\frac{1}{2\Delta a}\left[f_{y,5}\left(\Delta u_{y,1-3}\right) + f_{y,6}\left(\Delta u_{y,2-4}\right)\right] \tag{11}$$

$$G_{II} = -\frac{1}{2\Delta a}\left[f_{x,5}\left(\Delta u_{x,1-3}\right) + f_{x,6}\left(\Delta u_{x,2-4}\right)\right] \tag{12}$$

where $f_{x,i}$, $\Delta u_{x,j}$, and $\Delta u_{y,k}$ represent the nodal force, shear displacement and opening displacement, respectively. Equations (10) and (4) can then be used to calculate *G* and Ψ directly from the FEA results.

Key assumptions for this method are that two successive states of cracking are self-similar for an infinitesimally short crack advance; crack advance of Δa does not significantly change the stress state at the crack tip; and the crack tip elements are larger than oscillation zone and smaller than area dominated by geometric features, i.e., in K-dominate region. .

Both the J-integral method and the VCCT method can be used to evaluate *G*, but since the VCCT method allows for evaluation of *G* and Ψ in one step it is more user friendly. It is recommended that when evaluating *G*, the J-integral method should be calculated as a consistency check to ensure model stability.

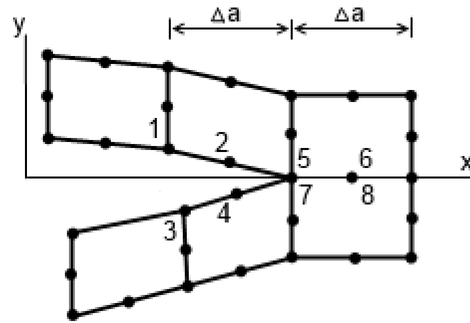

Figure 5. Schematic diagram of crack tip mesh.

2.3. Literature Review of Adhesion Testing in Rigid/Flexible/Rigid Multilayer Structures

Adhesion strength testing of key interfaces is a critical task for establishing the reliability of a packaging structure. Due to the material mismatch, the interface may be prone to delamination failure due to conditions during the manufacturing of the product or just from the day-to-day use. To assess the reliability of the interface adhesion strength testing can be performed during the design phase of the product. From the experimental results two key reliability parameters are then established to characterize the reliability of the interface: the critical interfacial energy release rate, G_c, and the mode mixity, Ψ. The critical interfacial energy release rate is an indication of the adhesion strength and represents the interfaces resistance to delamination, whereas the mode mixity indicates the ratio of shear-to-opening loading the interface is under.

Several conventional adhesion strength test methods that have been applied for adhesion strength testing of rigid/rigid interfaces include the double cantilever beam (DCB) [9-15], four-point bending (4PB) with side cracks testing method [20], and 4PB

with a central notch [10, 16-20]. These test method have been implemented in a variety of situations to evaluate the adhesion strength of interfaces in bimaterial structures and for critical interfaces within thin film multilayer stacks. Each technique has distinct advantages and disadvantages. Below is a review of the conventional adhesion strength testing methods for rigid/flexible/rigid multilayers and the key implementation of the techniques in regards to the semiconductor packaging industry.

2.3.1. Double Cantilever Beam (DCB) Testing Method

The double cantilever beam test is a commonly used method to measure the adhesion strength in a near mode I condition [9-15, 30-36]. For testing, there is a precrack placed in between two substrates with loading blocks attached to the end of the specimen.

As seen in Figure 6, tensile loading is applied at both ends of the cantilever beam at a constant displacement rate until the precrack propagates along the interface of interest. From the critical load and the precrack length the energy release rate can be assessed from the compliance of the system [1]. The system can be reset and tested again at a new crack length as seen in Figure 7 for multiple *G* calculations from a single sample.

Using the critical load and compliance found from the graph, the energy release rate can be determined [1]:

$$G = \frac{P^2}{2B}\frac{dC}{da} \qquad (13)$$

where B is the width of the specimen and C is the compliance of the structure. To assess the compliance for multilayer structures, authors have developed analytical expressions derived from the beam on elastic foundation model [13].

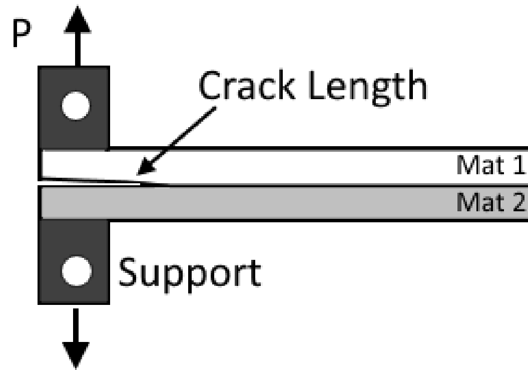

Figure 6. Schematic of bimaterial double cantilever beam test.

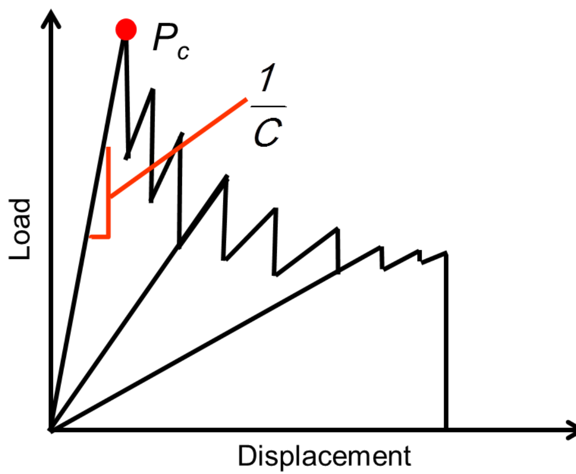

Figure 7. Schematic of typical load vs. displacement curve in DCB testing.

While this test does allow for multiple data points from a single sample and testing in a near mode I condition, the sample preparation for the precrack and alignment of the loadings is difficult to implement. This may add unwanted uncertainty to this method. Since the method assumes a perfect tensile loading, any unexpected in-plane shear loading (Mode II) or out-of-plane shear loading (Mode III twisting) may increase uncertainty.

Additionally, extra care should be taken for in-situ monitoring of the crack length to ensure accurate crack length measurements.

Advancements have also been made for accounting for the material mismatch across the interface to maintain a near mode I loading [14, 15]. By using unsymmetrical supporting layers, it has been shown that the mode mixity at the interface can be influenced to ensure the mode mixity is near mode I and the crack will stay in the interface. Key advantages of this test method is that a mode I energy release rate value can be assessed during testing, controlled, stable interfacial crack growth can be found, and closed form analytical solutions are available.

2.3.2. Four-Point Bending (4PB) with Symmetric Side Cracks

Another adhesion strength testing approach is the four-point bending (4PB) with side cracks method which involves two symmetric side cracks placed on a multilayer specimen [20, 37, 38]. A schematic of this setup is seen in Figure 8. The specimen is aligned in a 4PB fixture and monotonic displacement loading is applied until the cracks delaminate along the interface. Since both crack tips are within the inner loading pins, each side of the crack is subjected to the same constant moment. The displacement continues until both cracks delaminate along the interface of interest at a critical load. From that point the J-integral method [21, 22] is applied to evaluate the energy release rate of the interface. A major advantage of testing in 4PB is that the energy release rate can be determined without a crack length measurement. However some disadvantages of testing in this configuration stem from the larger mode mixity at the interface and the difficultly

of creating two perfectly symmetric precracks during sample prep which can lead to added uncertainty in testing results.

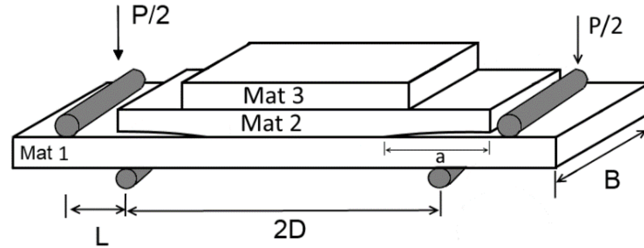

Figure 8. Schematic of symmetric side crack 4PB testing.

2.3.3. Four-Point Bending with Vertical Central Crack

The last major type of rigid/rigid adhesion strength testing considered is a 4PB test method with a central crack. This test method is quite similar to the previous 4PB method except that before testing only a vertical notch is made to the interface of interest in the middle of the bimaterial sample [10, 16] (**Error! Reference source not found.**). Loading is then applied in a similar manner until the crack initiates along the interface of interest at an initial load, $P_{initial}$. At this moment the load will drop as the crack begins to initiate. The crack then begins to stably propagate along the interface of interest at a critical load, $P_{critial}$, due to the constant moment region between the inner loading pins. This region is known as a steady state region. Figure 10 depicts a typical load vs displacement diagram for this type of testing. Using the critical load from testing the energy release rate can be evaluated from analytical methods.

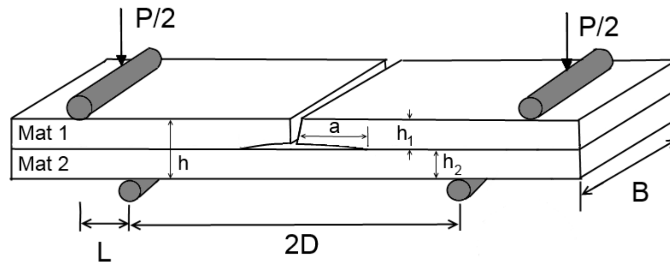

Figure 9. Schematic of a 4PB setup for a vertical center crack.

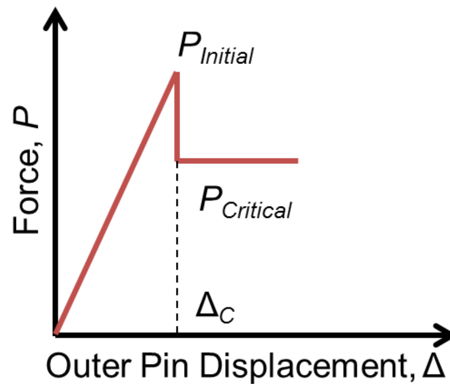

Figure 10. Schematic of typical load vs. displacement curve in 4PB test method with a vertical center crack

Similar to the previous 4PB testing method this method also has a larger mode mixity due to the nature of 4PB loading, but has the advantage of easier sample preparation and having a crack length independent method to calculate the energy release rate, which greatly reduces uncertainty in measurements. These advantages, in particular the reduced testing uncertainty and practicality to implement in reality have led to an uptick in recent years of 4PB with center crack applications. Following is a more in depth description of the 4PB test method with a vertical center crack, implementations of the method for specific problems and interfaces, and finally a look at the particular challenges when

extending this test method to evaluate key interfaces in thin multi-layer packaging structures.

2.3.3.1. Initially Proposed 4PB Method with Vertical Center Crack For Bimaterial Systems

Several authors have examined different application of the 4PB method with a vertical center crack and have helped to extend the technique [16-18, 20, 39-41]. The four-point bending adhesion strength testing method was initially proposed by Evans and Charalambides [10, 16] for assessing the adhesion strength of bimaterial interfaces in mixed mode conditions.

A schematic of a typical 4PB specimen can be seen in Figure 9. In this configuration, a bimaterial sample is notched in the center and a predefined crack length, a, was then created by applying clamps to the structure and applying load until the crack advanced to the end of the clamps. The specimen is then placed under a four-point bending loading fixture and outer pin displacement is increased monotonically. Since the precrack has already been established the load increases until the critical load, $P_{critical}$, is reached. At this point the crack will continue to delaminate stably along the interface due to the center of the specimen being under a constant moment condition as in Figure 10. The delamination will continue along the interface at the critical load until the crack reaches the inner loading pins. This critical load can be used to assess the energy release rate, G, of the interface-of-interest analytically by applying beam theory and assuming plane strain conditions [16]:

$$\frac{E_2 G h^3 b^2}{P_{crit}{}^2 l^2 \left(1-\nu_2{}^2\right)} = \frac{3}{2}\left\{\frac{1}{\left(\frac{h_2}{h}\right)^3} - \frac{\lambda}{\left\{\left(\frac{h_1}{h}\right)^3 + \lambda\left(\frac{h_2}{h}\right)^3 + 3\lambda\frac{h_1 h_2}{h^2}\left(\frac{h_1}{h} + \lambda\frac{h_2}{h}\right)\right\}}\right\} \quad (14)$$

where

- l = pin spacing,
- E_i = modulus,
- b = width,
- h_i = thickness,
- v_i = Poisson's ratio, and
- λ = plane strain constant.

Evans and Charalambides detailed the fundamentals of this test method and examined how the energy release rate and mode mixity are a function of the crack length, pin spacing, and modulus ratio between the two materials [16, 40]. The authors then applied this approach to evaluate an ideal interface of aluminum/PMMA materials. For this particular interface the typical adhesion strength results of this interface were on the order of 12 J/m^2.

2.3.3.2. "Essentially Homogeneous" Approach for Thin Film Stacks [17]

Later on Dauskardt implemented this approach to evaluate the adhesion strength of a SiO_2/TiN interface in thin film stacks. By sandwiching the thin film stacks between massively large silicon substrates, as seen in Figure 11, an essentially homogeneous structure was assembled and a simplified analytical solution was applied to evaluate the energy release rate from testing [17]:

$$G = \frac{21\left(1-v^2\right)M^2}{4Eb^2h^3} \quad (15)$$

where M is the critical moment and the material properties of the silicon substrates are used.

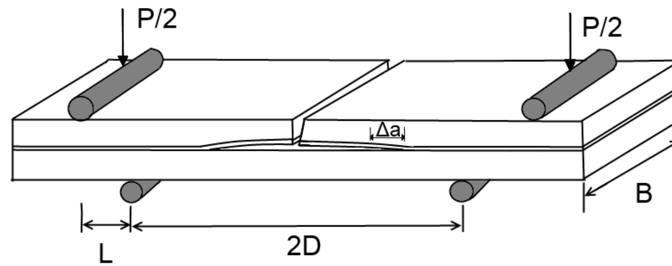

Figure 11. Schematic of a 4PB setup with a thin film stack sandwiched between two much larger substrates.

A weak intermetallic layer was used in the thin film stack (Figure 12a) to initiate a precrack to the interface of interest during testing. The benefit of this weak intermetallic layer is seen in the load vs. displacement curve in Figure 12b. The displacement is increased monotonically for the duration of the test. Once a critical initial load is reached, the crack propagates from the vertical notch to the weak copper bond layer of the thin film stack and then kinks downward to the interface of interest (depicted with the dashed red line in Figure 12a). As the displacement continues to be increased a load plateau is reached where steady state delamination is occurring at the interface of interest (depicted with the solid blue line in Figure 12a). For the SiO_2/TiN interface tested the energy release rate values were on the order of 10 J/m^2, representing a relatively weak interface.

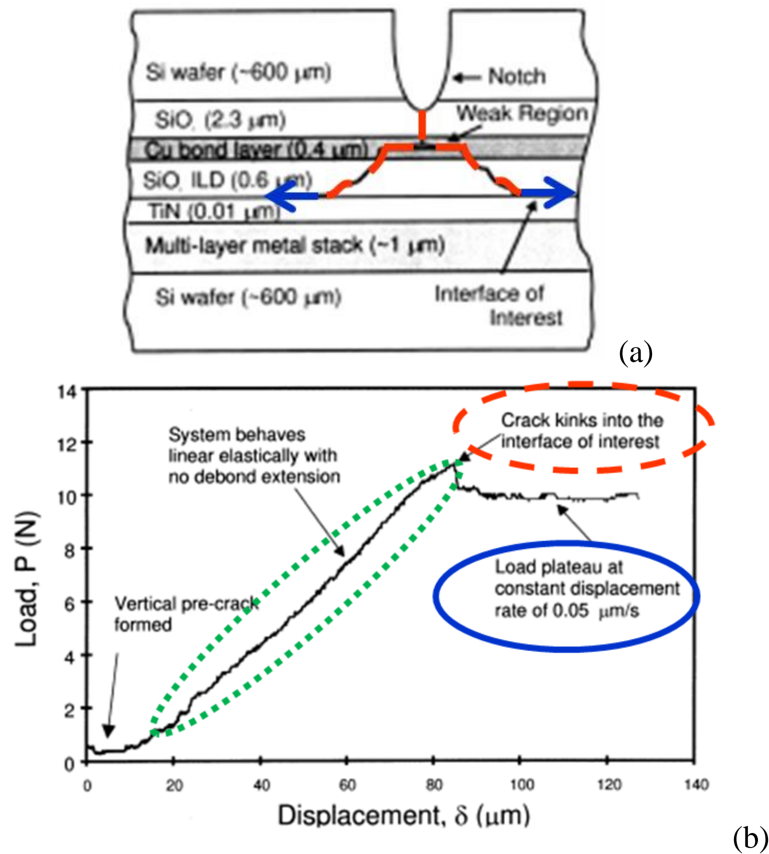

Figure 12. (a) Thin film stack sandwiched in Dauskardt's implementation, and (b) the load vs. displacement graph for 4PB testing of SiO_2/TiN interface [17].

2.3.3.3. Importance of Precrack [18]

Another key implementation assessed the importance of using a precrack at the interface of interest [18]. Similar to the previous extension, two massive substrates were used to create an essentially homogeneous material (Figure 13). The interface of interest for this case was a CDO/SiN interface in a thin multilayer stack as shown schematically in Figure 14a.

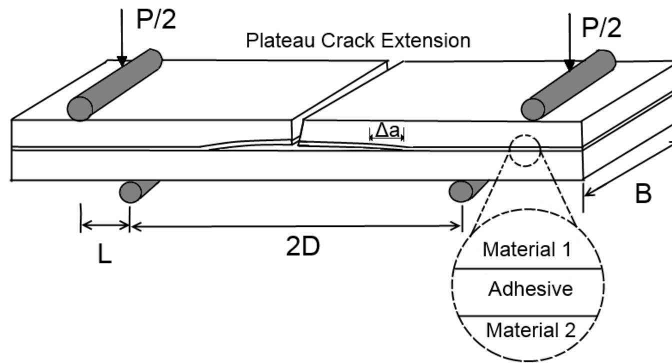

Figure 13. Schematic of a 4PB setup with a thin adhesive layer between two much larger substrates.

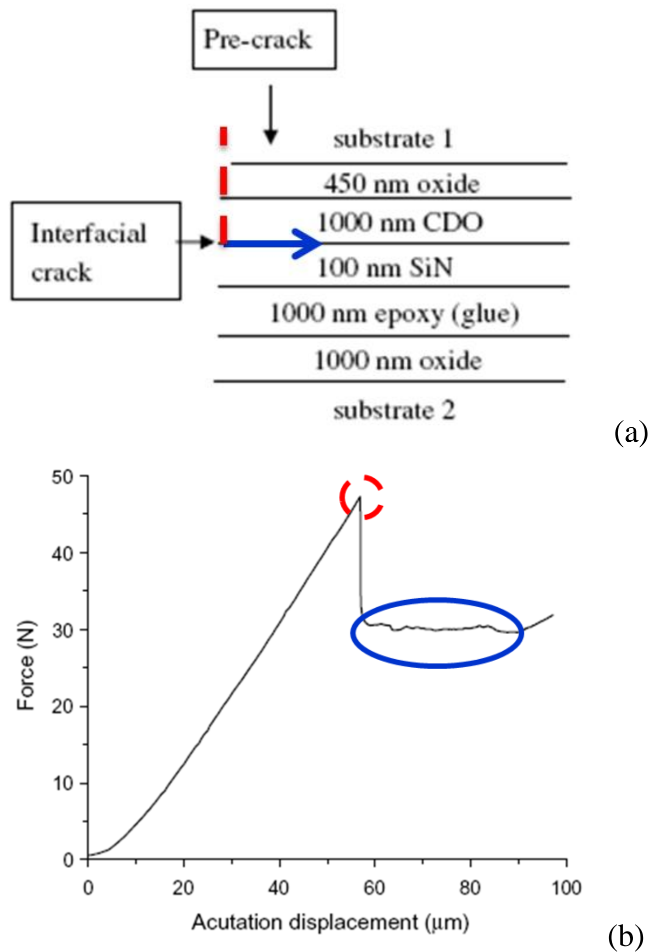

Figure 14. Second configuration for 4PB testing of CDO/SiN interface (a) schematic of multilayer stack sandwiched between two much larger substrates with epoxy below the interface of interest and (b) typical load vs. displacement curve of 4PB [18].

The layers were deposited on one silicon substrate and then a thin epoxy layer was used to sandwich the specimens. The top substrate was then notched close to the interface before testing, but no precrack was created. Upon testing under a constant displacement rate, the load would increase until at an initial load, $P_{initial}$. At this point the crack begins to initiate along the interface-of-interest while being accompanied by a load drop in the system (depicted with the dashed red line in Figure 14). As the outer pin displacement continues to increase the load will reach the critical load, $P_{critical}$. The crack will continue to delaminate stably along the interface due to the center of the specimen being under a constant moment condition system (depicted with the solid blue line in Figure 14). The delamination will continue along the interface at the critical load until the crack reaches the inner loading pins. This critical load can then be used to assess the energy release rate of the interface-of-interest.

An interesting takeaway from this work is that when testing without a precrack there will always be a larger load required to initiate the crack before the critical load required for delamination is reached. However, by employing a very thin precrack, it would be possible to eliminate the initial load overshoot which can prove problematic in certain cases. For example, the authors considered two configurations in this experiment: one with the epoxy below the interface-of-interest, and another with the epoxy above (Figure 15a) [18].

It was found that when testing with the epoxy layer above the interface-of-interest, the load required to initiate the precrack along the interface of interest was so large that instead of the crack arresting after reaching $P_{initial}$, the crack would rapidly propagate all the way to the inner loading pin without establishing a load plateau at the critical load

(Figure 15b). This case highlights a particular situation where if a precrack was first created, testing may have been possible. From the first case the evaluation of the energy release rate showed a relatively weak interface of 4 J/m^2.

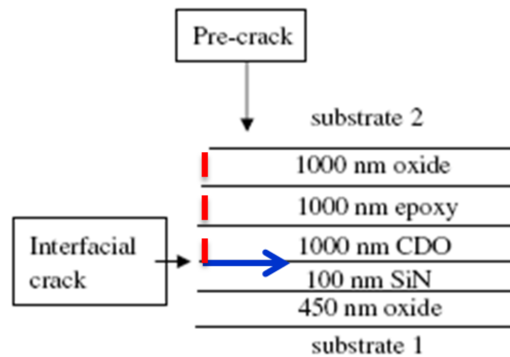

(a)

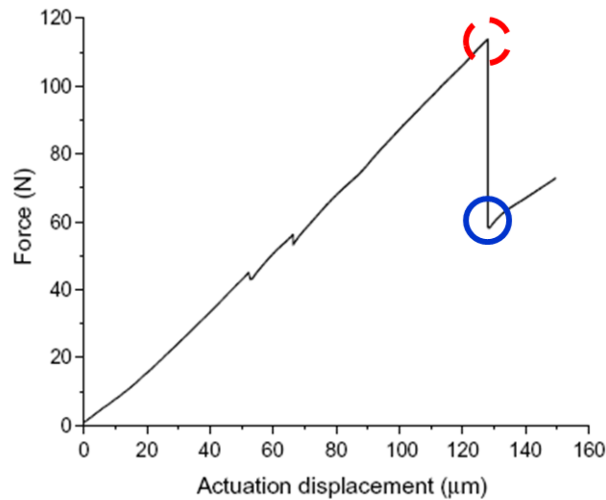

(b)

Figure 15. Second configuration for 4PB testing of CDO/SiN interface (a) schematic of multilayer stack sandwiched between two much larger substrates with epoxy above the interface of interest and (b) typical load vs. displacement curve of 4PB [18].

2.3.3.4. Application: Evaluating adhesion strength of bonds in Through Silicon Via (TSV)

One application of this technique is for the copper-copper direct bonds used in through silicon via (TSV) applications [41, 42]. Copper-copper direct bonds are typically cured under high temperature conditions. The authors were interested in evaluating the effect of curing conditions on the adhesion strength between the bonds.

Samples were made by depositing a layer of copper on to two larger silicon wafers (Figure 16) and then cured under various conditions. The samples were then tested (Figure 17) in 4PB and Dauskardt's simplified analytical solution, Equation (15), was applied to assess the adhesion strength. Adhesion strength results were relatively small, ~3 J/m^2 and varied based on the temperature and pressure conditions applied. Adhesion strength increased with bonding temperature and post-bond annealing temperature.

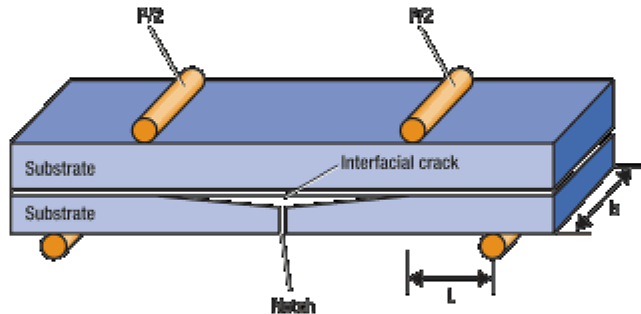

Figure 16. Schematic of copper-copper bonding samples created on larger silicon substrates [41].

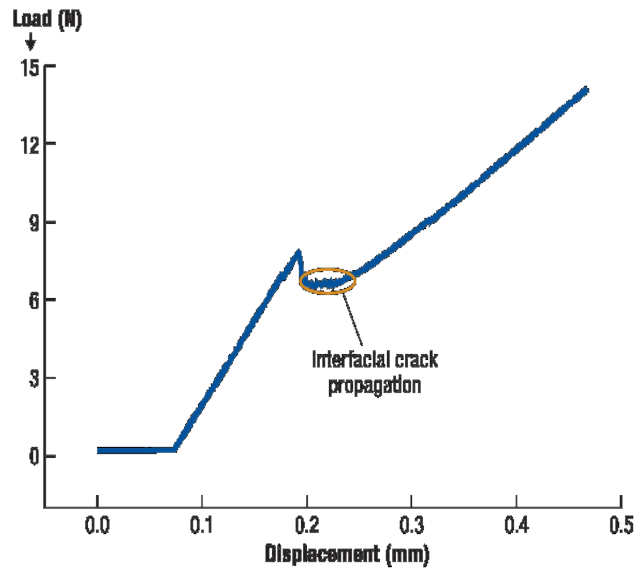

Figure 17. Load vs. displacement curve for Cu-Cu direct bond 4PB adhesion testing [41].

2.3.3.5. Application: Evaluating Adhesion Strength of EMC/Copper Bonds

Another interface of interest that has been investigated by several authors with the 4PB method is the interface between epoxy molding compound (EMC) and copper leadframe [19, 43-45]. Figure 18 provides an example of the type of package where this interface ca be found. Epoxy molding compound is typically employed to protect the critical components and connections of the chip from the outside environment and moisture exposure. However, since the properties of the EMC are subject to change from long term exposure to moisture and temperature conditions, the initial adhesion strength and the adhesion strength degradation over time exposed to these conditions are critical to determine for characterizing the device reliability.

To evaluate this interface authors typically employ a simple bimaterial strip of EMC/copper. After creating the bimaterial strips, a vertical notch is cut in the center of the sample and then 4PB loading is employed. As documented before, the displacement is

increased until an initial load is reached where the crack initiates along the interface. The load then drops to a critical plateau load where the crack delaminates in a steady state condition to the end of the inner loading pin.

To evaluate the energy release rate the equations initially proposed by Charalambides et. al. [16] are employed. For testing performed immediately after sample creation authors have reported energy release rates on the order of 20 J/m^2. The authors were also able to test after exposing samples to high temperature and humidity conditions and characterized the degradation of the adhesion strength with time.

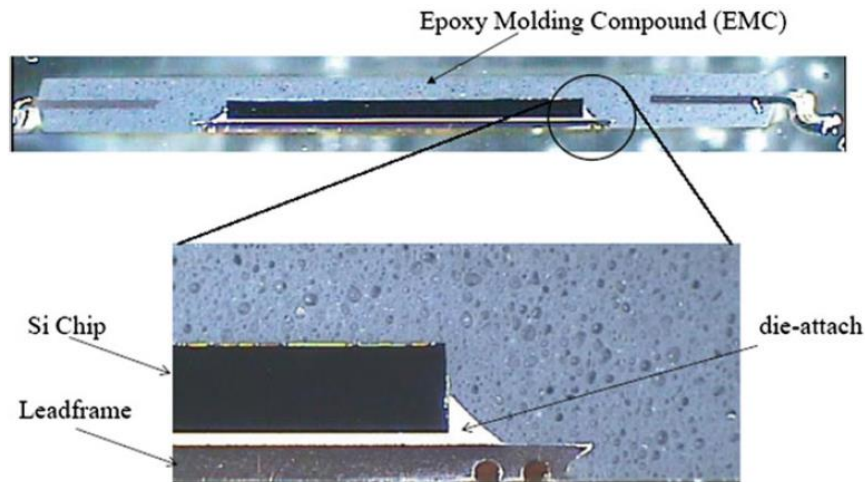

Figure 18. Cross section image of typical microelectronic package with EMC/copper leadframe interface [19].

2.3.3.6. Remarks on Further Extension of 4PB Method

The four-point bending method with a vertical center crack is an effective test method for evaluating the critical interfacial energy release rate for a bimaterial interface in mixed mode loading conditions. Previous implementations in the community have shown the method is very effective when evaluating interfaces with small adhesion strengths in comparison to the adherend materials.

However, difficulties with using this technique are met when extending to the thin multilayer structures that are common in semiconductor packaging systems. Samples are thinner than ever and are multilayered and with non-ignorable volume stiffness of the intermediate layers. Additionally with the advancement of materials engineering the adhesion strength of interfaces of interests are larger than ever. When large adhesion strength interfaces are mixed with low fracture toughness adherends, such as with high filler epoxy molding compounds (EMC) or other brittle layers, crack kinking into the adherend instead of delamination during testing also becomes a concern. Further investigation must be made for evaluating the adhesion strength at critical interfaces in thin-multilayer samples. Additional consideration must be made for the high toughness interfaces where crack kinking out of the interface is a distinct possibility.

Chapter 3: Applicable Testing Domain of Four-Point Bending Adhesion Test Method for Assessing Critical Interfaces in Thin Multilayer Microelectronic Systems

Abstract

The four-point bending (4PB) test method is a conventional adhesion strength test method that has been used to evaluate the adhesion strength at many critical interfaces. However, the test has typically been limited to evaluation of low strength interfaces. As new materials are introduced, there is an increased need to evaluate if conventional test methods can be extended to areas with increasing large adhesion strength values. With the goal of evaluating stronger material interfaces, the 4PB with central notch adhesion strength testing method is investigated to assess a applicable testing domain for a given material set in a thin multilayer microelectronic system.

Before testing, a theoretical approach considering the fracture toughness and structural material properties of the material set in question, the specimen configuration, the global loading configuration, and the mode mixity at the crack tip in order to determine the applicable testing domain where the 4PB test can be used to successfully evaluate the adhesion strength of an interface. This approach is then implemented for a high strength epoxy molding compound (EMC) and photo solder resist (PSR) interface.

3.1. Introduction

Delamination at critical interfaces inside electronic devices is a major reliability issue that can occur during the manufacturing process or during normal use of the device. With advancing thin-profile designs and closer line spacing, delamination is not only a mechanical durability issue, but also a functionality issue. With the quick time-to-market requirements within industry, it is important that design feasibility and reliability are assessed at early stages of the product development cycle. The reliability of the interface can be assessed by adhesion strength testing of the interface. A conventional test that is employed to characterize the adhesion strength is the four-point bending (4PB) test. As previously discussed in Chapter 2, this technique provides a clear advantage of having a steady state region where the adhesion strength can be evaluated leading to much less scatter in testing results, but at the cost of a larger inherent mode mixity at the crack tip due to the global loading condition.

To date, the 4PB test method has been employed successfully for many different interfaces which are typically weaker interfaces where the energy release rate was on the order of ~10 J/m^2 or less [1-4]. As new designs and more advanced material combinations are introduced to electronic packaging systems, it is of interest to investigate extending the applicability of this conventional testing technique to evaluate higher adhesion strength interfaces.

A theoretical approach is proposed that investigates the crack tip condition during a 4PB test for a given specimen configuration. A FEA analysis is then carried out to assess the propensity for an interfacial crack to delaminate or kink into an adjacent adherend based on the crack competition at the interface. The key considerations for this approach consist

of the known fracture toughness and structural material properties of the material set in question, and the specimen configuration which establishes the global loading configuration. From this information a numerical model of the specimen can be created and the mode mixity at the interface of interest can be assessed. From here a virtual crack closure technique (VCCT) [5-7] can be employed at the crack tip to assess the propensity for the crack to delaminate or kink into an adherend at a given kink angle. Through this analysis an applicable testing domain can be established for a given specimen configuration that can provide guidelines on the maximum adhesion strength this 4PB test configuration is capable of assessing depending on the fracture toughness of the given adherends.

3.2. Crack competition in an interface

Consider a crack that is inside a homogeneous body. When the sample is loaded to the point of crack propagation, the crack will potentially change its orientation, or kink, in to the direction that maximizes G [8]. However, for an interfacial crack in a bimaterial sample (Figure 19) the potential crack propagation becomes more complicated. Whenever there is crack trapped in an interface, one of two outcomes can occur: the crack delaminates along the interface, or it kinks into an adjacent material [8-10]. When the sample is initially loaded, there will be some degree of mode mixity at the crack tip. If the adhesion strength is weak in comparison to the fracture toughness of the adjacent materials, then the crack can propagate along the interface with a mode mixity.

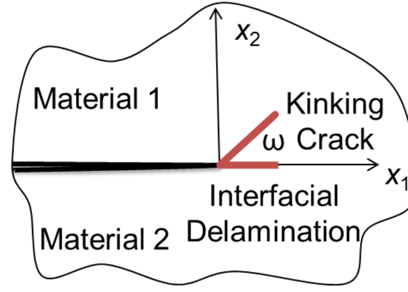

Figure 19. Schematic of crack trapped in the interface with two outcomes.

This concept is especially important to consider when evaluating interface properties in electronic packaging systems. If the adhesion strength is too large, or the fracture toughness of the individual adherends is too weak, there will be the potential that the crack will kink out of the interface before delamination occurs. If kinking occurs, then testing in the given configuration will not be able to evaluate the adhesion strength of the interface-of-interest. Mathematically, this is best represented through the following crack kinking equation:

$$\frac{\mathbf{Max}\left[G_{kink}\left(\omega\right)\right]}{G_0} < \frac{\Gamma_{IC}^{(2)}}{\Gamma_C^{(\mathbf{interface})}\left(\psi\right)} \tag{16}$$

where G_0 and G_{kink} are the energy release rate for the interface and lower material, respectively, $\Gamma_c^{(\text{interface})}$ and $\Gamma_{IC}^{(2)}$ are the fracture toughness for the interface and lower material, respectively, Ψ is the mode mixity at the interface, and ω is the associated kinking direction into the bulk of a material. Since this relationship is dependent on the mode mixity at the interface, each new test configuration (sample dimensions, load configuration, material properties, ect.) should be modeled to evaluate Equation (16) to determine if

testing is feasible. This concept can be repeated over several test configurations, crack tip mode mixity values, to establish an applicable testing domain.

3.3. Approach

3.3.1. Numerical model for a thin multilayer 4PB specimen

To numerically evaluate the energy release rate and the mode mixity, a FEA model must first be established. Consider the multilayer structure in Figure 20. This multilayer structure can be modeled using commercially available FEA software (ANSYS). Due to symmetry, a 3D quarter model can be created using solid elements. Each layer is associated with its own linear elastic material properties. The layer boundaries are bonded unless a predefined area is prescribed. At the interface-of-interest, the area past the crack tip is bonded whereas two traction free lines are used along the length of the predefined area to represent the crack front. The crack tip consists of a shared crack tip node and can be modeled using either a square elements or singular crack tip elements. Each mesh type poses its own advantages and disadvantages which will be discussed later on. The model should be meshed using a mapped meshing procedure for model efficiency while retaining a high mesh density near the crack tip. A mesh sensitivity study must be performed to assure the model results are insensitive to mesh size near the crack tip.

The boundary conditions for the model consist of the u_x displacement at the center of the model, u_z displacement on the front side of the specimen, and the u_y displacement along the inner loading pin. A distributed line load is applied along the outer loading pin. After establishing them numerical model the critical delamination condition can be evaluated. When delamination occurs along the interface at the load plateau, the critical load, P_{Crit} is

found. Using this critical load, the model is run to determine the critical stress and displacement fields around the crack tip. At this point the J-integral and VCCT methods previously described in Chapter 2 can be applied to evaluate the adhesion strength and mode mixity at the crack tip.

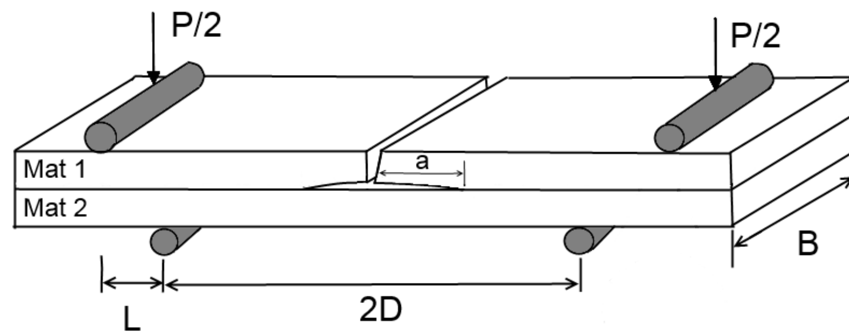

Figure 20. Schematic of bimaterial 4PB sample.

3.3.2. Evaluation of $G_{kink}(\omega)$ at various kinking angles

When interested in evaluating the energy release rate for a kinked crack into an adherend a single step VCCT method can be employed [7]. This method considers a radial mesh of singular elements at the crack tip as seen in Figure 21. The energy release rate of a hypothetical kinked crack can then be determined by considering the crack kinking angle, the nodal forces and nodal displacements for the nodes near the crack tip. Repeating this procedure over several ω angles the maximum G_{Kink} can be determined.

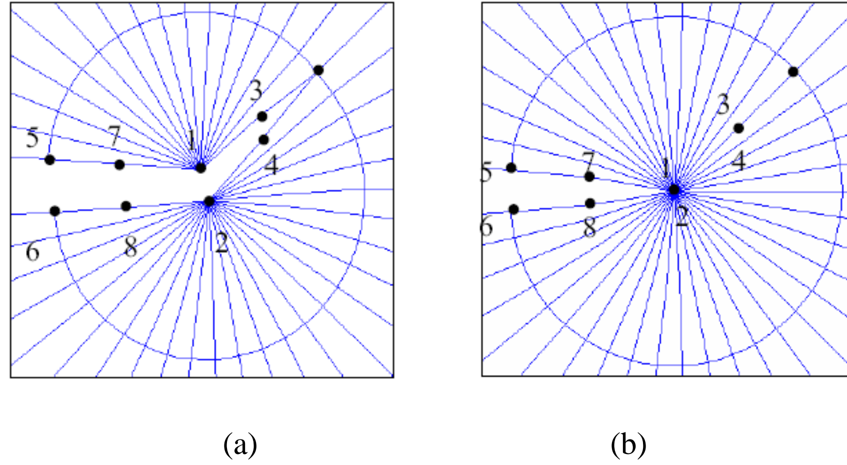

Figure 21. Singular crack tip elements used for evaluating $G_{kink}(\omega)$ (a) before and (b) after crack closure [7].

Using the modeling results and the known bulk fracture toughness of the adherends, Equation (16) can then be used to assess if this test configuration will be more likely to result in interfacial delamination, or crack kinking into an adjacent material.

Consider a bimaterial 4PB specimen that consists of a top and bottom layer that are each 1 mm thick with a Poisson's ratio of 0.3, but different elastic modulus, *E*. The modulus of the bottom layer is E_2 = 25 GPa and the top layer's modulus, E_1, is allowed to vary to analysis the effect moduli ratio plays on the mode mixity and the propensity for crack kinking at the crack tip. Figure 22 shows an example of this VCCT procedure to determine G_{kink} as a function of kink angle for several different moduli ratios. In the figure, the ratio of $G_{Kink}(\omega)/G_0$ is plotted vs. the kink angle. From this chart the preferred kinking direction and the maximum G_{Kink}/G_0 can be established for each case. It is important to note that the crack tip mode mixity is different in each case due to the different material mismatches at the interface. The largest G_{Kink}/G_0 ratio occurs for the highest mode mixity, indicating a greater chance for the crack to kink instead of delaminate under large mode

mixity configurations. As the mode mixity increases so does the angle at which the crack will kink into the bottom adherend. When evaluating weak interfaces, the propensity for a crack to kink into an adherend is not an important consideration since the adhesion strength is typically significantly less than the bulk fracture toughness of the adherends. However when evaluating more advanced material sets that have a combination of larger adhesion strength and lower bulk fracture toughness this can become an issue. Analysis must be run prior to testing to confirm that a particular testing configuration will allow for the evaluation of the expected adhesion strength of the interface.

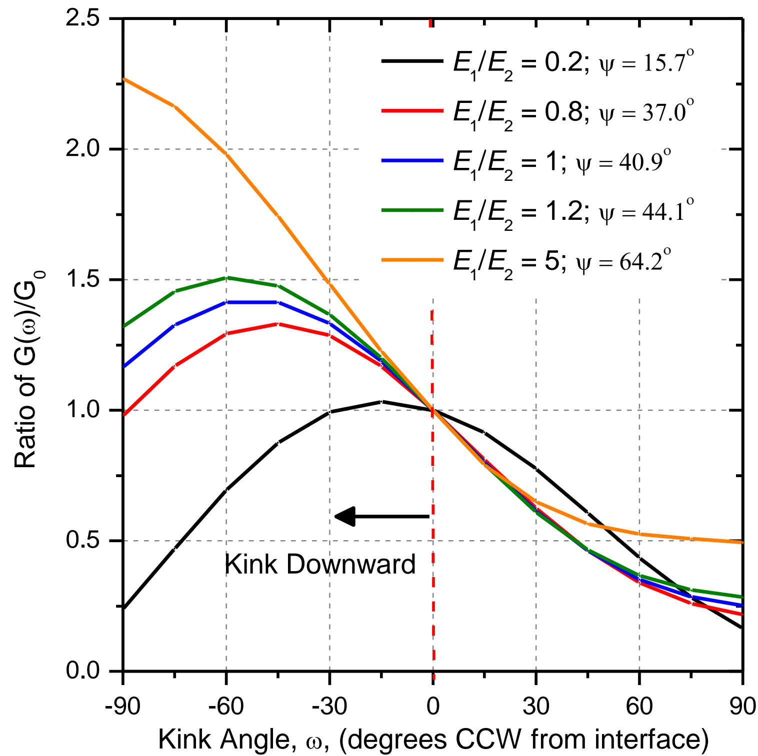

Figure 22. Several $G_{Kink}(\omega)/G_0$ vs. kink angle curves for different material combinations.

3.3.3. Establishing an applicable testing domain

When interested in selecting a specific testing configuration to evaluate the adhesion strength of a given material set, it is helpful to first establish an applicable testing domain. An applicable testing domain can be used to determine the maximum adhesion strength, which can be evaluated when considering the interface-of-interest, interfacial properties, specimen configuration, and the bulk fracture toughness properties by plotting the adhesion strength, or interfacial fracture toughness, Γ_0, against the bulk fracture toughness of the bottom material.

For the example specimens in Figure 22 the maximum G_{kink}/G_0 was determined for each case and used to establish an applicable testing domain in Figure 23. It is clear from the graph that as the mode mixity of the test configuration decreases, the applicable testing domain increases. For a specified bulk fracture toughness, the maximum interfacial fracture toughness that can be evaluated increases as mode mixity decreases.

This procedure can be repeated by creating a numerical model for a given specimen configuration and calculating the G_0, mode mixity and $G_{kink}(\omega)$ to provide insight into if this testing configuration is appropriate for the expected critical adhesion strength of the interface-of-interest.

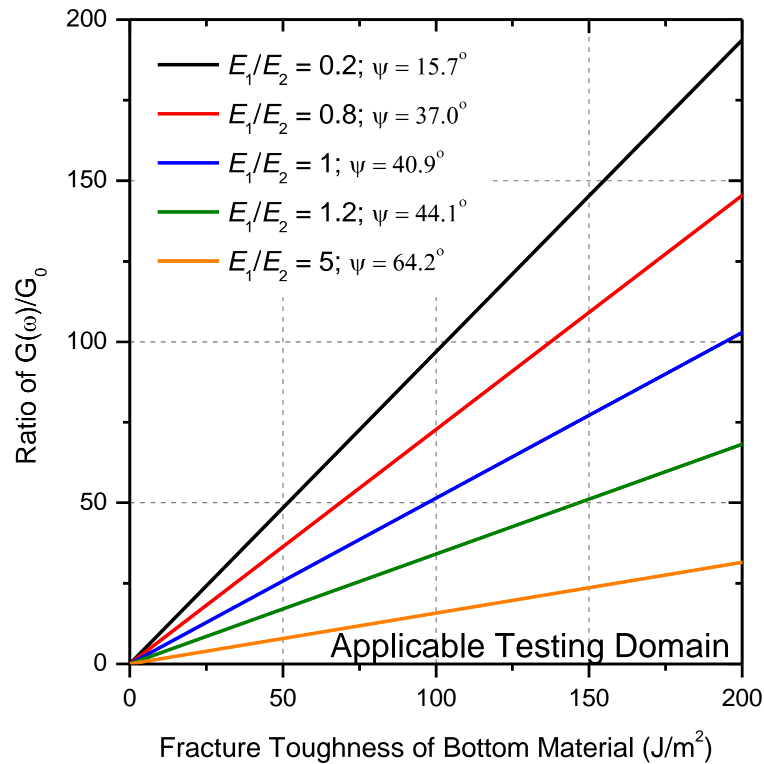

Figure 23. Applicable testing domains over several test configurations for a bimaterial 4PB specimen.

3.4. Implementation of the Applicable Testing Domain for EMC/PSR Interface

To illustrate how the applicable testing domain can be used to determine the maximum adhesion strength that can be tested for a given interface-of-interest in 4PB configuration, an EMC/PSR samples will be studied. The EMC/PSR interface is particularly challenging due to the make-up of the sample (Figure 24). The entire structure is very thin, less than one mm thick, meaning that a reinforcement layer system must be employed to test the specimen. When loaded without any reinforcement there are

excessively large deformations of the specimen as seen in Figure 25. The PSR material is a 25 μm thin, soft, compliant material with a modulus of 4.2 GPa. The EMC material at the interface has a modulus of 24 GPa. The EMC is made with a high-filler content, which also leads to a weak EMC fracture toughness. The specimen dimensions are provided in Table 1.

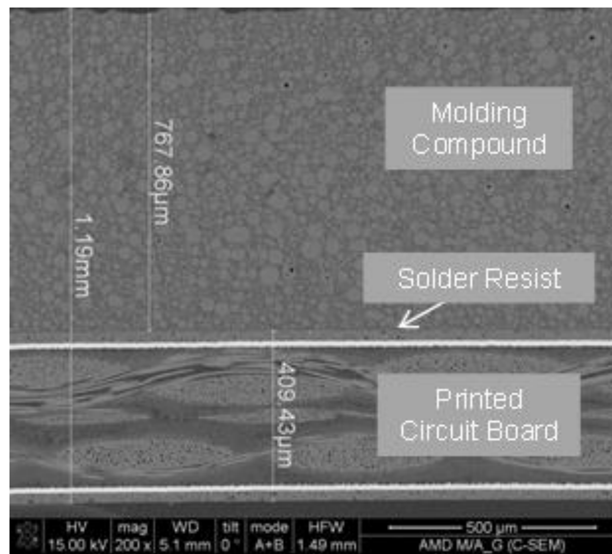

Figure 24. SEM image of EMC/PSR specimen tested.

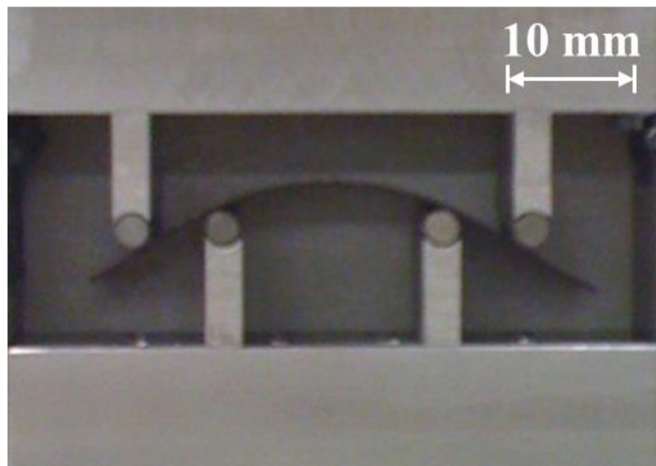

Figure 25. Large deflection in 4PB samples prior to testing thin multilayer structure.

Table 1. Specimen configuration for EMC/PSR specimen tested in 4PB.

Layer	Thickness	Modulus	Poisson’s Ratio
EMC	770 µm	24 GPa	0.28
PSR	25 µm	4.2 GPa	0.38
PCB	410 µm	27 GPa	0.22
Support	1 mm	70 GPa	0.33

The main challenge of testing this sample will be making sure that interfacial delamination occurs before crack kinking can happen. Due to the global loading configuration of the 4PB test, the mode mixity will dictate that the preferred crack direction is downward into the bottom material. Since the PSR layer is so compliant with the lowest fracture toughness, the specimen must be configured with the EMC as the bottom material of the interface as seen with the reinforcement layers in Figure 26.

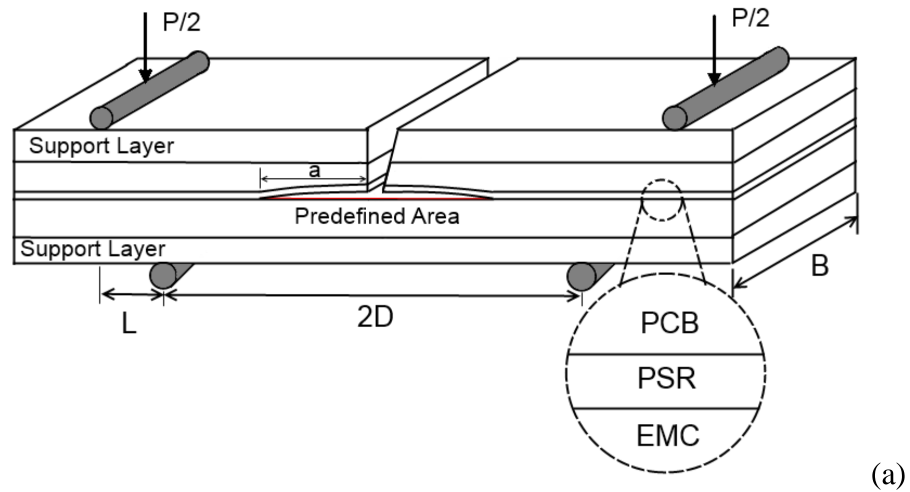

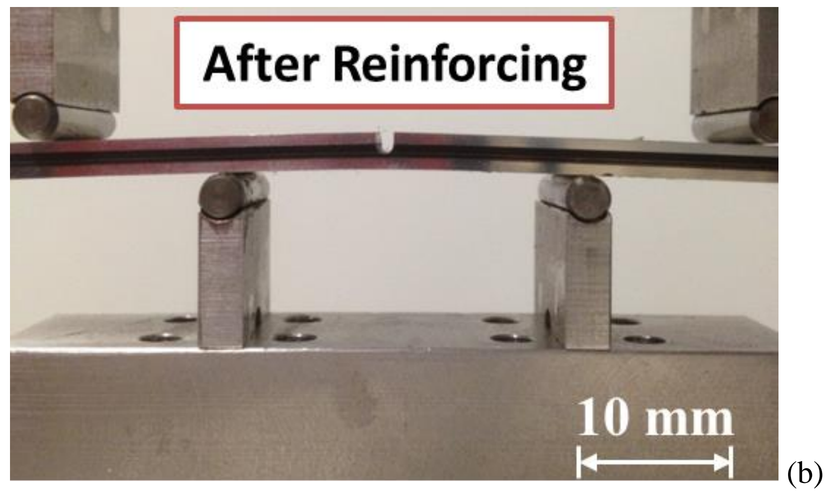

Figure 26. Reinforcement system for EMC/PSR specimen shown a) schematically, and b) during testing.

For the given specimen dimensions and material properties, a FEA model of the 4PB specimen was generated using the circular crack tip mesh field. The model was then run to determine the crack tip stress and displacement fields at the critical state. Post processing routines were then run using the VCCT method to determine G_0, Ψ, and G_{kink} as a function of kink angle, ω. In Figure 27, the ratio of $G_{Kink}(\omega)/G_0$ is plotted vs. the kink angle. From the figure it is clear that the maximum G_{Kink}/G_0 occurs at a preferred kinking

direction of -30° for this configuration, which is downward into the EMC layer. The maximum G_{Kink}/G_0 is 1.20 for the given specimen configuration with a crack tip mode mixity of 45°.

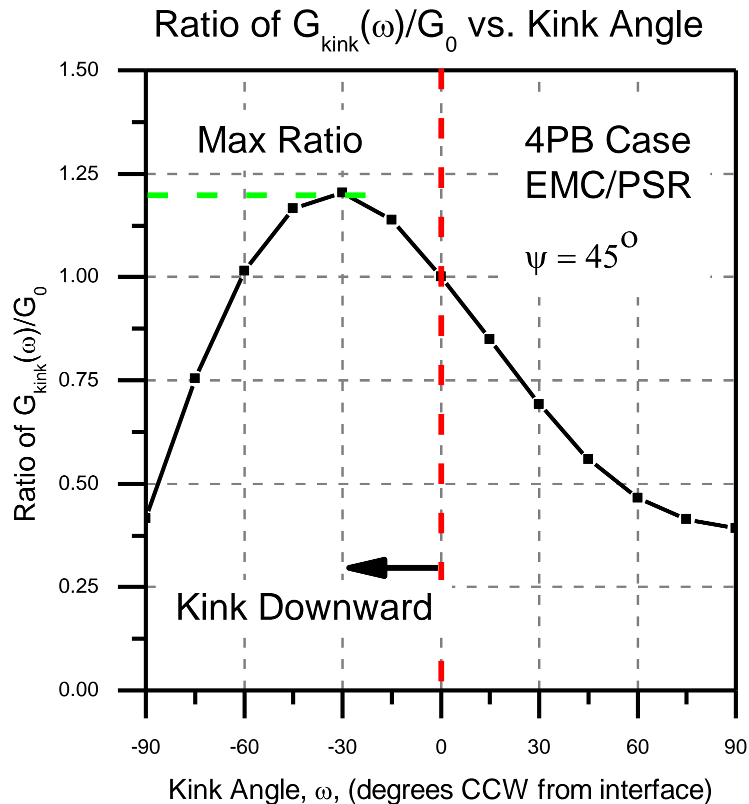

Figure 27. Example of evaluating preferred crack kinking direction when establishing the applicable testing domain for a EMC/PSR interface.

Since the preferred kinking direction is into the EMC layer, the bulk fracture toughness must be assessed. A single edge notched bend test was performed for eight EMC specimens to determine the bulk fracture toughness of the EMC was determined to be approximately 150 J/m^2. Using the energy release rate ratio and the bulk fracture toughness of the high-filler EMC, the applicable testing domain can be established. Figure 28 depicts the applicable testing domain for the specified EMC/PSR specimen. According to the

analysis the maximum adhesion strength that can be evaluated in this configuration is approximately 125 J/m^2. The large mode mixity of the 4PB case is simply unavoidable in the 4PB test configuration, which limits the maximum adhesion strength value that can be assessed prior to crack kinking into the EMC layer.

Samples were fabricated and tested in this configuration. The load vs. displacement curve is shown in Figure 29. The results were not as expected. Towards the end of the load vs. displacement curve instead of reaching a load plateau there was an increase in the compliance shortly before the crack kinked into the interface. Analyzing the sample after testing revealed about 0.5 mm of delamination before the crack kinked into the EMC as shown in Figure 30.

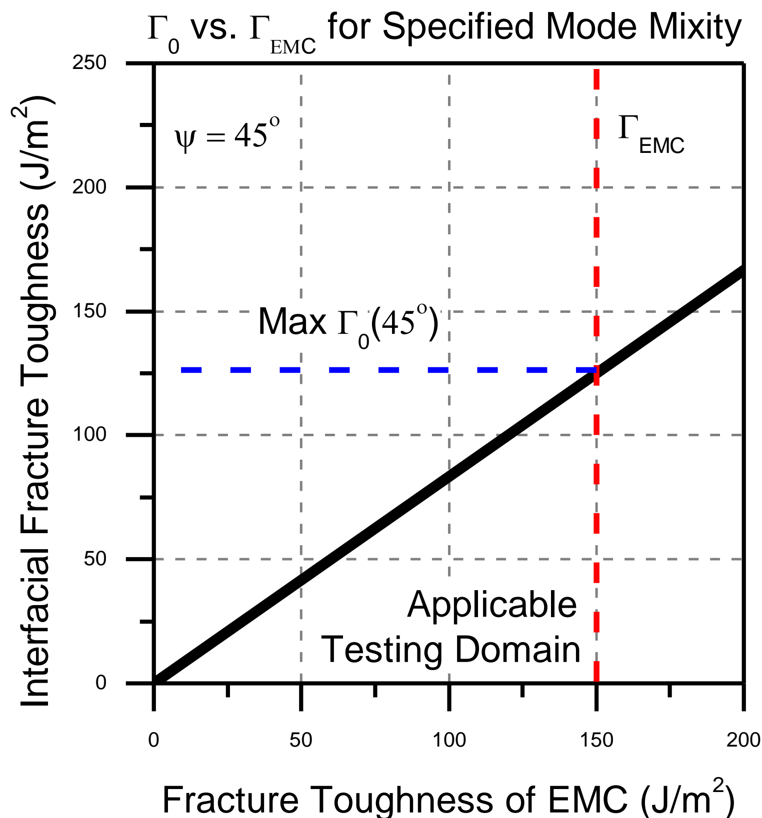

Figure 28. Establishing applicable testing domain over several test configurations.

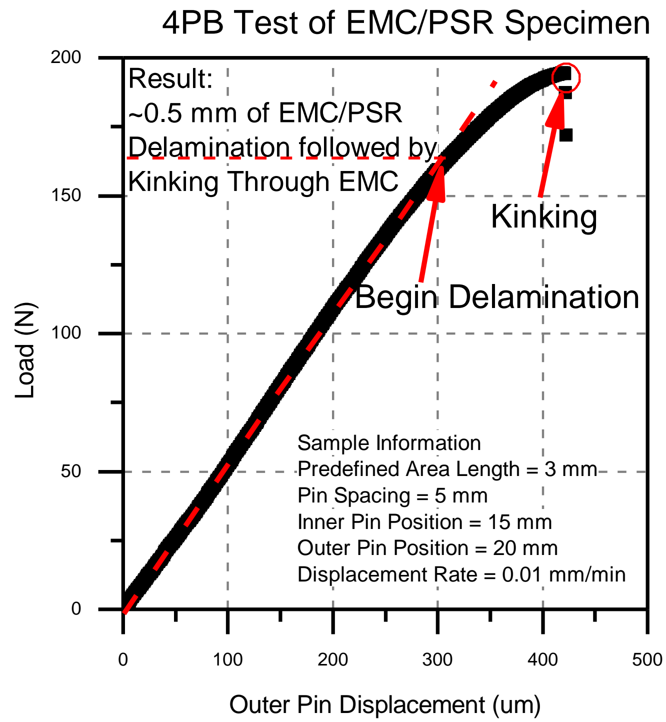

Figure 29. Load vs. displacement curve for reinforced EMC/PSR interface sample.

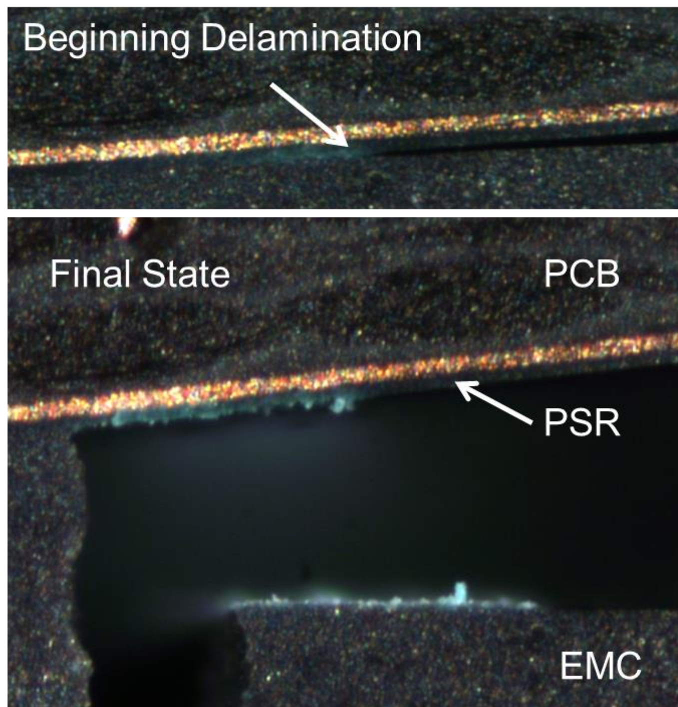

Figure 30. Initial and final states of EMC/PSR sample testing

Using the critical load from the load vs. displacement curve where delamination began, the energy release rate was calculated to be roughly 120 J/m^2. When plotting this in the applicable testing domain, shown in Figure 28, it is obvious that the 4PB test failed because the condition was at the very extent of the applicable testing domain. In order to have clear test results for this interface a different test configuration must be considered that allows for testing at a lower mode mixity.

3.5. Conclusion

An approach for establishing an applicable testing domain for evaluating the adhesion strength of an interface in the 4PB configuration was presented. Numerical methods were employed to establish the propensity for a crack to kink out of the interface depending on a number of critical factors. The approach to establish an applicable testing domain was then carried out for a high strength EMC/PSR interface, and was shown theoretically that testing would be at the edge of the applicable testing domain due to the large adhesion strength of the interface, the low fracture toughness of the EMC and the large mode mixity of the system configuration. 4PB testing was then carried out for this specimen to demonstrate these findings. By carrying out this approach to establish an applicable testing domain prior to specimen fabrication, the experimenter can be guided to select an appropriate test method that will allow for successful adhesion strength testing of their interface-of-interest.

Chapter 4: Single Cantilever Adhesion Test for Interfaces in Thin Multilayer Semiconductor Packages[1]

Abstract

We propose and implement a novel adhesion test configuration called "single cantilever adhesion test (SCAT)" that can be employed to determine the adhesion strength at interfaces in thin multilayer semiconductor packages. The proposed SCAT method is optimal for quick and quantitative testing of strong interfaces inside thin multilayer structures as sample preparation and testing are considerably simpler than double cantilever beam tests while still maintaining a lower mode mixity at the crack tip than four point bending tests. Following detailed sample preparation and experimental testing to determine the critical load required for delamination, a numerical model of the sample is created and run at the critical condition to assess the stress and strain fields around the crack tip at the point of delamination, thus allowing for the J-integral method to be employed to determine the critical energy release rate, G_{Crit}. The proposed approach is carried out for thin multilayer structures with two different interfaces. The results show excellent repeatability, which allows for the test method to be used effectively to select the most ideal material set for given applications.

---

[1] This chapter was submitted to the *Journal of Microelectronics Reliability* under the title of "Single Cantilever Adhesion Test for Interfaces in Thin Multilayer Semiconductor Packages" by K. Mahan, B.Y. Kim, B. Wu, B. Han, I. Kim, H. Moon, and Y. Hwang

4.1. Introduction

With the advancement of thin-profile designs, in-situ adhesion strength testing of products directly off of manufacturing lines is a critical challenge. If potential delamination failures due to inadequate adhesion strength can be detected early in the design cycle, unreliable designs can be ruled out leading to quicker product turn around. This is especially important in the fast-pace environment of the electronic packaging industry where quick and effective adhesion strength testing methods are required.

One such interface that must address these challenges is the high adhesion strength interface found between epoxy molding compound (EMC) and photo solder resist (PSR). The interface is shown in Figure 31, where the PSR is sandwiched between the EMC and the printed circuit board (PCB) substrate. The EMC/PSR interface can delaminate during manufacturing processes and/or operating conditions. Thus, it is critical to assess the adhesion strength of any newly proposed material combinations to assure the adhesion strength of selected material sets is strong enough for the intended product application.

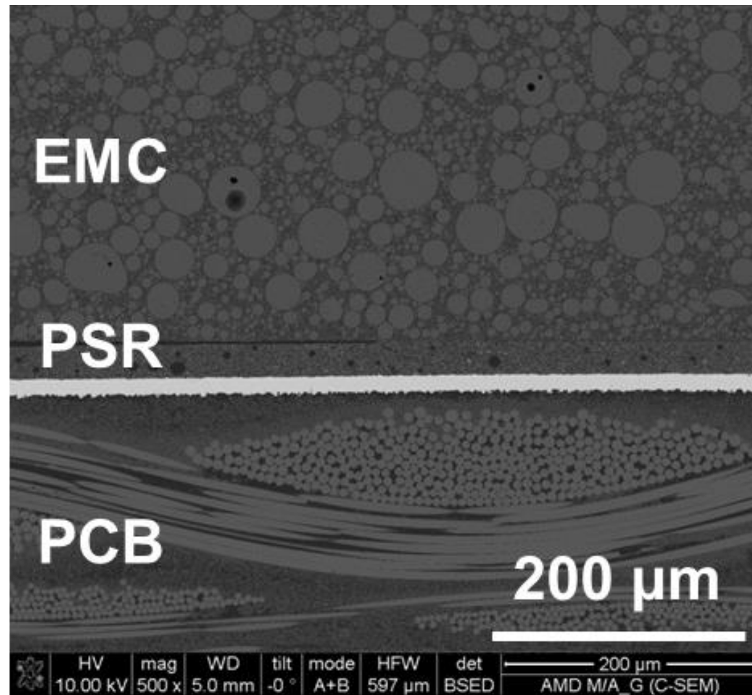

Figure 31. Close up SEM image of thin multilayer stacks consisting of EMC, PSR, and PCB.

The adhesion strength is often characterized using the energy release rate of the interface [1]. The energy release rate, *G*, is a measure of the energy available for an increment of crack extension. When a specimen with an interfacial crack is loaded, energy is stored inside until a critical loading state is reached. At this point, the crack propagates, and energy is released from the system while creating a new surface area along the interface. For this case, *G* can be evaluated directly from a typical load vs. displacement graph.

The second critical property to consider is the mode mixity at the crack tip. The mode mixity can be defined as the ratio of in plane shear (mode II) to opening (mode I) loading at the crack tip [1-5]:

$$\tan^{-1}\Psi = \sqrt{\frac{G_{II}}{G_{I}}} \tag{17}$$

where G_I and G_{II} represent the mode I and II energy release rate contribution at the interface, respectively. The energy release rate is known to increase with respect to the mode mixity due to the increased presence of in-plane shear loading; when comparing different material sets, it is important to compare them at similar mode mixity values [1-5].

Energy release rate testing methods, such as the double cantilever beam (DCB) method [4, 6-12] and the four point bending (4PB) method [3, 4, 13-28], have been practiced widely, but when faced with the increasingly strong interfaces and thinner layers of interest, complications in testing arise. For instance, the DCB testing offers near mode I energy release rates by applying opening mode loading to the end of a beam specimen. However, DCB testing requires complex sample preparation to maintain near mode I loading [10, 11] when dealing with thin multilayer structures.

The 4PB test method offers the advantage of crack length independent energy release rates due to the constant moment region inside the loading pins. Due to the global loading condition, however, the mode mixity at the crack tip is much larger in this configuration [3]. When faced with large crack tip mode mixity and a high adhesion strength interface, it can be difficult to obtain delamination along the interface before the crack kinks into an adjacent material. This issue is apparent for the EMC/PSR interface due to the increasingly large high-filler content of EMCs that are being used in newer products. High-filler content leads to a reduced EMC fracture toughness, which makes a precrack at the PSR/EMC interface more susceptible to kinking out of the interface. A new adhesion testing approach is required to address the particular challenges of this EMC/PSR interface.

This paper proposes and implements a novel adhesion test configuration called "single cantilever adhesion test" (SCAT) that can be employed to determine the adhesion strength at strong interfaces in thin multilayer stacks. Following detailed sample preparation and experimental testing to determine the critical load required for delamination, a numerical procedure to determine the critical energy release rate and the mode mixity of the interface is described. The results obtained from the proposed approach are presented to discuss the effectiveness of the proposed SCAT method.

4.2. Background

Several fundamental concepts are employed to develop this adhesion test method. They are presented here first as background for the method.

4.2.1. J-integral Approach

A J-integral method is employed to evaluate the critical energy release rate. The energy release rate, G, was proposed by Irwin as a measure of the energy available for crack extension when materials remain linear elastic [29]. Rice later went on to expand upon Irwin's approach by idealizing elastic-plastic deformation as nonlinear elastic. This allowed for the extension of fracture mechanics beyond the linear elastic deformation by use of the J integral [30]. The J integral considers an arbitrary path going counter-clockwise around a crack tip:

$$G = J = \int_c \left(w n_i - T_i \frac{du_i}{dx} \right) ds \tag{18}$$

where w is strain energy density:

$$w = \int_{0}^{\varepsilon} \sigma_{ij} d\varepsilon_{ij} \tag{19}$$

n_i is the normal vector to c, and T_i is the traction vector:

$$T_i = \sigma_{ij} n_j \tag{20}$$

c is an arbitrary contour around the tip of the crack; σ , ε, and u are the stress, strain, and displacement field, respectively [30]. The J-integral remains equivalent to the energy release rate as long as the sample is under small scale yielding. This can be readily shown in other source material [1, 30, 31]. Another key criterion is that the J-integral is path independent. This derivation can also be found in source material [1, 32] and holds true for a crack in a multilayer structure as long as the structure is under small scale yielding and the crack is parallel to the layered structures [32].

Once the critical condition of the specimen is modeled using a commercial FEA package, the critical stress and displacement fields can be assessed on the contour around the crack tip. A contour path is then selected around the crack tip to evaluate the J-integral. Several contours should be analyzed to assure that the selected contour is indeed path-independent. A post-processing routine can be run to determine the stress and displacements along the contour to evaluate the J-integral.

4.2.2. Virtual Crack Closure Technique

To verify the integrity of the J-integral, a virtual crack closure technique (VCCT) is run that can evaluate the energy release rate and mode mixity in a single step. According to Irwin, the work required to close a crack by an infinitesimal crack length, Δa, is equal to the work required to close the crack to its original length [29]. For homogeneous,

isotropic materials, this interpretation allows for the mode I and mode II components of the energy release rate to be expressed as [2, 5]:

$$G_I = \lim_{\Delta \to 0} \frac{1}{2\Delta} \int_0^\Delta \sigma_{yy}\left(\Delta - r\right)\delta_y\left(r\right)dr \tag{21}$$

$$G_{II} = \lim_{\Delta \to 0} \frac{1}{2\Delta} \int_0^\Delta \sigma_{xy}\left(\Delta - r\right)\delta_x\left(r\right)dr \tag{22}$$

$$G = G_I + G_{II} \tag{23}$$

where Δ is an infinitesimal crack extension, σ_{yy} and σ_{xy} are the normal and shear tractions at a distance *r* ahead of the crack tip, and δ_x and δ_y are the displacement jumps at a distance *r* behind the crack tip along the *x* (sliding mode) and *y* (opening mode) directions.

This theoretical interpretation can be extended to a numerical finite element model. Considering the crack tip mesh in Figure 32, the energy release rate can be expressed in terms of the nodal forces and displacements as [5]:

$$G_I = -\frac{1}{2\Delta a}\left[f_{y,5}\left(\Delta u_{y,1-3}\right) + f_{y,6}\left(\Delta u_{y,2-4}\right)\right] \tag{24}$$

$$G_{II} = -\frac{1}{2\Delta a}\left[f_{\mathrm{x},5}\left(\Delta u_{\mathrm{x},1-3}\right) + f_{\mathrm{x},6}\left(\Delta u_{\mathrm{x},2-4}\right)\right] \tag{25}$$

where $f_{x,i}$, $\Delta u_{x,j}$ and $\Delta u_{y,k}$ represent the nodal force, shear displacement and opening displacement, respectively. Equations (17) and (23) can then be used to verify the energy release rate and determine the mode mixity at the crack tip directly from the FEA results.

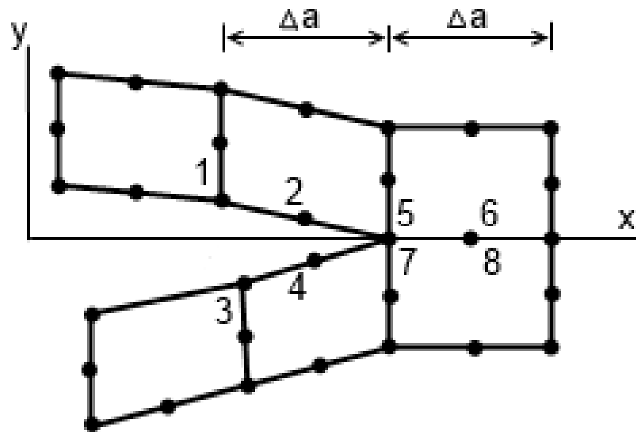

Figure 32. Schematic diagram of crack tip mesh for VCCT method.

4.2.3. Crack Tip Mode Mixity

The larger the mode mixity, the more susceptible the interfacial crack will be to kinking out of the interface [33-35]. Additionally, crack kinking is of greater risk when dealing with high adhesion strength interfaces and adherends with low fracture toughness. Care should be taken to design the SCAT specimen in the lowest possible mode mixity possible to be able to test a wide range of interfaces.

It is well known that the mode mixity of a crack in the interface of two materials is influenced by the mismatch of the elastic material properties, namely the elastic modulus, E, and Poisson's ratio, v [36]. Consequently, for an interfacial cracked specimen, even when the sample is loaded in a global mode I loading condition, such as DCB, there is still a non-zero mode mixity at the crack tip.

Suo and Hutchinson have investigated the effect of this material mismatch for several conditions [15, 16, 37-39]. Of interest is that even when pure mode I loading is globally applied, the specimen will still have a mixed mode loading condition at the crack tip due

to the material mismatch. This inherent mode mixity plays a role regardless of the global loading condition.

4.3. Single Cantilever Adhesion Test (SCAT) Method

4.3.1. Physical Description

The SCAT configuration comprises of a thin multilayer specimen with a precrack at the interface-of-interest that is secured to a supporting block. The material above the interface-of-interest extends further so that a cantilever arm is offset past the fixed area to allow for direct loading. A schematic of a typical SCAT specimen and test configuration can be seen in Figure 33a.

The specimen is secured to a mechanical test stand and pin loading is applied to the offset cantilever arm. A typical load vs. displacement curve that can be expected from the SCAT is shown in Figure 33b. As the displacement increases monotonically, the load increases until a critical load, P_{Crit}, is reached and delamination begins at the end of the predefined area. From a load vs. displacement graph the critical load will be the maximum load on the graph. Once delamination begins, stored energy must be released from the body to create the new surface area. In the experimental results this is seen as a load drop corresponding with the beginning of delamination. Since the test is run in displacement control, the displacement will continue to increase, resulting in steady delamination along the interface of interest until the test is stopped.

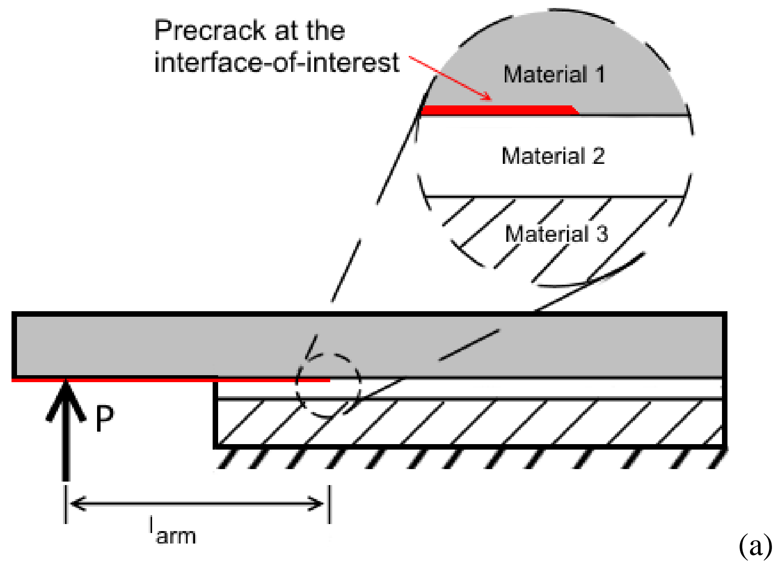

(a)

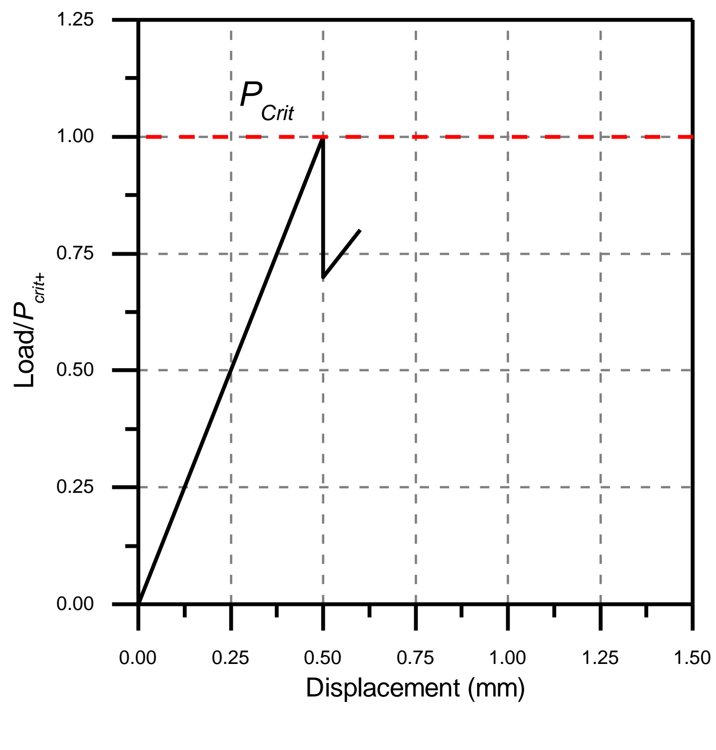

(b)

Figure 33. Schematic of (a) test configuration for SCAT specimen with a precrack and (b) load vs. displacement graph for a SCAT test.

4.3.2. Numerical Analysis

A numerical analysis is employed to extract the energy release rate and mode mixity from the experimental results. A 2D model of the specimen is first established with plane strain elements. A meshing strategy can be used to minimize the total number of elements while still retaining a dense mesh at the crack tip. Maintaining a concentrated mesh near the crack tip is essential for thin structures as it allows for more accurate stress and strain fields to be assessed. A sensitivity analysis should be run to assure that the element size near the crack tip is small enough to be mesh independent. The model can then be run to evaluate the critical state by applying the critical load from the experiment. From the results a post-processing routine can be run to evaluate the critical energy release rate, G_{Crit}, and the mode mixity, Ψ, of the interface.

4.3.3. Mode Mixity in SCAT Method

When establishing the specimen dimensions for the test, it is important to consider the mode mixity at the crack tip when testing. For the SCAT, the most critical parameters that influence the mode mixity at the crack tip are the modulus and thickness of the top material and the moment arm of the applied loading. When designing a specimen, the material properties of the top layer are typically fixed due to the interface-of-interest being testing. The specimen designer can still optimize the height of the top layer to minimize the mode mixity at the crack tip. By increasing the height of the top layer the flexural rigidity of the loaded beam is greatly increased, thus resulting in a greater mode I opening loading condition when pin loading is applied to the offset cantilever beam. Using FEA modeling this can be clearly shown for a given material pair.

Consider a three-layer specimen with a predefined area precrack placed between the top and middle layers creating a moment arm, l_{arm}, of 5 mm. The bottom layer has a thickness of h_3 = 300μm and an effective modulus of E_3 = 27.5 GPa. The middle layer is a thin film layer of thickness, h_2 = 25 μm and the modulus of the top layer is E_1 = 24 GPa. These parameters were set as a baseline for later consideration of a specific case on interest. Using the plane strain numerical model, the mode mixity at the crack tip vs. the increasing top layer thickness for several material combinations width different elastic moduli mismatches was calculated and plotted in Figure 34. It is clear from the figure that in each case increasing the height of the top layer will allow for a smaller crack tip mode mixity to be evaluated.

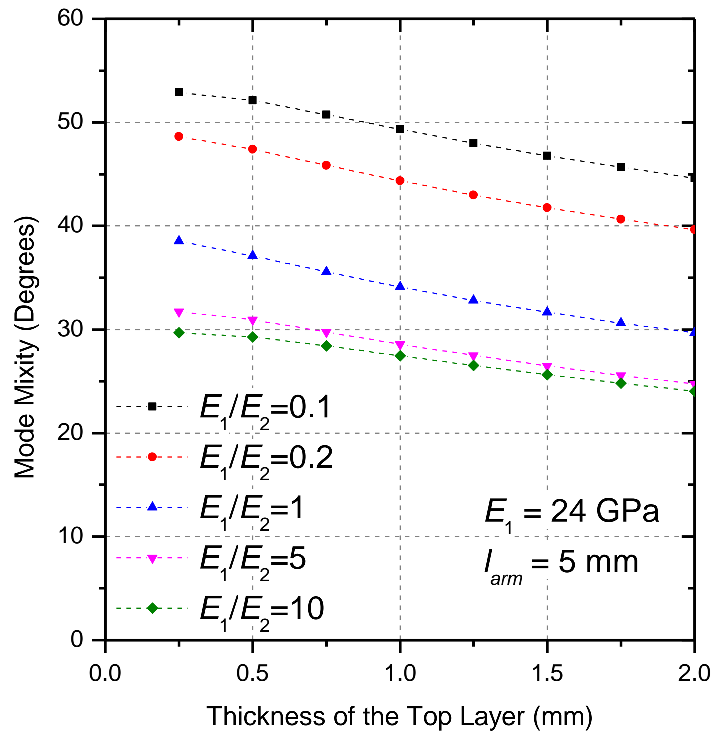

Figure 34. Mode mixity vs. upper layer thickness for several material combinations in SCAT test configuration.

The second factor to consider is the moment arm. To evaluate the effect of moment arm length on the mode mixity, the mode mixity was plotted against multiple moment arm lengths in Figure 35. For the plot the lowest mode mixity case from Figure 34 was selected with the moduli ratio $E_1/E_2 = 10$, and an upper layer thickness of $h_1 = 2$ mm. As the moment arm length increases, the mode mixity at the crack tip also increases. The results suggest that the shortest moment arm length should be used during testing to minimize mode mixity.

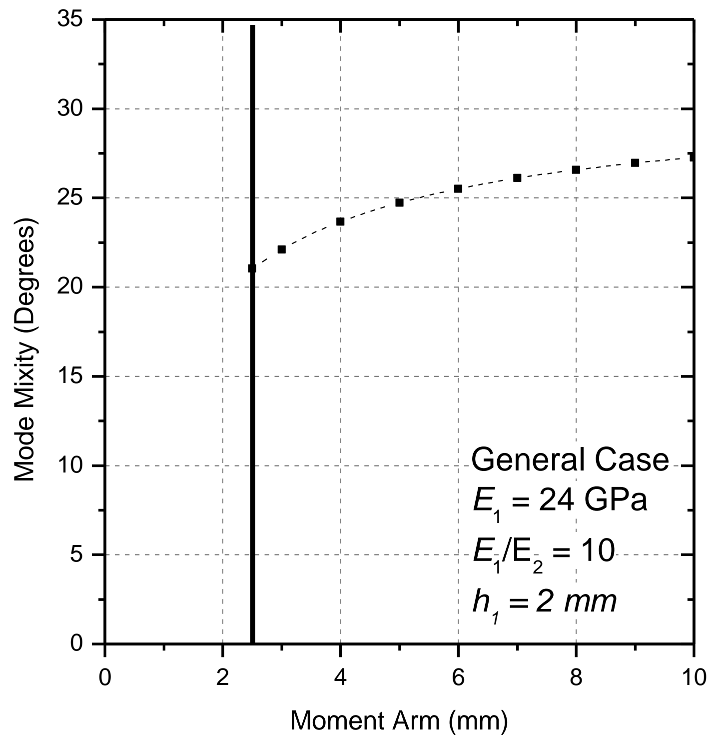

Figure 35. Mode mixity vs. moment arm length for $E_1/E_2 = 5$ and $h_1 = 2$ mm in SCAT test configuration.

4.4. Test preparation

Two separate material sets consisting of an EMC/PSR interface on top of a thin PCB were selected to implement the SCAT procedure. Each material set is consistent except for two potential PSR materials of interest (will be referred to as PSR1 and PSR2).

4.4.1. Specimen Design

While the PSR and PCB thicknesses were fixed due to manufacturing specifications, the thickness of the EMC was a variable to consider when designing the specimen. The previous numerical analysis (Figure 34) clearly indicated that the largest possible EMC thickness should be selected to minimize the mode mixity. Due to height restrictions of the mold, the maximum allowable EMC height was 950 μm. Following this logic, the mode mixity of the specimen configuration was ~28.5°. Material properties of the individual layers can be found in Table 2.

Table 2. Material properties for the EMC/PSR specimen.

Material	Thickness	Modulus	Poisson's Ratio
EMC	950 μm	24 GPa	0.28
PSR	25 μm	4.2 GPa	0.38
PCB	300 μm	27.5 GPa	0.22

Another key consideration for creating samples is to make sure the specimen is under the plane strain condition. Plane strain testing is required for assessing the critical energy release rate as an intrinsic material property since a specimen in plain strain has the

most concentrated tri-axial stress state [1]. After the cross-section of the specimen has been designed to obtain the desired mode mixity at the crack tip, a 3D numerical analysis was performed to assess the minimum specimen thickness required to maintain a plane strain state in the specimen.

The energy release rate was assessed at the center of the model. This process was repeated over several specimen widths. Figure 36 shows the results normalized by the energy release rate obtained from the 2-D plane model ($G_{3D}/G_{Plane\text{-}strain}$) and plotted as a function of the specimen width. As expected, the specimen approaches a plane strain condition as the sample width increases. For this specific sample configuration, the sample is within 1% of a plane strain configuration with a width of 16 mm. Since any further increase in width only fractionally increases the plane strain condition and considering the difficulty in testing very wide specimens, a 16 mm sample width was selected for all samples.

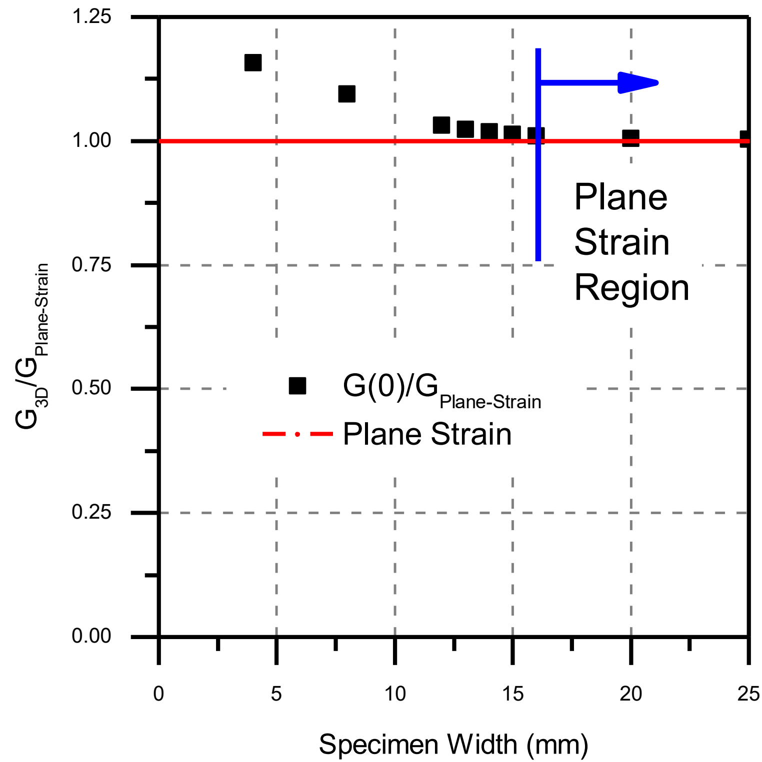

Figure 36. Plot of 3D energy release rate normalized by plane strain energy release rate vs. specimen width for a EMC/PSR SCAT sample.

4.4.2. Specimen Preparation

Samples were prepared in individual boards designed to fit with a typical molding process. Figure 37a depicts a schematic of the board layout used for creating a sample batch. After the PCB board was created with a top PSR layer, dicing marks were etched on the bottom of the board. The individual specimens were created by laser cutting through the etched intersections. On the top of the board, the predefined area is created on the PSR surface.

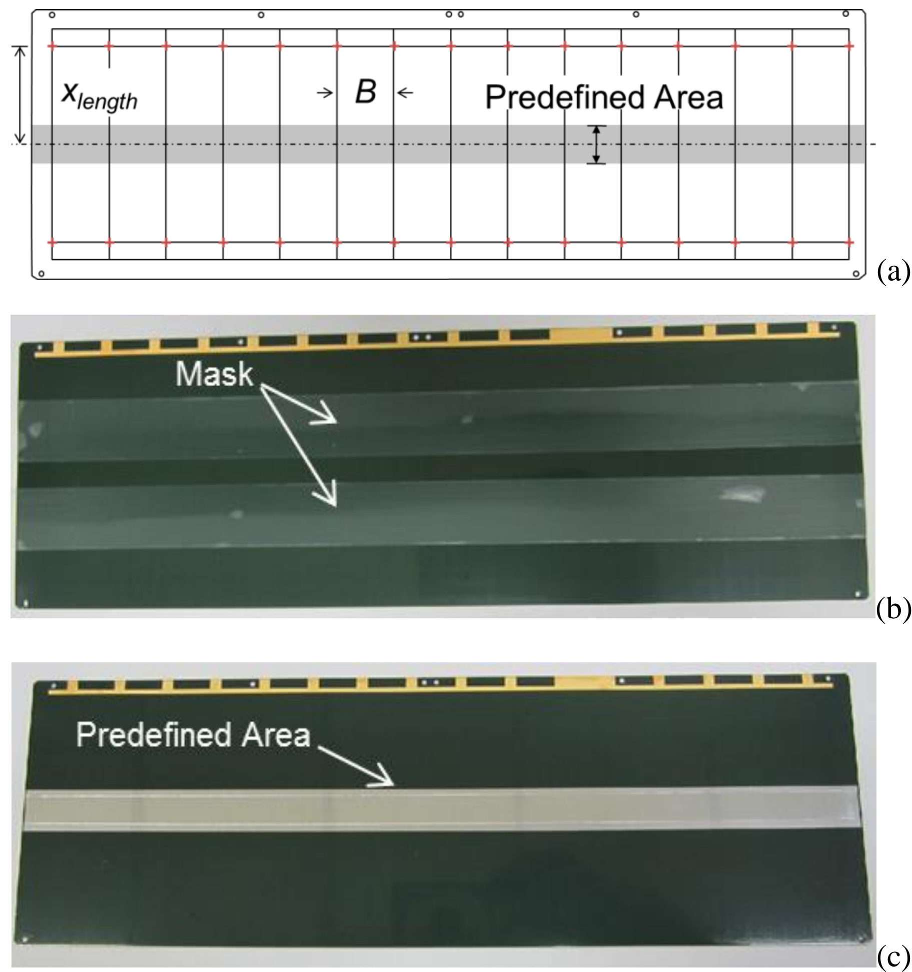

Figure 37. Sample preparation steps: a) schematic of board layout with dicing markers and planned predefined area, b) masked area on top of PSR/PCB layers for predefined area, and c) finished silicon oil/aluminum sputtered predefined area on PSR surface.

The most important function of this specimen fabrication is the creation of a low-adhesion predefined area at the interface-of-interest. The predefined area provides a thin, natural crack front that is essential to accurate testing using the SCAT method. To create the predefined area (PDA), the following approach was implemented.

A temporary mask was placed on the PSR surface to establish the length of the predefined area for two specimens on the row (Figure 37a). A thin layer of silicon oil was

applied in between the masked area and allowed to dry. An aluminum layer was then deposited by sputtering aluminum over this area. The masked area was then removed, revealing the finished predefined area as seen in Figure 37c.

The silicon oil greatly reduced the adhesion in this area, which resulted in very small loading requirements to delaminate this area. The aluminum sputtering layer acted as a barrier layer between the silicon rubber and the top adherent. This barrier layer was critical since the specimen went through the high pressure and temperature EMC molding process. Without the aluminum sputtered layer, the predefined area could be modified undesirably (non-ideal plane crack).

The board was then put through the molding process to create the upper EMC layer. A cross-sectional view of the PCB/PSR/EMC specimen is shown schematically in Figure 38 along with a close-up SEM image of the silicon oil/aluminum layers of the predefined area. It is clear through the SEM image that a thin, continuous silicon oil layer remains intact after the molding process on top of the PSR layer due to the sputtered aluminum layer. Specimen were then laser cut using the dicing marks shown in Figure 37a to establish individual specimens of the desired length and width.

Figure 39a highlights two specimens from a given row on the sample board. Cut A in Figure 39a was made via the laser to arrive at the individual specimen. Prior to testing, the PCB side of the specimen was bonded to a rigid aluminum support block using a thin layer of a structural epoxy. In this configuration, the end of the specimen is aligned with the supporting block with part of the predefined area offset over the edge of the fixed support (Figure 39b). During this process, the sides of the specimen were temporarily covered with tape to prevent epoxy from potentially bonding to the interface-of-interest.

Any excess epoxy at the interface-of-interest could potentially lead to artificially large adhesion strength results. After the epoxy cured over a twelve hour period, the tape was removed. Finally the offset area under the interface-of-interest was removed to allow for direct pin loading to the EMC (Cut B in Figure 39a).

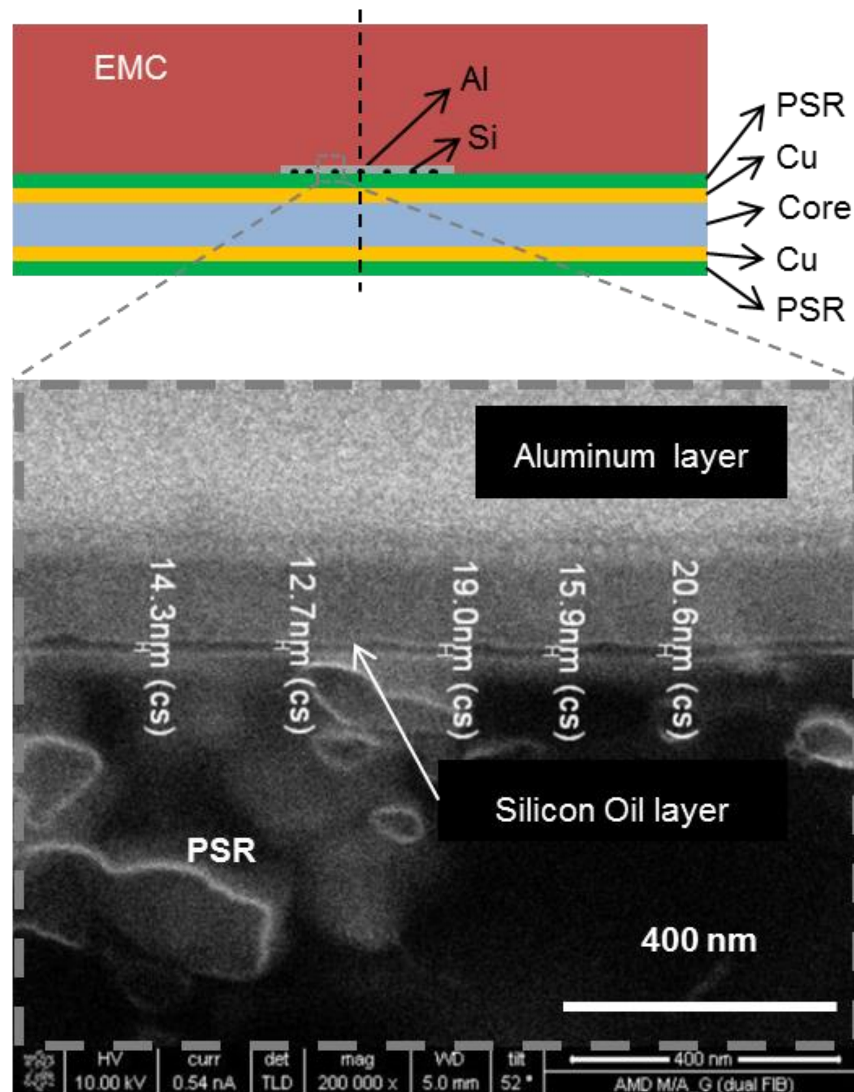

Figure 38. Cross-sectional schematic view of predefined area creation for EMC/PSR SCAT specimens along with an inset of a zoomed in SEM image of silicon oil and aluminum sputtered layers of predefined area.

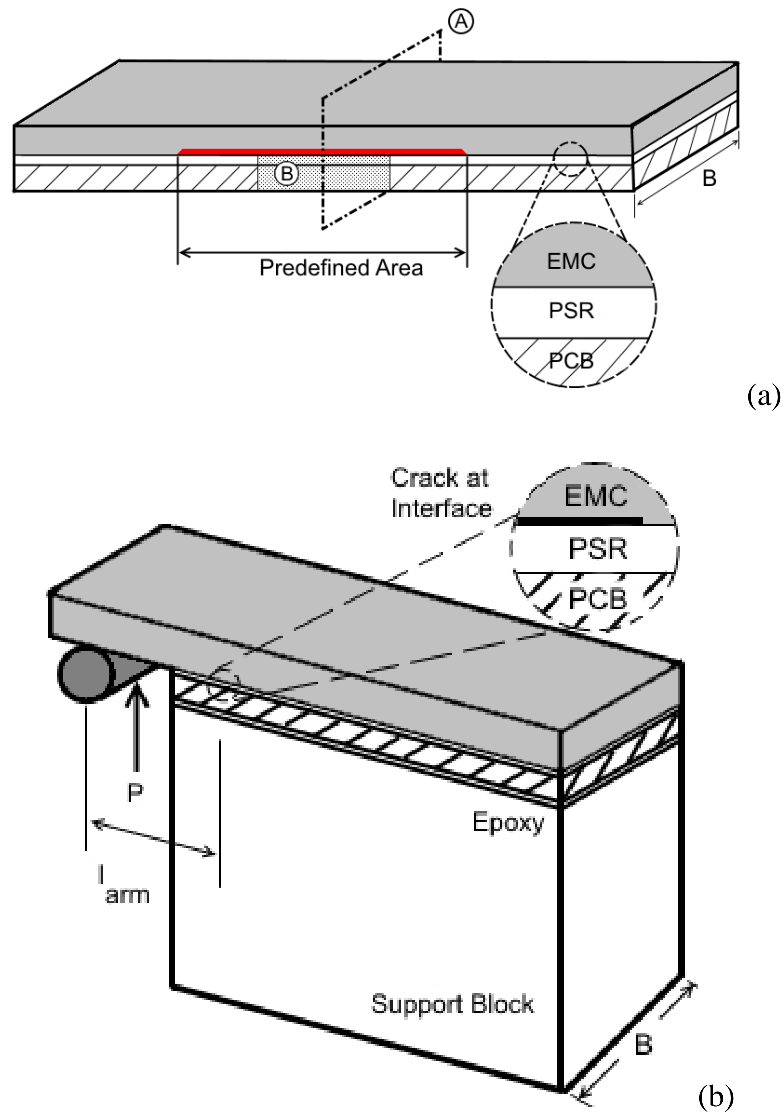

Figure 39. Schematics of typical (a) two SCAT specimen with predefined area prior to dicing, and (b) test configuration for a SCAT test.

4.5. Experiment and Results

4.5.1. Testing

For testing, the specimen was secured on a mechanical test stand with a specially designed test fixture (Figure 40a). The test fixture should allow for direct loading of the

EMC with a greased pin while maintaining alignment throughout testing. A fixture that allowed for self-alignment in the out-of-plane direction was ideal to prevent twisting during testing which would result in erroneous test results. A camera was also setup to capture the initial pin position on the offset arm and to take video of the following delamination.

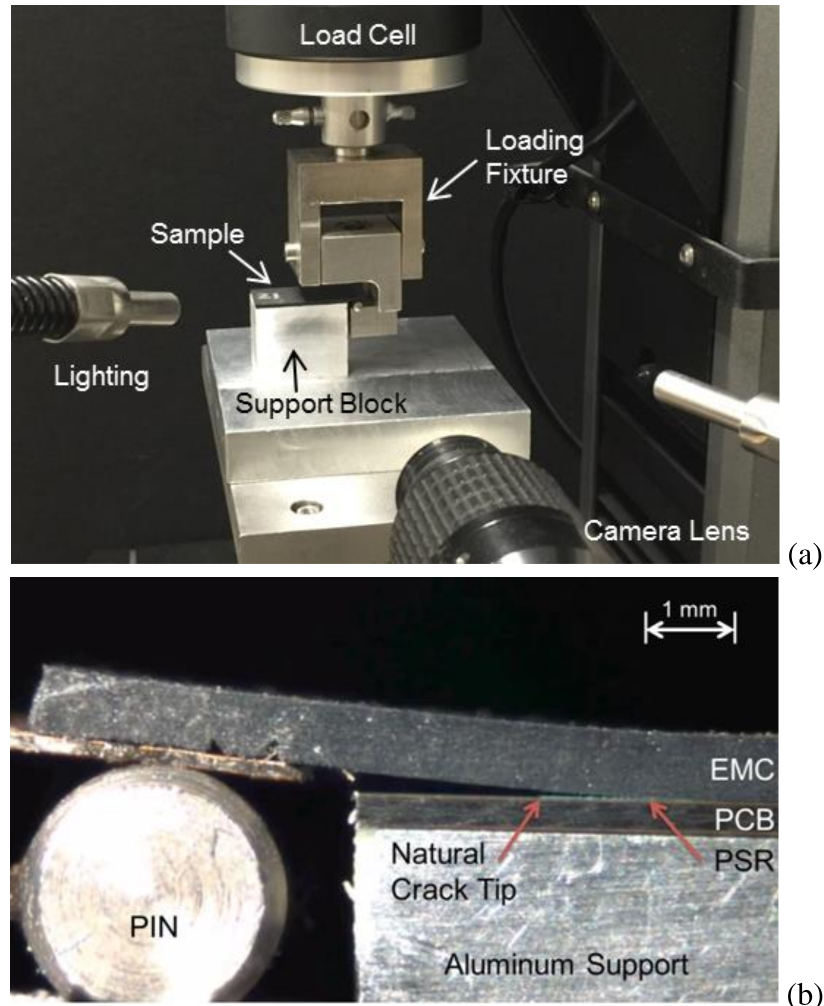

Figure 40. SCAT a) test setup with EMC/PSR specimen, test stand, loading fixture, and camera used to monitor delamination; and b) in-situ camera image of delamination occurring at EMC/PSR interface during testing.

Once the specimen was set up, a displacement rate of 100 μm/sec was applied to the pin monotonically until delamination occurred at the interface at a critical load, P_{crit}.

As seen in Figure 40b, the camera captured this initial crack propagation and the following steady state delamination along the interface as the load decreased with increasing pin displacement.

Following the test, the moment arm, l_{arm}, from the experiment was determined for each specimen to use in the numerical model. There was a slight variation in the moment arm from specimen to specimen resulting from alignment of the loading pin and from the dicing of individual specimens. The initial position of the moment arm was determined from a still image from the camera prior to testing, shown schematically in Figure 41a. The offset distance from the center of the pin to the edge of the specimen was then recorded. Next by evaluating the delaminated side of the specimen the extent of the predefined area was determined.

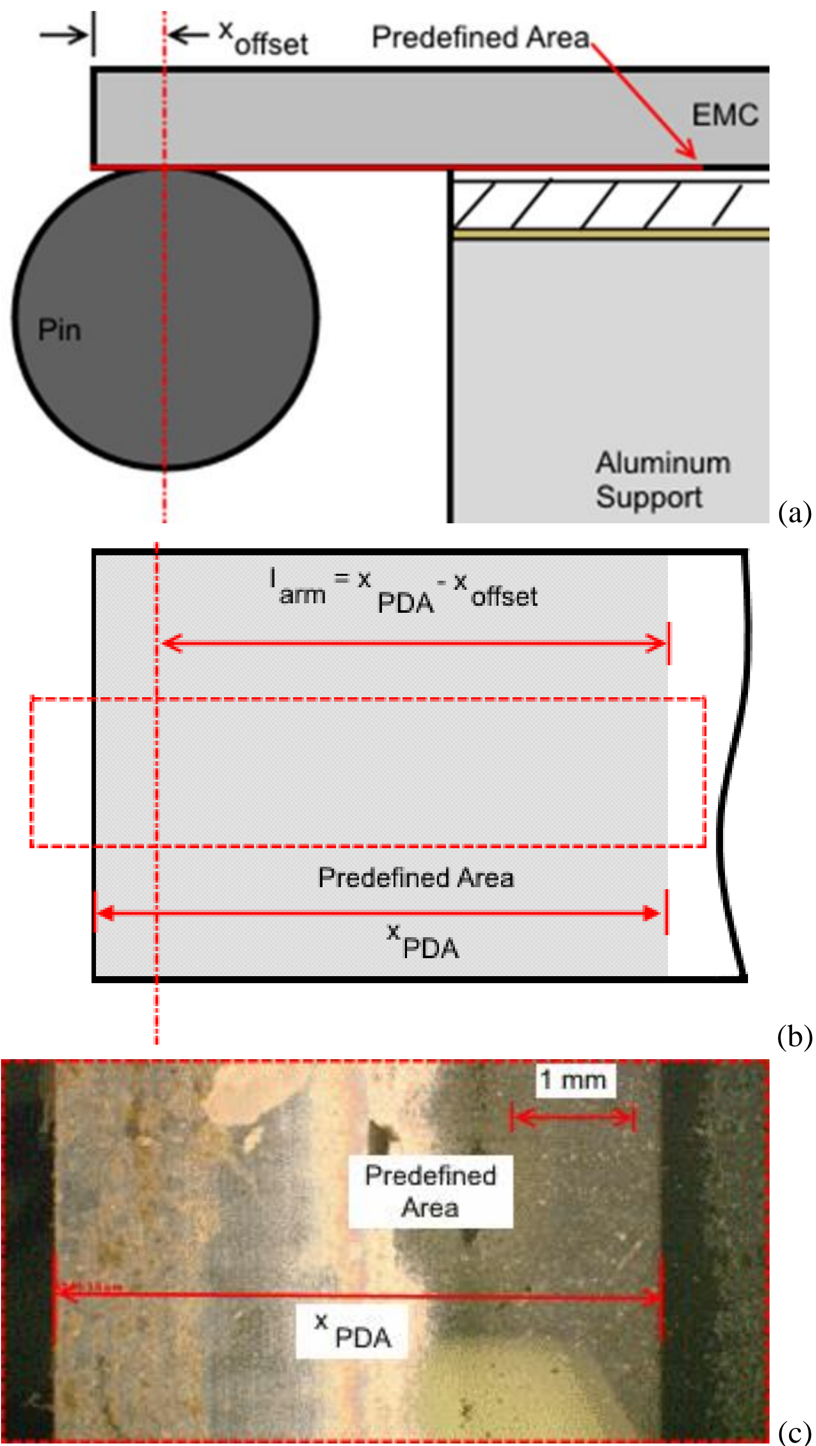

Figure 41. Determining the moment arm in a SCAT test a) cross-sectional schematic used to determine the offset distance, b) schematic of delaminated EMC side of specimen, and c) inset from b) highlighting a delaminated specimen used to verify the extent of the predefined area.

This method is shown schematically in Figure 41b. The distance from the edge of the specimen to the end of the predefined area is recorded and from these two measurements the moment arm of the specimen can be specified. Figure 41c shows how the predefined area is determined from the delaminated EMC surface. Using the critical load and moment arm, the numerical model is used to evaluate G_{crit} and Ψ.

4.5.2. Evaluation of Adhesion Strength

Specimens from both EMC/PSR1 and EMC/PSR2 sample sets were tested until a critical load was reached, resulting in a significant load drop and delamination along the interface. Each specimen was reloaded several times, resulting in several distinct load drops corresponding to increased delaminated area. Figure 42 shows a load vs. normalized displacement curve for each material set where the relationship is based off of simple cantilever beam displacement:

$$P = E_{EMC}\left(\frac{wBh_{EMC}^{3}}{4l_{arm}^{3}}\right) \tag{26}$$

where E_{EMC} represents the modulus of the EMC layer. Since the loading is dominated by the EMC layer, this figure can be used to verify the modulus of the EMC and quickly identify any potential testing outliers due to bad sample preparation or testing alignment.

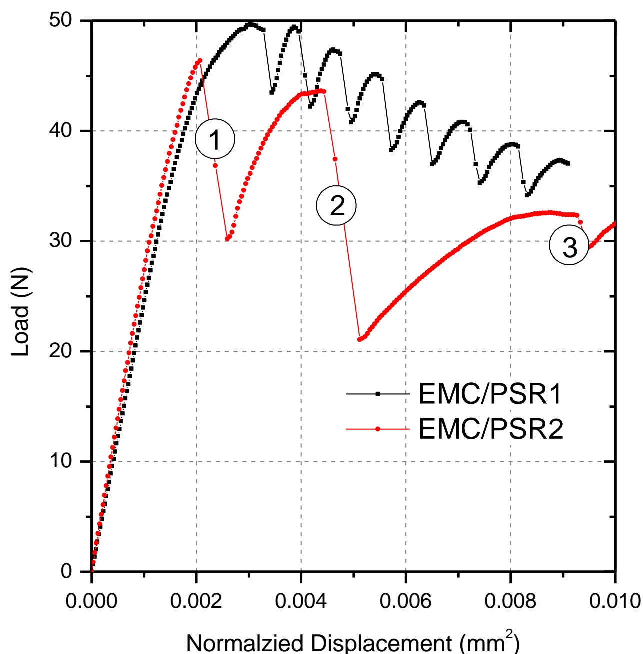

Figure 42. Comparison of load vs. normalized displacement curves for both EMC/PSR material.

As seen in Figure 43, by examining the EMC surface of a tested specimen, clear delamination can be seen at the onset of crack propagation corresponding to each peak load during testing. Of note is how the delamination patterns varied between material sets with the EMC/PSR2 set showing much larger load drops following delamination. The PSR1 specimens showed very small incremental delamination corresponding to each load drop. After testing the EMC layer was yanked off to create the distinct change in pattern after the test. Since the only difference between sample sets is the PSR material used, this behavior can be attributed to differences in the PSR materials.

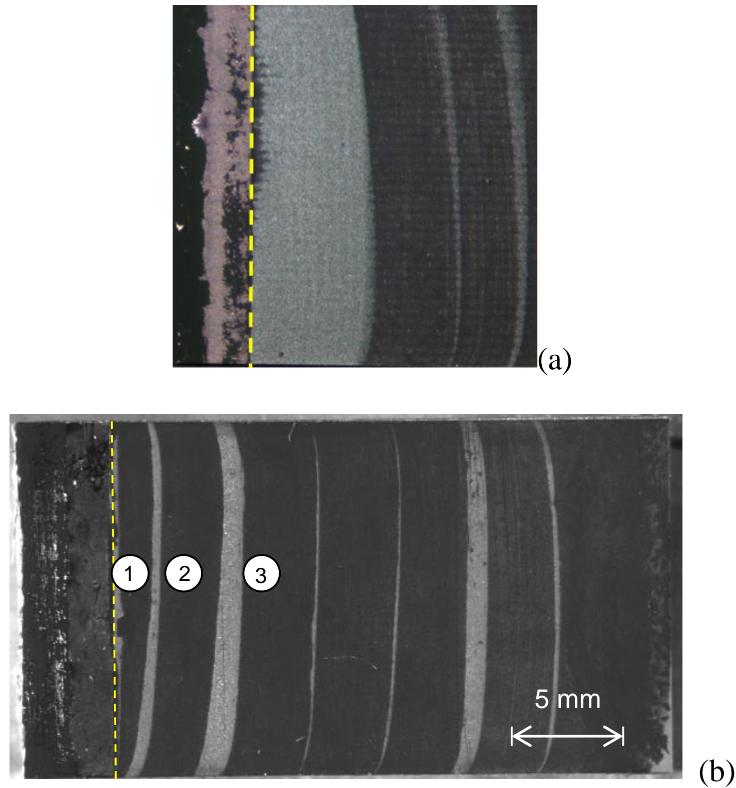

Figure 43. Delaminated surfaces from SCAT tested specimens with crack propagation corresponding to load drops during testing for the a) EMC/PSR1 and b) EMC/PSR2 material sets.

Testing for the EMC/PSR1 material set was repeated over six specimens. The average critical load and moment arm from the testing was 50.5 N and 7.5 mm, respectively. Each sample was then evaluated using the 2D plane strain numerical model to determine the energy release rate and mode mixity. The average G_{crit} was 147 J/m^2 and the average Ψ = 29.2°. The variation in the sample was only +/- 3% showing very good repeatability for an adhesion strength test.

Six specimens were tested from the EMC/PSR2 material set with an average critical load and moment arm of 48.2 N and 6.9 mm, respectively. The average G_{crit} was 115 J/m^2 and the average mode mixity was 29.0°. The variation in the PSR2 set was noticeably

larger at <12% variation. This can be attributed to the difference in crack growth on the delaminated surfaces. The delamination in the PSR2 set was larger and less stable than the PSR1 set. Additionally for comparison purposes between the two sets, the PSR1 set has a definitively stronger energy release rate than the PSR2 set. A comparison of the energy release rate of each set can be seen in Figure 44 and a breakdown of the mode I and mode II components of the energy release rate are recorded in Table 3 and Table 4 for each material set.

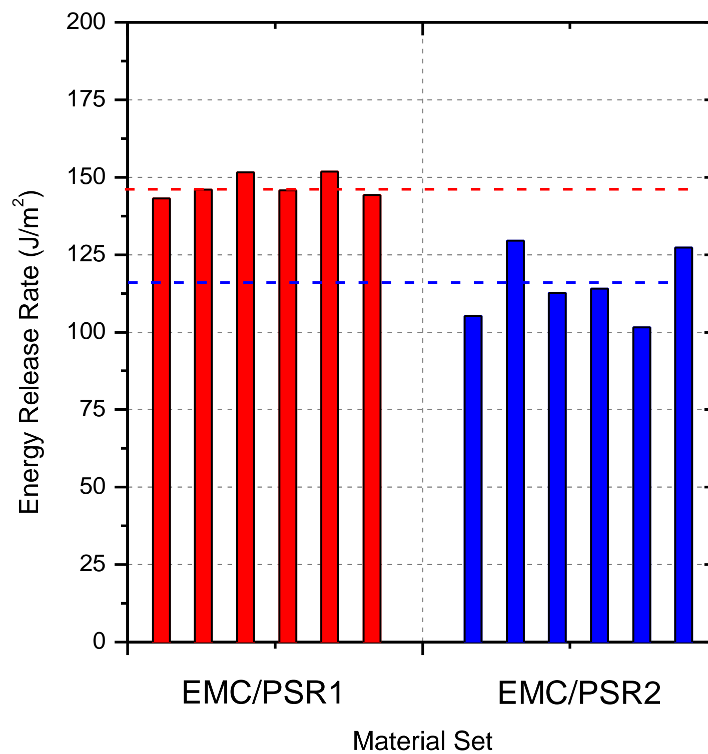

Figure 44. Comparison of adhesion strength results for both EMC/PSR material sets.

Table 3. Energy release rate results for EMC/PSR1 material set.

Set 1	G (J/m^2)	G_I (J/m^2)	G_{II} (J/m^2)	Mode Mixity (°)
1	143	109	34	29.2
2	146	111	35	29.2
3	152	115	36	29.3
4	146	111	35	29.2
5	152	116	36	29.2
6	144	110	34	29.2

Table 4. Energy release rate results for EMC/PSR2 material set.

Set 2	G (J/m^2)	G_I (J/m^2)	G_{II} (J/m^2)	Mode Mixity (°)
1	105	81	25	29
2	130	99	31	29.1
3	113	86	27	29
4	114	87	27	28.9
5	102	81	20	26.7
6	127	98	30	28.9

4.6. Discussions

4.6.1. Validity of LEFM

In order to employ numerical approaches to assess the interfacial energy release rate, namely the J-integral and VCCT methods, it is critical to assure that the linear elastic fracture mechanics assumption is not violated. For LEFM to be maintained any plasticity

near the crack tip must be limited to a very small area around the crack tip [1]. To verify that this is the case during SCAT testing a moiré interferometry approach was employed.

Moiré interferometry allows for the in-plane displacement fields to be assessed during testing by first placing a moiré grating with a distinct pattern on the sample prior to testing [40]. Tuning this system prior to testing allows for the establishment of a null field of zero strain on the sample. After applying load to the sample the interferometer can be used to assess the in-plane displacement field that occurs after calibrating a null field.

To assess if the plasticity that occurs is confined to a near crack tip region, the SCAT specimen with the grating was tested until delamination occurred at the interface-of-interest and then unloaded. The specimen was then returned to the moiré interferometer and the u_x and u_y displacement fields were assessed. Figure 45 shows the residual deformation after delamination seen in the sample for both the u_x and u_y displacement fields. The fringe lines in the delaminated portion of the EMC cantilever beam mean that there is some rigid body rotation of the cantilever beam. This is an indication of some plastic deformation at the crack tip that is preventing the beam from returning to its original position.

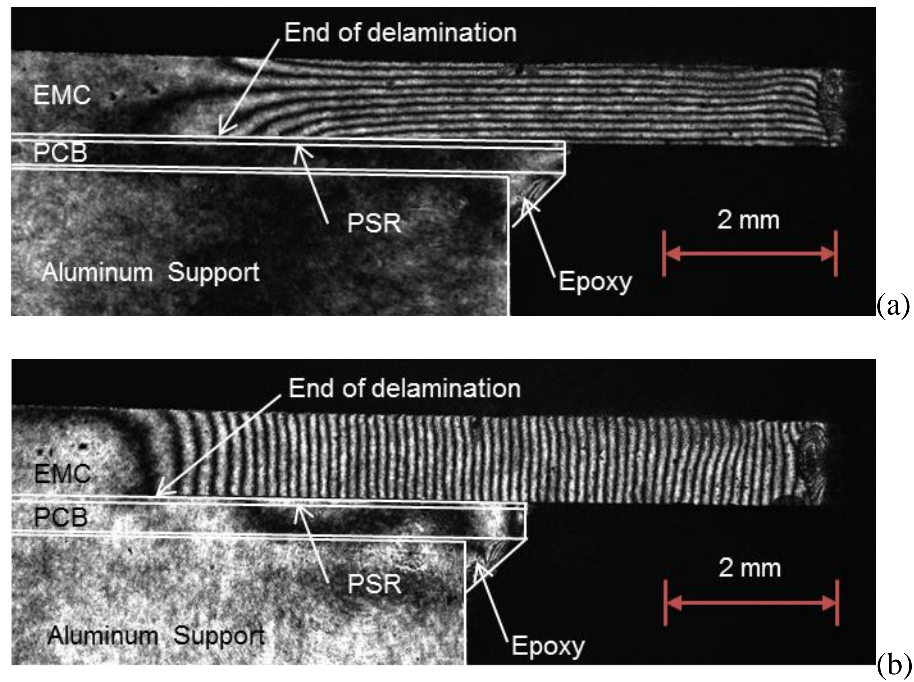

Figure 45. Moiré fringe patterns on EMC/PSR specimen after delamination along interface for a) u_x displacement field and b) u_y displacement field.

Examining the moiré field near the crack tip in Figure 46 it is apparent that there is a small plastic wake that does occur in the area where the interface has already delaminated. The development of this plastic wake prevents the cantilever arm from returning to its initial position. This is why rigid body rotation of the cantilever arm is seen in Figure 45.

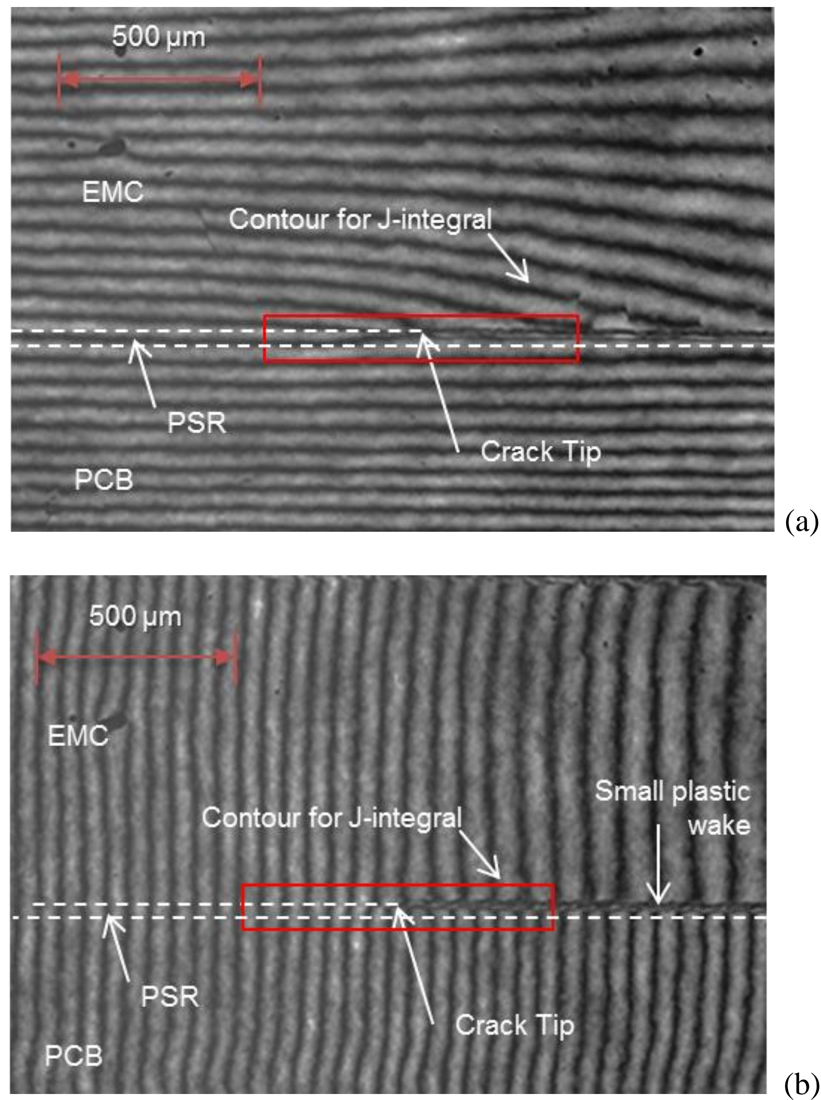

Figure 46. Near crack tip moiré images before and after applying load for a EMC/PSR SCAT specimen for a) u_x displacement field and b) u_y displacement field.

However, for assessing the energy release rate, the concern is that the extent of the plastic deformation near the crack tip is small enough so as to use linear elastic fracture mechanics concepts. The J-integral method is calculated using a contour away from the crack tip. As long as the selected contour is not within the near crack tip plasticity region then the J-integral can be used to represent the energy release rate of the interface. In

Figure 46, carrier rotations were applied to the image to provide a better contrast near the interface. Deviations from the constant contour lines near the crack tip are an indication of plastic deformation. Using this micro moiré setup to examine the fringe patterns, very little plasticity near the crack tip is seen. Calculating the potential extent of the near field plasticity using the camera and digital software, the plastic region was found to be confined to 10 µm around the crack tip. Since the J-integral is evaluated at a contour that is roughly 50 µm away from the crack tip, it is safe to assume that LEFM is still valid and the numerical methods can be used to calculate G and Ψ for the SCAT method.

4.6.2. Uncertainty Analysis: Effect of Moment Arm on *G* in SCAT

The length of the moment arm is an important parameter in SCAT for determining the energy release rate and minimizing the mode mixity. When a shorter moment arm length is used in the specimen design, the natural of the global loading condition is altered to create a lower mode mixity condition at the crack tip. However, a shorter moment arm means that any uncertainty in the moment arm measurement will be amplified leading to increased uncertainty in the energy release rate measurement. Both factors should be considered when designing the moment arm of a specimen.

While the well-defined natural of the predefined area aides in reducing measurement uncertainty, some uncertainty will inevitably exist. This uncertainty stems from minimal pixel spacing in our imaging system and making two measurements for both the predefined area length and the offset length to the pin loading position. Depending on the engineer this uncertainty could vary from 50 µm to 500 µm. To analysis this effect an FEA model was run and the amount of uncertainty in G introduced from the moment arm

measurement was considered as a function of moment arm length. In this model the dimensions of the EMC/PSR specimen were used and a critical load was set for a typical energy release rate value of G =150 J/m^2 for the true moment arm length case. The model was then run at multiple moment arm lengths with several different uncertainty deviations.

Figure 47 shows the plot of the uncertainty in G vs. moment arm length for different uncertainty levels. It is clear from the graph that increasing the moment arm length will reduce the uncertainty in the G calculation. This finding is intuitive since the percent deviation in the total moment arm is less for a larger moment arm length. For the typical case reported in this dissertation, a moment arm of 7.5 mm was used with an uncertainty in the moment arm measurement of 100 μm, resulting in a G uncertainty of +/- 2.5%.

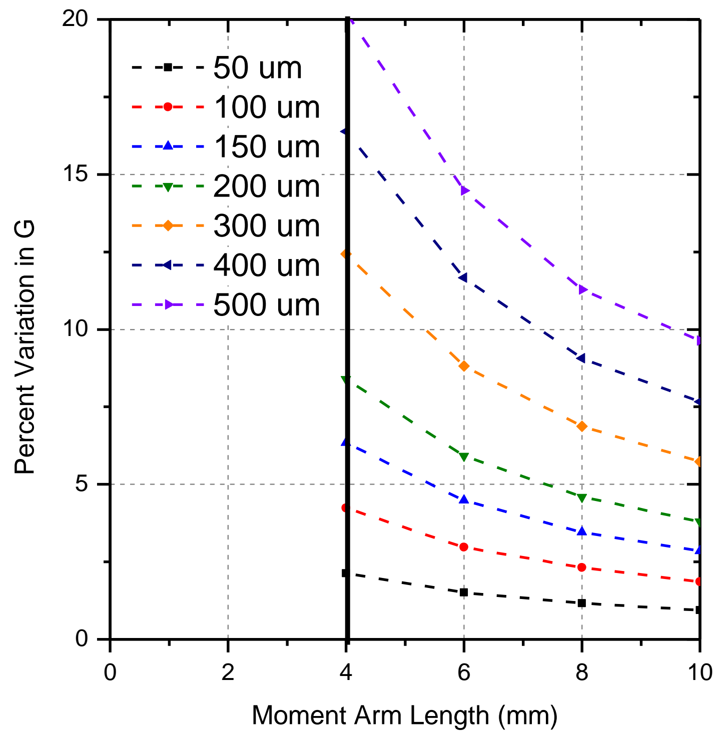

Figure 47. Uncertainty in G as a function of moment arm for several levels of moment arm length uncertainty in the EMC/PSR SCAT configuration.

The effect of the moment arm uncertainty can be further shown in Figure 48 where the percent uncertainty in the energy release rate is plotted against the moment arm length normalized by the deviation in the moment arm length. Independent of the initial moment arm length, the percent uncertainty in *G* follows the same relationship where the uncertainty becomes significantly larger as the deviation in the moment arm measurement becomes a greater percentage of the actual moment arm length.

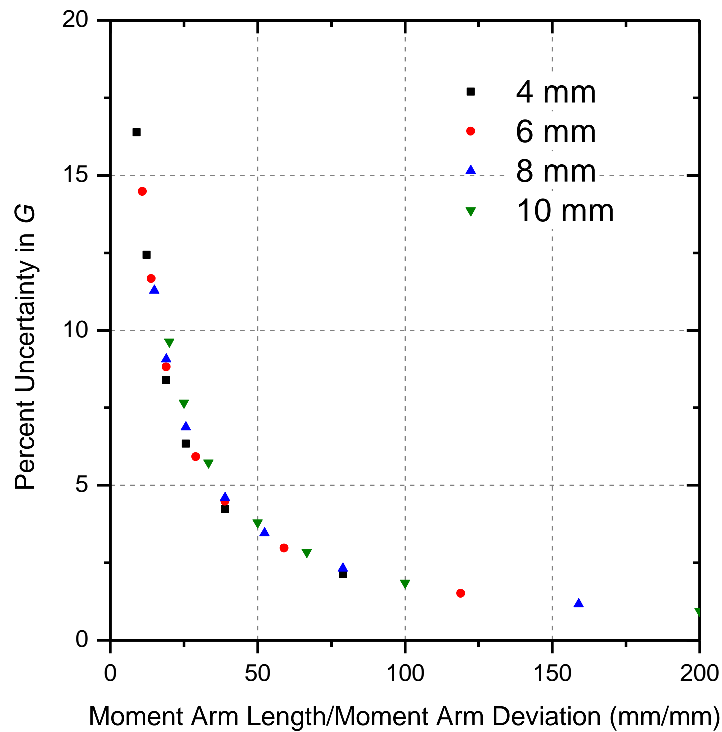

Figure 48. Uncertainty in G vs. normalized moment arm length per moment arm deviation.

When comparing PSR1 and PSR2 values, it is of interest to note that the typical moment arm value used in the PSR2 case was 0.6 mm shorter on average. Using Figure 47 it is clear that the expected uncertainty in *G* is larger for the PSR2 case. The

consequence of this larger deviation partly contributes to the larger energy release rate variation in the PSR2 material set.

4.7. Conclusion

The SCAT method was proposed and implemented for two separate material sets to assess which PSR provides the greater adhesion strength to a given EMC. The method allows for quick and quantitative adhesion strength evaluation of the EMC/PSR interface while maintaining a high level of repeatability. Detailed sample preparation, experimental testing, and numerical processing steps were shown. For baseline as-is testing excellent repeatability was obtained with less than 3% variation in energy release rate results due to the well-defined precrack and testing method. Furthermore the small testing scatter allowed for the test method to clearly distinguished that one material set had larger adhesion strength than the other.

This simple configuration allows for quick and quantitative testing of the interface with great repeatability. Additionally as compared to 4PB configuration, relatively small mode mixity configurations can be achieved, allowing for testing of interfaces with strong adhesion strength and/or weak fracture toughness of their adherends while still maintaining enhanced repeatability.

Part II Adhesion Strength Testing of Flexible Membranes on Rigid Substrates

Chapter 5: Background and Literature Review of Adhesion Strength Testing Methods of Flexible Membranes on Rigid Substrates

5.1. Background

For the flexible membrane on rigid substrate interface there are several adhesion strength tests available. There are several variations of the peel test [1], blister test [64-95], and constrained blister test [96-98] which are specifically developed for thin films. By examining the advantages and disadvantages of each conventional technique, it is possible to find areas to extend existing test methods that will allow for more accurate, quantitative evaluation of a wider range of polymer film/rigid substrate interfaces with increasingly high adhesion strength.

5.2. Literature review of adhesion testing in flexible membranes on rigid substrates systems

5.2.1. Peel test

A commonly used adhesion test for flexible adhesives is the peel test [1]. The experimental procedure to conduct this test is very simple and straightforward. A flexible membrane on a rigid membrane is placed on an electro-mechanical test stand. The membrane layer is connected to the crosshead of the test stand. The crosshead displacement increases monotonically until the membrane is peeled off of the substrate.

By determining the average pull force (*F)* along the debond length, the adhesion strength can be quantified. A schematic of the 180° peel test can be seen in Figure 49. This is just one configuration of the peel test. Engineers in industry prefer the simplicity of this test method. It allows for a quick comparison of different interfaces. Although testing adhesives in this matter is simple to do, the analysis is quite difficult due to the complex stress states that arise when the adhesive undergoes this configuration. A full description of the nonlinear material properties of the film is required. In addition, the test is very sensitive to parameters such as peel angle, width, and thickness of the adhesive. Finally, the peel test does not provide any insight on the adhesive's mechanical properties. Rather, it only indicates its resistance to peeling forces [99, 100]. Nevertheless, due to its straightforward testing it receives wide use for qualitative evaluation of different material sets.

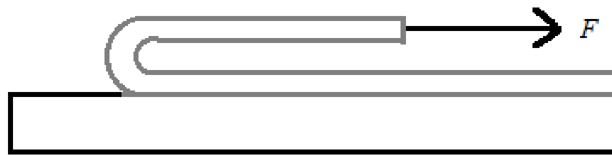

Figure 49. Schematic of the 180° peel test.

5.2.2. Blister test

The blister test was developed as an adhesion testing methods ideal for thin flexible membranes on rigid substrates [64-95]. Thin-film layers are very common in electronic packaging applications ranging in application from die attach films to conformal coating

layers for tin whisker mitigation. A known thickness of a polymer in question is adhered to the top side of a rigid substrate above a small pressure hole (Figure 50). An increasing pressure load is applied to the underside of the polymer via the pressure hole, thus eventually creating a circular debond (blister) which grows in size. The height of the blister is recorded, providing a pressure and height relationship. Analysis of this relationship in conjunction with the debond radius can allow one to gain insight into the energy release rate of a material. The disadvantages to this approach include difficulty in dynamically measuring the debond radius and inaccuracies when the blister height exceeds a value known as the spherical limit. In addition, this approach assumes a constant Young's modulus for all loading conditions which may not be accurate when considering the rate-dependent modulus of many polymers.

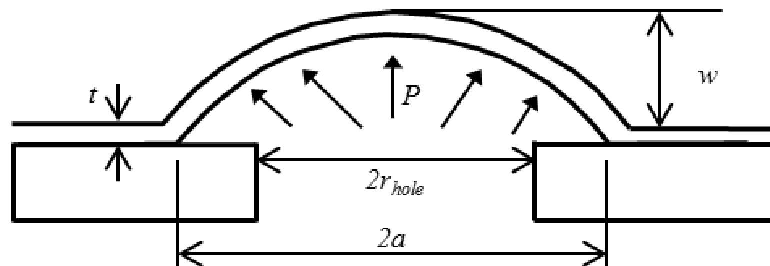

Figure 50. Schematic of a traditional blister test.

5.2.3. Constrained blister test (CBT)

The constrained blister test (CBT) differs from the traditional blister test by restricting the deflection of the blister with a rigid plate [96-98]. The test is performed similar to the blister test where pressure is applied through the pressure port in the bottom

of the film. As the pressure is increased monotonically, the blister begins to inflate and makes contact with the rigid plate. As the blister begins to delaminate, contact increases with the top plate. A schematic of the test can be seen in Figure 51. From the critical pressure and the fixed height between the plate and film layer, h_c, the energy release rate can be determined from testing [97]:

$$G = P_c h_c q \tag{27}$$

A correction factor, q, is then used to account for the amount of contact the blister has with the top surface at delamination:

$$q = \left(1 - \frac{d}{2a}\right) + \left(\frac{d}{3a} - \frac{1}{2}\right)\frac{\partial d}{\partial a} \tag{28}$$

The correction factor makes assumptions about the volume of the blister and that the film forms a straight line connection between the rigid plate and the end of the debond area. Additionally, because the plate is rigid, the method assumes no energy is stored in the rigid plate when determining the energy release rate.

One advantage of this test method is that time-dependent adhesion strength can be assessed for a constant pressure [97]. This type of testing is good for investigating sub-critical debonding. This is investigated by fixing the pressure and characterizing the rate of delamination with time. However there are disadvantages to the test method on a couple of points. Uncertainty is added to the solution due to the correction factors used to calculate the energy release rate. Additionally, when testing very high adhesion strength interfaces the rigid constraint may not be applicable due to a bulging out effect of the film when pressurized. As pressure increases in this situation, assumptions over the shape of the blister would no longer be valid.

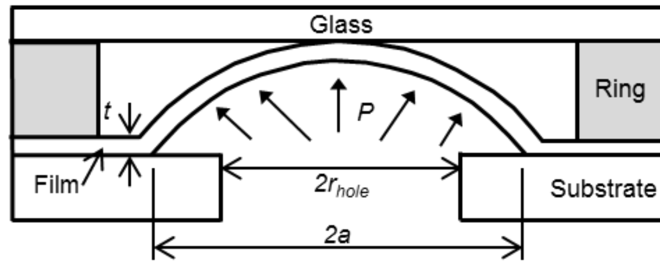

Figure 51. Schematic of a constrained blister test.

Chapter 6: Adhesion and Puncture Strength of Polyurethane Coating Used to Mitigate Tin Whisker Growth[2]

Abstract

Reliability of conformal coatings used to mitigate tin whisker growth depends on their ability to contain tin whiskers. Two key material properties required to assess the reliability of a polyurethane coating are documented experimentally: adhesion strength and puncture strength. A modified blister test using a predefined blister area is employed to assess the adhesion strength and a puncture test is employed to evaluate the puncture strength of the coating. After measuring the properties at time zero, the coatings are subjected to accelerated testing conditions (high temperature/humidity storage and temperature cycling) and the degradations of the coating properties are documented.

6.1. Introduction

The ongoing movement to replace lead (Pb) from electronics has made pure tin plating a major choice for lead-free components. The issue with the pure tin plating is the single crystal metal hair-like growth from the tin surface, called the tin whisker [101, 102]. Tin whiskers can be straight or kinked with diameters on the order of 1 to 5 μm [102].

---

[2] This chapter was published in the *Journal of Electronic Packaging* under the title of "Adhesion and Puncture Strength of Polyurethane Coating Used to Mitigate Tin Whisker Growth" by K. Mahan, Y. Sun, B. Han, S. Han, and M. Osterman

They are electrically conductive and can bridge adjacent interconnect, causing circuit shortage, or they can be dislodged and obstruct or interconnect with other components. Tin whiskers are regarded as a major safety, reliability, and potential liability threat to high reliability electronics and associated hardware. The extensive review [103] of the tin whisker bibliography and mitigation practice provides good knowledge of tin whisker.

Several options are currently available to mitigate tin whisker growth [104]. One commonly implemented mitigation option is to apply a conformal coating over a tin coated area [105, 106]. A conformal coating is a polymeric layer that can contain the whisker and prevent it from bridging adjacent interconnects. Even though conformal coatings cannot prevent tin whisker formation, it can reduce the rate of growth and contain the tin whisker with the electrically insulated coating [107]. The ability of different conformal coatings to suppress tin whisker formation and growth has been examined under long-term accelerated test conditions [108, 109]. The study shows that whiskers can still penetrate the conformal coating at thin coated areas. Two key material properties required to assess the ability of a polyurethane coating to contain tin whiskers are adhesion strength and puncture strength. The adhesion strength assesses the resistance to delamination between the coating and tin surface when a whisker begins to nucleate, while the puncture strength characterizes the coatings resistance to puncture of the whisker. Together the adhesion strength and puncture strength can be used to characterize the reliability of the coating.

In this paper, the adhesion strength and puncture strength of a conformal coating are determined experimentally. A polyurethane coating is selected for testing since it has been proven to mitigate tin whisker growth effectively [105, 108, 109]. A modified blister test using a predefined blister area larger than the pressure application hole is employed to

assess the adhesion strength. A puncture test is employed to evaluate the puncture strength of the coating. The properties were determined after initial curing and then again after the samples are subjected to accelerated testing conditions (high temperature/ humidity storage and temperature cycling) to investigate the effect of the conditions on the degradation of the coating.

6.2. Test Method

The two test methods, namely a modified blister test and a puncture test, are described briefly with their governing equations that relate experimentally measured quantities to adhesion strength and puncture strength.

6.2.1. Adhesion Strength Test: Modified Blister Test

Analytical solutions for the blister test configuration have been discussed in many different ways [65, 110-113]. Let us consider a thin membrane adhered to a rigid substrate with a central hole for pressure application and a larger predefined area of low adhesion (Figure 52). When pressure is applied, the thin membrane is assumed to take on a spherical blister form when the deflection of the blister is much smaller than the opening radius. From the geometrical considerations in Figure 52, the strain can be expressed as [114]:

$$\varepsilon = \frac{2w^2}{3a^2} \tag{29}$$

where w is the blister height and a is the opening radius. Considering the force equilibrium, the normal stress of the thin membrane can be expressed as [114]:

$$\sigma = \frac{Pa^2}{4wt} \tag{30}$$

where P is the applied pressure and t is the thickness of the membrane. As testing continues, the pressure is monotonically increased until a critical pressure, P_{crit}, is reached and the thin membrane delaminates from the surface. From the experimentally measured critical pressure, the adhesion strength is determined analytically.

The polyurethane conformal coating tested in this study has high adhesion strength, and usually deforms plastically during blister growth. If the conventional elastic blister model is used, the energy dissipated by plastic deformation will lead to an overestimation of the adhesion strength. To cope with this behavior, the well-known work-hardening power law relationship is employed as the elastic-plastic constitutive equation.

The power law relationship can be expressed as:

$$\varepsilon = \frac{\sigma_0}{E}\left(\frac{\sigma}{\sigma_0}\right)^{1/n} \qquad \begin{array}{l} n = 1 \text{ for } \sigma < \sigma_0 \\ n = n_0 \text{ for } \sigma \geq \sigma_0 \end{array} \tag{31}$$

where σ_0 is the yield stress, n is the power-hardening exponent, and E is Young's modulus.

Substituting Eqs. (29) and (30) into (31), the blister height as a function of the pressure and opening radius can be expressed as:

$$w = C_1^{\frac{-1}{2n+1}} P^{\frac{1}{2n+1}} a^{\frac{2n+2}{2n+1}} \quad \text{where } C_1 = \frac{2^{n+2} E^n t \sigma_0^{1-n}}{3^n} \text{ and } \begin{array}{l} n = 1 \text{ for } \sigma < \sigma_0 \\ n = n_0 \text{ for } \sigma \geq \sigma_0 \end{array} \tag{32}$$

Using the notations shown in Figure 52, the blister volume can be expressed as:

$$V = C_2 \pi a^2 w \tag{33}$$

where C_2 is a numerical constant to accommodate the volume difference of the spherical cap due to the clamped end condition of the blister; $C_2 = 0.518$ for a typical Poisson's ratio of polymers has been reported in the literature [64, 110, 111].

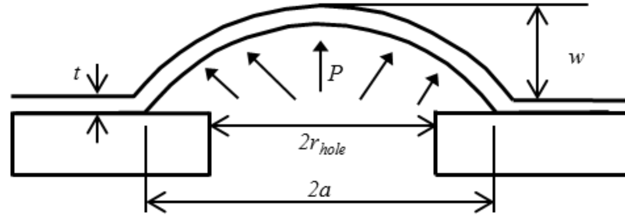

Figure 52. Schematic illustration of a modified blister test specimen.

The energy release rate, G, is a measure of the energy available for an increment of crack extension, and is an indication of the adhesion strength [1]. Following the procedures established in Refs. [64, 110, 111, 115], the energy release rate during delamination can be expressed by:

$$G = \frac{3n+2}{n+1}\frac{PV}{2\pi a^2} \quad \text{where} \quad \begin{matrix} n = 1 \text{ for } \sigma < \sigma_0 \\ n = n_0 \text{ for } \sigma \geq \sigma_0 \end{matrix} \tag{34}$$

Using Eqs. (33) and (32), the energy release rate can be expressed in terms of the experimental parameters (pressure, opening radius, and material properties) as [115]:

$$G = \frac{3n+2}{2n+2} C_1^{-\frac{1}{2n+1}} C_2 \left(Pa\right)^{\frac{2n+2}{2n+1}} \quad \begin{matrix} n = 1 \text{ for } \sigma < \sigma_0 \\ n = n_0 \text{ for } \sigma \geq \sigma_0 \end{matrix} \tag{35}$$

6.2.2. Puncture Strength Test

In general, the puncture strength of a coating depends on the force required for a tin whisker to puncture the coating, and the contact area between the two surfaces. The

puncture strength of polymer films can be determined experimentally by measuring the force required for a probe to puncture the coating normalized by the probe perimeter [116]:

$$T_p = F_P / P_P \tag{36}$$

where T_P is the puncture strength, F_P is the puncture force, and P_P is the probe perimeter. When testing with a flat probe tip [116]:

$$T_p = F_P / 2\pi r \tag{37}$$

where r is the probe radius. The above definition results in units of N/m. When testing with flat probe tips, the puncture strength is linearly proportional to the probe diameter [116].

6.3. Experimental Procedure

6.3.1. Modified Blister Test

From Eq. (35), it is obvious that the opening radius is critical to accurate determination of the adhesion strength. In conventional blister testing, the hole in the substrate used for pressure application is defined as the opening radius (r_{hole} in Figure 52). After curing the conformal coating on the substrate, any excess adhesive between the walls of the pressure hole will directly affect the adhesive strength of the specimen. To address this issue, an opening radius larger than the pressure application hole is created with a low adhesion release agent before the test (a in Figure 52). A procedure developed to produce an accurate opening radius while accommodating the highly "acidic" environment of tin electroplating is presented below.

Figure 53 shows a simplified schematic view of the rigid copper substrate with a 4 mm diameter pressure application hole which will act as a base for tin plating, and the rigid copper plug mold used to form the epoxy plugs. Before the tin plating process can begin, the four pressure application holes in the rigid copper substrate must be temporarily filled with an epoxy material as seen in Figure 54. The purpose of creating a temporary epoxy plug is twofold: (1) prevent tin from being plated on the inner perimeter of the pressure hole and (2) create a level surface for applying the release agent and conformal coating layers. The plug mold defines the shape of the temporary epoxy plug, allowing for easy epoxy injection and removal of the plug after curing the conformal coating layer.

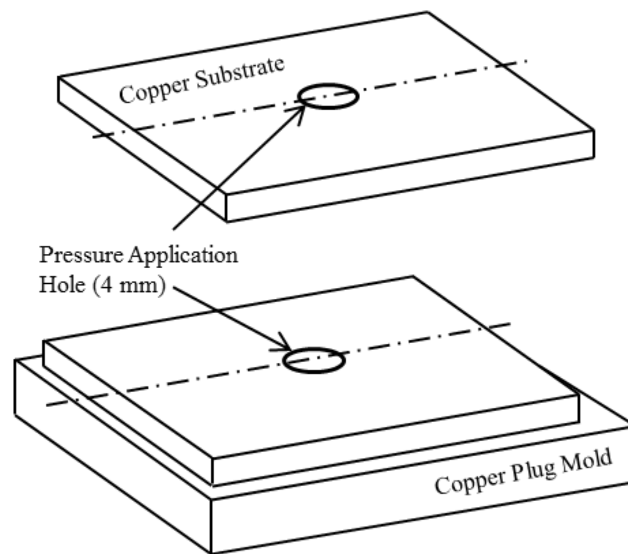

Figure 53. 3D view of (a) copper substrate and (b) copper plug mold.

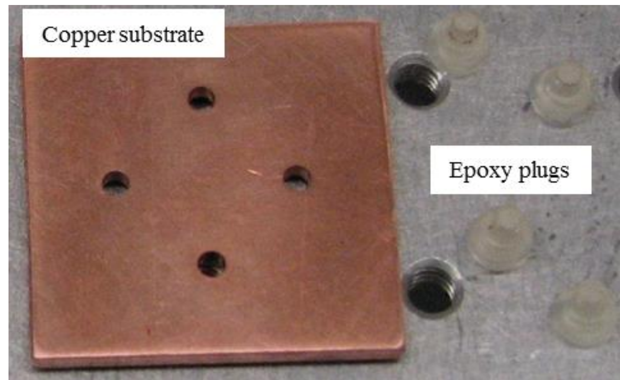

Figure 54. Copper substrate with epoxy plugs.

To facilitate easy separation of the plug, a release agent (20-8185-002 Release Agent: Buehler) is applied on the surfaces of the holes. Next the substrate is placed with the side to be tin plated face down and the plug mold aligned on top of the substrate. A two-part epoxy (EpoKwick Resin/Hardener: Buehler) is mixed in a 5:1 ratio and injected into the hole and allowed to cure at room temperature for 24 hours. After curing, the surface is grinded and polished to remove excess epoxy and to prepare the surface for tin plating.

A tin plating bath solution is employed with tin attached to the anode end of a power supply and the sample to be plated attached to the cathode side. When voltage is applied, the metal is oxidized at the anode to form metal ions, and transferred through electrolyte to a negatively-charged cathode to be reduced on its surface. After the process the copper substrate has a thin layer of tin on its surface as illustrated in Figure 55a. Figure 55 depicts the cross-sectional view of the sample preparation process for one test hole in Figure 53.

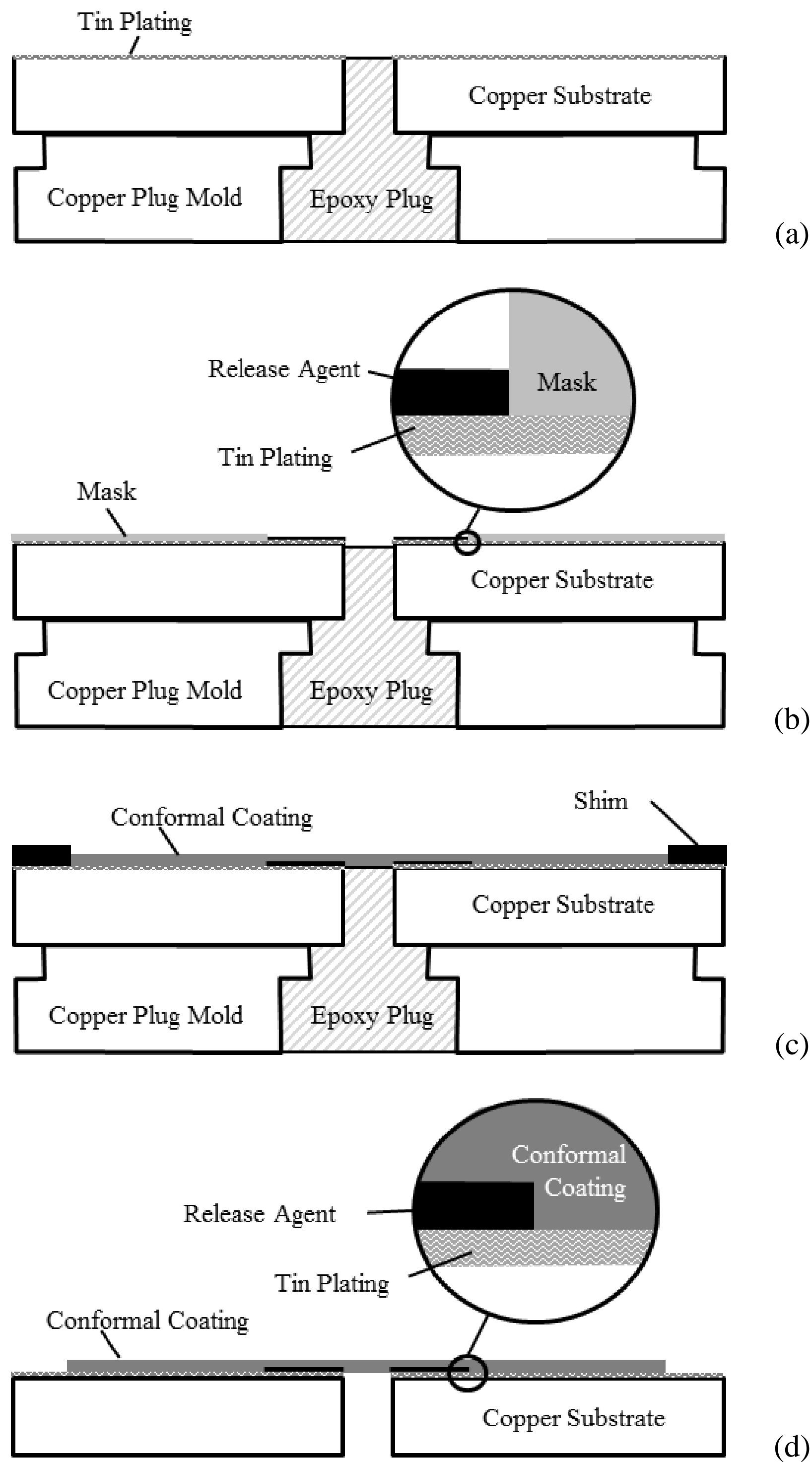

Figure 55. Schematic cross sectional view of sample preparation process: a) tin plated substrate and plug mold; b) temporary mask and release agent application; c) temporary shim for conformal coating curing; and d) final blister test specimen.

The release agent and coating application process is also depicted in Figure 55. After the plating process is completed, a circular mask is placed concentrically around the pressure application hole (Figure 55b). Next a small layer of release agent is placed inside the mask and allowed to dry. The addition of the release agent layer significantly reduces the adhesive strength around the pressure application hole. Before testing, a small preload pressure is first applied to debond the release agent area at a very low pressure. This creates a well-defined, accurate opening radius at the perimeter of the release agent area.

Upon removal of the mask, a shim is placed around the top of the substrate, and a thin layer of the conformal coating is applied and allowed to cure at room temperature for 24 hours (Figure 55c). Finally the plug mold is removed to clear the pressure port for testing leaving the final blister test specimen (Figure 55d).

6.3.1.1 Experimental Setup and Test Procedure

A schematic diagram and actual test setup employed for the adhesion strength test are seen in Figure 56 and Figure 57, respectively. A conformal coating thickness of $50\ \mu\text{m}$ and a crack opening radius of $a = 3.2$ mm are used for the test. The blister test specimen is aligned over a pressure port. A pressure regulator (ER3000: Tescom) applies pressure at 0.1 psi/sec and records the pressure to an accuracy of 0.1 psi. A laser triangulation sensor (LTC-050-10-SA: MTI instrument) simultaneously records the blister height within 2 μm. As the pressure increases monotonically, the blister continues to grow until a critical pressure is reached and the film delaminates from the tin-plated surface. The critical height and pressure can be determined from the pressure vs. blister height results.

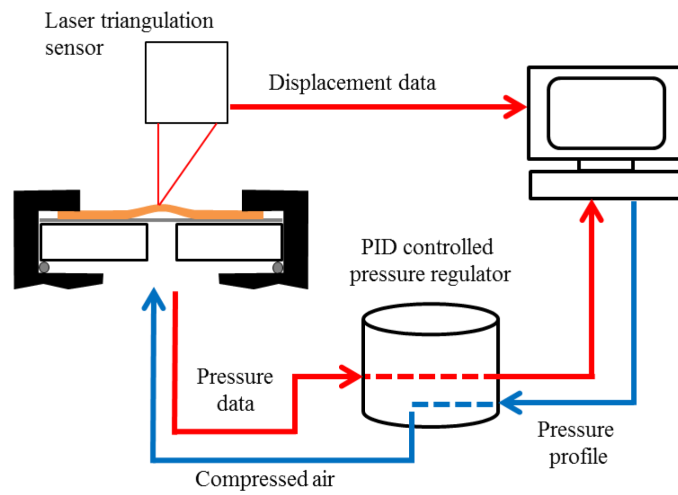

Figure 56. Schematic diagram of the blister test setup.

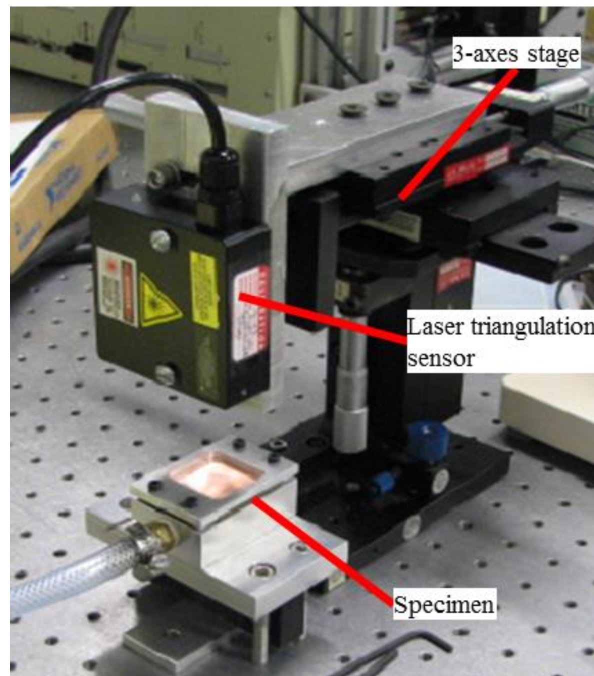

Figure 57. Blister test setup.

6.3.2. Puncture Test

For puncture testing, a thin film conformal coating specimen is required. A non-stick, Teflon substrate was placed on a level surface, and a shim of a desired film height placed on top. Next a spray conformal coating was transferred to a test tube, and then poured slowly onto the Teflon substrate. Any excess coating above the shim was removed to create a level film thickness. Extra care was also given to removing any excess bubbles that formed on top of the coating. The coating was then allowed to cure, diced into test specimens, and removed from the Teflon substrate.

6.3.2.1 Experimental Setup and Test Procedure

A schematic diagram and actual test setup employed for the puncture test setup is depicted in Figure 58 and Figure 59, respectively. The test probe is fitted to a 10 N load cell on the cross head of an Instron test stand. The load cell is accurate to +/-0.05 N. A conformal coating of 50 μm thickness is clamped between two aluminum plates with central test holes. The radius of this hole does not affect the puncture strength. An x-y stage aligns the probe in the center of the test hole before testing.

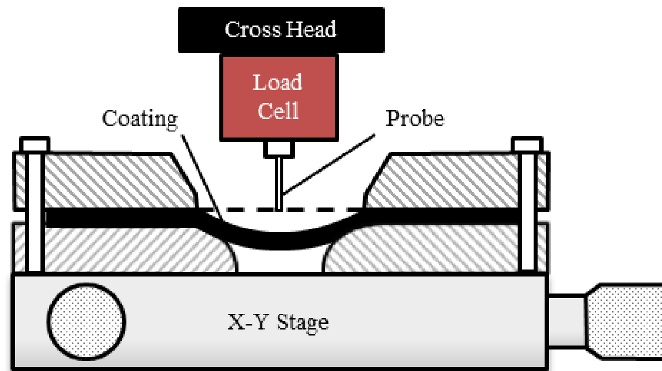

Figure 58. Schematic diagram of the puncture test setup.

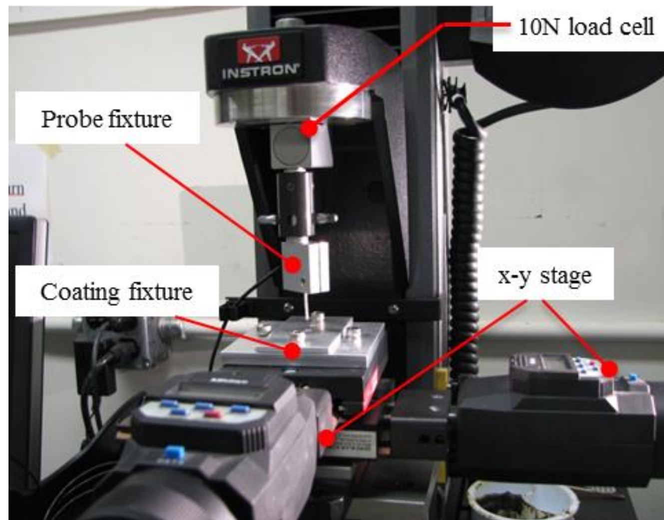

Figure 59. Puncture test setup.

After alignment, the probe is extended at a rate of 0.5 mm/min into the coating. The probe extends into the coating until a critical puncture force is reached and the probe punctures the coating. The load and displacement data are measured simultaneously.

Test probes with three different radii are used for testing: 50 μm, 65 μm and 80 μm. Probes with flat tips are employed to ensure repeatability of the experimental results.

6.4. Experimental Results

The two properties of the polyurethane conformal coating are characterized at room temperature first, and then after subjecting the coatings to two accelerated testing environments: high temperature and humidity (T/H) storage and temperature cycling (T/C).

6.4.1. Adhesion Strength

Two representative blister height vs. pressure tests for the polyurethane coating prior to aging are shown in Figure 60. The critical pressure is determined from the discontinuity of the blister height vs. pressure graph. The critical pressure for the sample shown in Figure 60 is 25 and 27 psi, respectively.

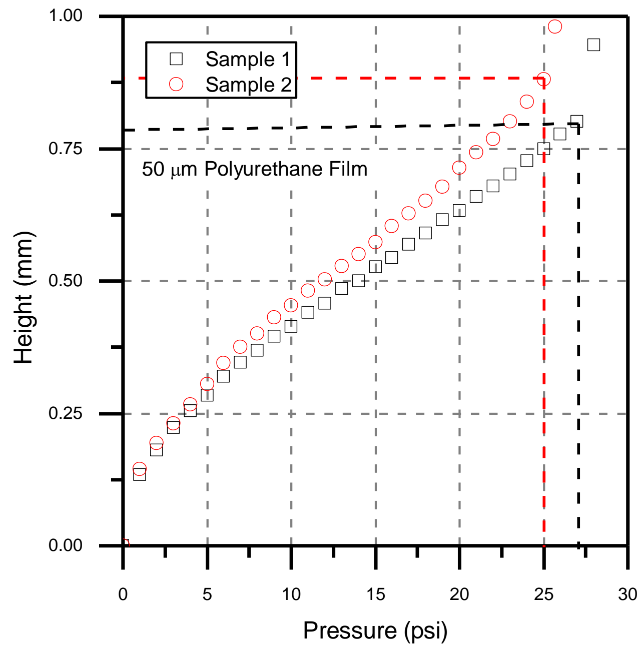

Figure 60. Typical pressure vs. blister height results for the blister test of a polyurethane conformal coating before aging.

An advantage of the blister testing formation is that the initial portion of the elasto-plastic properties of the coating. The unknown elasto-plastic properties are: the modulus, E, the hardening constant, n, and the yield strength, σ_y. To determine the elasto-plastic properties of the coating, a nonlinear regression analysis is performed to fit the

experimental data to the analytical height from Eqn. (32). Before the nonlinear regression analysis, the blister height vs. pressure results was smoothed using the well-known Savitzky-Golay method.

A two part process is then employed to extract the elasto-plastic properties. The modulus is determined first by using a nonlinear regression to fit the initial, elastic portion of the pressure vs. blister height curve. Setting $n=1$ in Eqn. (32) reduces the blister height analytical equation to the linear elastic relationship which is valid before the stress is greater than the yield stress.

Using the modulus from the elastic fit, a second nonlinear regression is performed over the entire elasto-plastic curve to determine the hardening constant and the yield strength of the coating. The results of the fit are shown in Figure 61. The resulting elasto-plastic properties are listed below:

$$E = 956\,MPa$$
$$n = 0.333$$
$$\sigma_y = 5.90\,MPa$$

With the elasto-plastic material properties, and the critical pressure from the experiment, the adhesion strength of the polyurethane/tin plating interface before aging is calculated by Eq. (35):

$$G = 94.9 \pm 11\ J/m^2$$

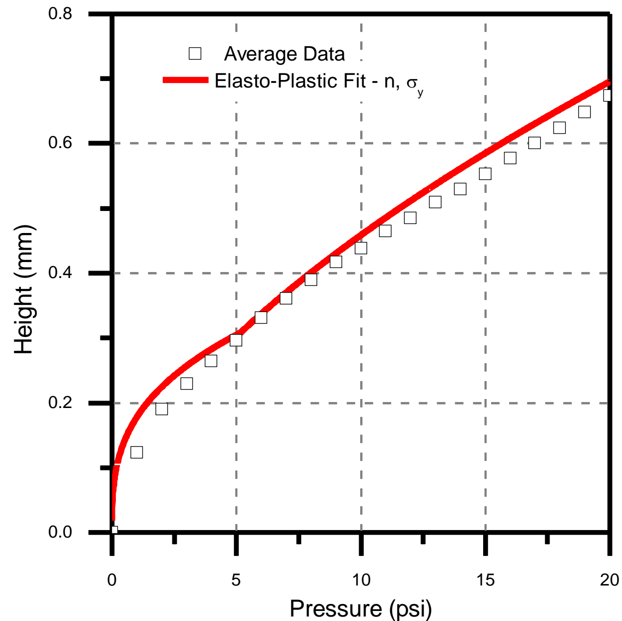

Figure 61. Nonlinear regression results of the elasto-plastic curve to determine the hardening constant and yield strength of the coating.

6.4.1.1 Accelerated Testing Results

The blister test samples were subjected to a suggested JEDEC T/H standard for tin whiskers [117] of 55°C/85% RH and tested after 0, 1000, and 2000 hours. Figure 62 shows how the average adhesion strength changes with time in T/H testing conditions. After 1000 hours of T/H conditions, the adhesion strength increased by 40%. It is speculated that the initial increase in adhesion strength is caused by additional crosslinking of the polymer coating. After another 1000 hours in the chamber, the coating did not degrade and the adhesion strength remains nearly constant.

Another set of blister test samples were subjected a temperature cycling condition. The suggested JEDEC T/C standard for tin whiskers is -55˚C to 85˚C. Due to the slow rate of degradation, a harsher test condition, -55˚C to 125˚C, was employed. Samples were

then tested after 0, 500, and 1000 cycles in the T/C testing chamber. Figure 63 shows how the average adhesion strength changes with T/C testing cycles. After 500 cycles, the adhesion strength increased 27%. Again, this may be attributed to additional crosslinking of the polymer coating. Over the next 500 cycles the adhesion strength degrades by 22%.

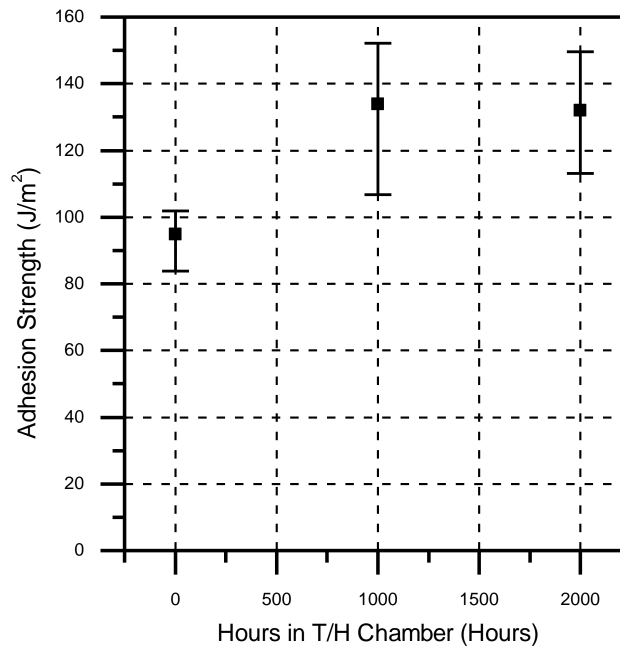

Figure 62. Adhesion strength versus hours in a T/H chamber.

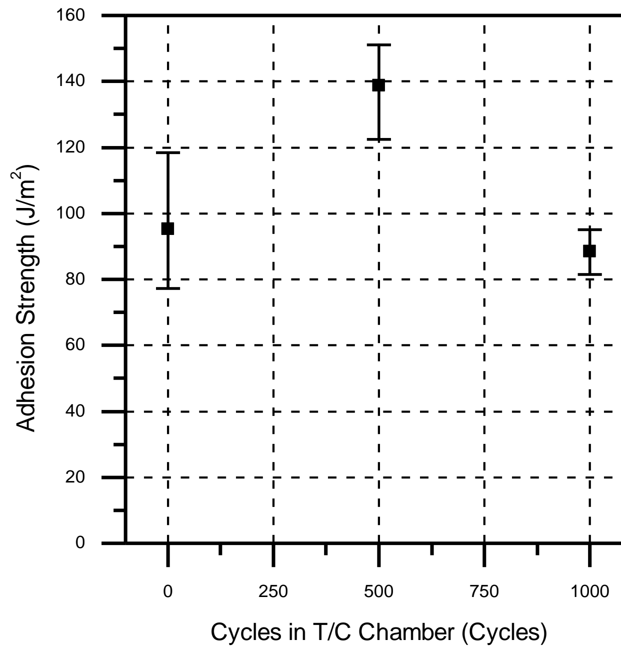

Figure 63. Adhesion strength versus cycles in a T/C chamber.

6.4.2. Puncture Strength

Typical puncture force vs. deflection results for the polyurethane coating are shown in Figure 64 for three different probe radii and the corresponding puncture strength results are recorded in Table 5 . As seen in the table, the puncture strength of the coating has a variation of less than 3% with probe radii. It follows that for a given whisker radius, the puncture force of the coating can be calculated from the puncture strength using Eq. (37).

Table 5. Puncture strength with different probe radii.

Probe radius (μm)	Puncture strength (J/m^2)
50	1343±78
65	1341±24
80	1282±19

Puncture test samples were subjected to IPC standard [118] T/H testing condition of 85°C/95% RH, and tested after 0, 168 hours, 336 hours and 504 hours in the testing chamber. Figure 65 shows that the average puncture strength of the coating steadily decreased with time in this accelerated environment.

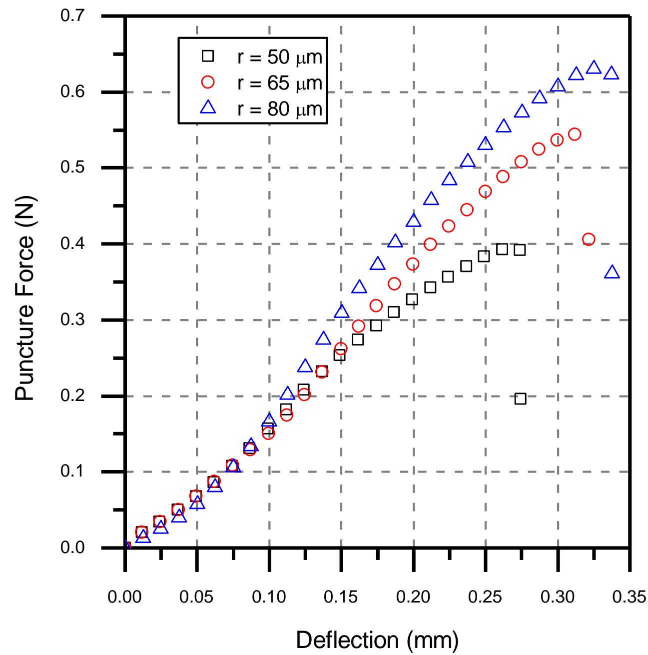

Figure 64. Typical load vs. deflection results for the puncture test of a polyurethane conformal coating.

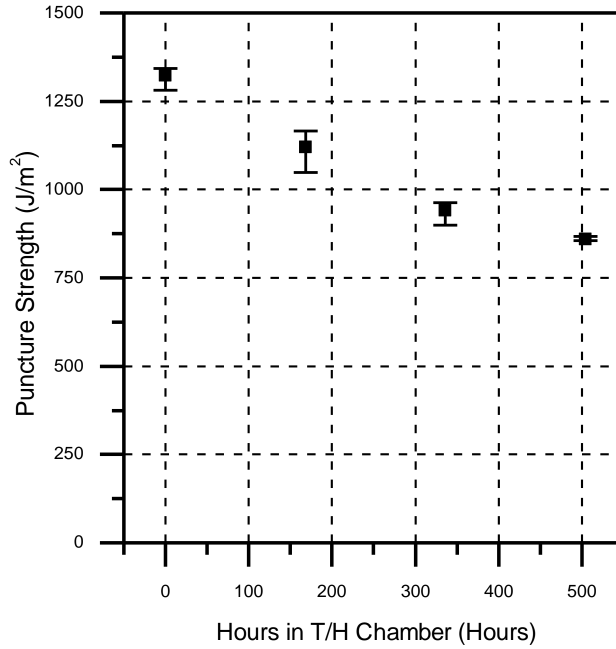

Figure 65. Puncture strength versus hours in a T/H chamber.

6.5. Discussions: Failure Modes

This paper has focused on the failure mechanisms due to tin whisker nucleation and growth from underneath the coating as seen in Figure 66. As discussed, the puncture strength characterizes the failure of the conformal coating due to cohesive penetration by tin whisker nucleation. The puncture force of the coating can be calculated when the puncture strength, T_P, and the whisker radius, d_w, are known by the following equation [116]:

$$F_P = \pi d_w T_p \tag{38}$$

As the whisker continues to grow from underneath the coating, a competing mechanism to puncture, buckling, is introduced. If the whisker buckles before reaching the puncture strength of the coating, the whisker will be contained within the coating,

preventing a failure due to penetration. To compare the competing mechanisms, the buckling force of a tin whisker can be calculated by [106]:

$$F_b = \frac{\pi^3 E_w d_w^4}{32L^2} \tag{39}$$

where L is the length of the whisker, E_w is the modulus of the tin whisker, and d_w is the diameter of the whisker. From Eq. (38) and (39), we can see the puncture force is independent of the whisker length and the buckling force is inversely proportional to the whisker length squared.

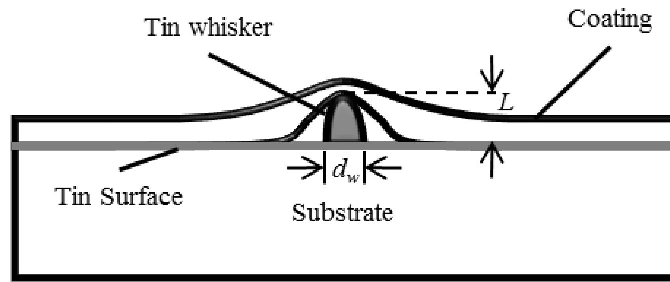

Figure 66. Schematic of tin whisker nucleating on tin coated substrate.

Figure 67 depicts the puncture and buckling force plotted vs. the whisker length. In the figure, three different whisker diameters are considered, $d_w = 2,\ 4,\ 6\ \mu\text{m}$, the tin whisker modulus is assumed to be $E_w = 42$ GPa [103], and the puncture strength of the tested conformal coating is $T_P = 1322\ \text{J/m}^2$. For a given whisker diameter and puncture strength there exists a critical whisker length at which the critical force required to puncture the coating becomes larger than the critical buckling force:

$$L_{Critical} = \sqrt{\frac{\pi^2 E_w d_w^3}{32 T_p}} \tag{40}$$

Figure 68 plots the critical whisker length for buckling versus whisker diameter. For whiskers longer than the critical whisker length, the whiskers buckle and are contained by the conformal coating and do not result in failure. The critical whisker length increases with increasing whisker diameter therefore as expected, thinner diameter whiskers are much easier to contain. So given the above coating properties, a 6 μm diameter whisker will buckle and be contained if it grows longer than 150 μm in length. This approach could be applied to set a design point to identify required thicknesses of conformal coatings.

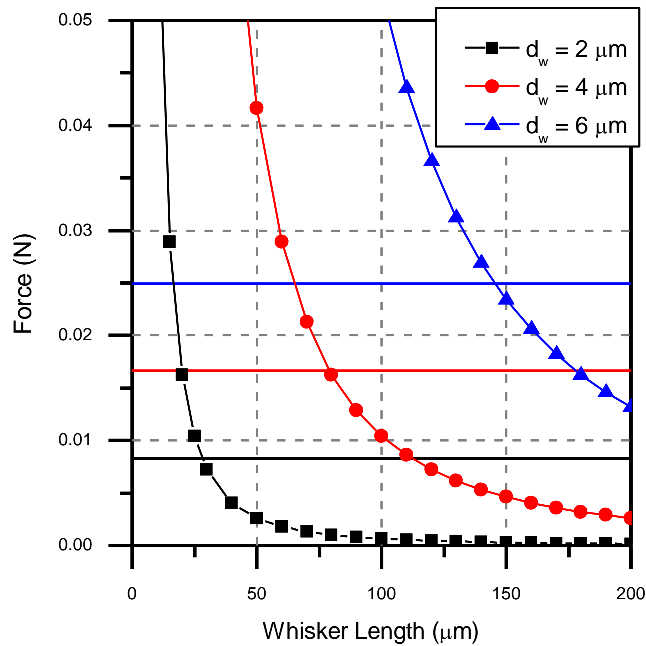

Figure 67. Puncture force and buckling force versus whisker length.

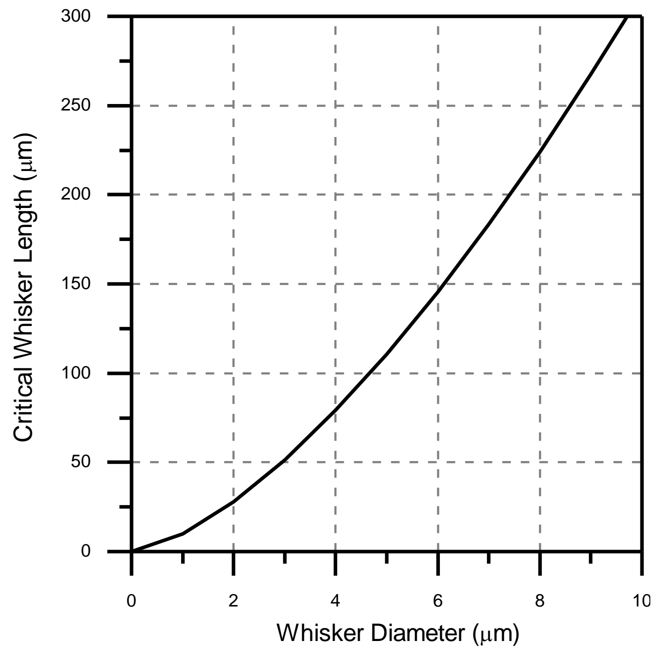

Figure 68. Critical whisker length for buckling versus whisker diameter.

The adhesion strength between the coating and tin layer also affects the reliability of the coating because whiskers can escape from exfoliated areas of the coating. Additionally, delaminated openings resulting from a growing whisker lifting the coating affect the delamination configuration and alter the puncture force of the whisker. As the delaminated area increases, both the puncture and buckling forces are reduced. Because of the delaminated surface, the critical whisker length would increase significantly compared to the puncture strength, allowing for even longer whiskers to be contained.

Future work can expand on this concept through advanced numerical modeling to determine what will occur once a tin whisker nucleates on a conformally coated surface. A sequential approach can be applied considering a contact analysis and an indentation analysis for the initial nucleation of the whisker into the coating. This initial stress analysis

determines the stress/strain distribution around the whisker tip as well as the total force exerted on the whisker. The former can be compared to the puncture strength of the coating to assess if puncture occurs first while the latter can be input to a buckling analysis. The lifting force on the whisker can also be used to calculate the stress along the interface of the coating/tin plating surface. If the stresses at the interface are large enough to overcome the adhesion strength of the interface, delamination occurs, which redefines the deformation configuration of the analysis.

6.6. Conclusion

Two key material properties required to assess the reliability of a polyurethane coating were obtained: adhesion strength by blister testing and puncture strength by puncture test. A procedure to prepare blister samples for tin-plated surfaces was proposed, including a method for creating a well-defined pre-defined area. A blister test procedure was employed to determine the elasto-plastic properties of a urethane conformal coating. The elasto-plastic properties of conformal coatings were then considered in adhesion strength calculations leading to a more realistic determination of the adhesion strength. A puncture test was employed to determine the puncture strength of the coating. Blister test and puncture test samples were tested before and after accelerated testing conditions and the degradation of the coating properties was reported.

Adhesion strength samples in both T/H and T/C environments both experienced an initial increase in the adhesion strength ranging from 27 – 40%. This increase in adhesion strength is speculated to be attributed to additional crosslinking of the polymer coating. Continued T/H testing resulted in little change in the adhesion strength, whereas the T/C

testing environment resulted in 22% decrease in adhesion strength over the next 500 cycles. The puncture strength saw 35% decrease in strength after 500 hours in a T/H testing environment. The results indicated that a polyurethane coating would be an effective solution to mitigate the tin whisker growth problem.

Chapter 7: Blister Testing for Adhesion Strength Measurement of Polymer Films Subjected to Environmental Conditions[3]

ABSTRACT

A blister testing method combined with a numerical procedure can be used effectively for characterizing the adhesion strength. A challenge arises when it is implemented after subjecting samples to various environmental conditions. The concept of pseudo property is introduced to cope with the problem associated with property changes during environmental testing. The pseudo property set is determined directly from a deflection vs. pressure curve obtained from a typical blister test. A classical energy balance approach is followed to evaluate the energy release rate from the critical pressure and pseudo property set. The proposed approach is carried out for an epoxy/copper interface after subjecting samples to full moisture saturation and a high temperature storage condition. In spite of significant change in property, the energy release rates are calculated accurately without extra tests for property measurements.

---

[3] This chapter has been submitted for review to the *Journal of Electronic Packaging* under the title of "Enhanced Blister Testing for Adhesion Strength Measurement of Polymer Film Subjected to Environmental Conditions" by K. Mahan, D. Rosen, and B. Han.

7.1. Introduction

In microelectronics, there are many interfaces that come together to create a product. One such interface is found between flexible polymer films and rigid substrates. Whenever two materials are structurally bonded together, a potential reliability issue is created that must be monitored. If the adhesion strength at the interface is weak, delamination can occur, leading to failure of the device. Therefore, it is imperative to assess the reliability of the interface under the same conditions the device will be subjected to in order to avoid failure under device operating conditions.

The reliability of the interface can be quantified by experimentally measuring the critical energy release rate of the interface. The energy release rate, G, is an indication of the adhesion strength of the interface since it quantifies the energy required to create new surface area for interfacial crack propagation [1]. A common adhesion strength testing method that is effective for this type of flexible/rigid interface is the blister test [64-68, 73-75, 77, 87]. Previous challenges with this technique involving creation of a well-defined blister area have been addressed, leading to more consistent blister test results [95]. Analytical solutions for the blister test exist when testing under idealized bending only or stretching only domains. However, challenges exist when the material properties of the film or the testing domain is not known prior to testing.

It is well known that long term exposure to high temperature and moisture conditions, as well as the presence of moisture at the interface, can lead to a decrease in the adhesion strength of an interface [119-122]. To fully characterize the reliability of the interface, testing is typically performed at as-manufactured and environmentally degraded conditions such as thermal aging, moisture absorption, etc. However, any degradation or

change in the polymer during environmental conditioning can affect the structural properties, the Young's modulus, E, and the Poisson's ratio, ν, of the polymer [123, 124]. In addition, polymers are known to have rate dependent properties [125-127]. Due to the prescribed rate and/or the degradation from environmental aging the structural properties of the polymer can potentially shift the deformation mode of the film to some mixture of stretching and bending deformation modes, which adds to the uncertainty in using analytical solutions for long term degradation testing. Without knowledge of the appropriate testing domain and/or the structural properties of the polymer at the time of testing, the analytical solutions cannot be applied with confidence to assess the energy release rate.

One approach to account for variation of the material properties between test conditions is to run additional material characterization tests of the polymer prior to each data point. However, running separate and simultaneous tests to obtain the polymer's structural properties is time consuming and often impractical.

To cope with the problem, we introduce the concept of "pseudo" material properties that can be determined from the pressure-displacement data. In general, only the maximum pressure, which causes interface delamination, is used in the analysis and the pressure-displacement data is often ignored because an additional data is required to determine both Young's modulus and Poisson's ratio. A typical numerical procedure is implemented with the blister test that takes a classical energy balance approach to evaluate the energy release rate from the maximum pressure, but a "pseudo" properties based hybrid approach extends its applicability to the cases where the properties are not known. This approach is proven most useful when investigating the effect of environmental conditions on the adhesion

strength since the structural properties of a polymer film can degrade over time leading to added uncertainty in the original properties of the film.

7.2. Background: review of analytical solutions

A schematic of a blister test sample with a predefined area is illustrated in Figure 69. In a typical blister test experiment, pressure loading is applied through the hole in the substrate layer to load the film layer. Pressure is increased monotonically causing the film to inflate like a blister of radius a, until the film delaminates along the interface at a critical pressure, P_{crit} and critical blister height, w_{crit}.

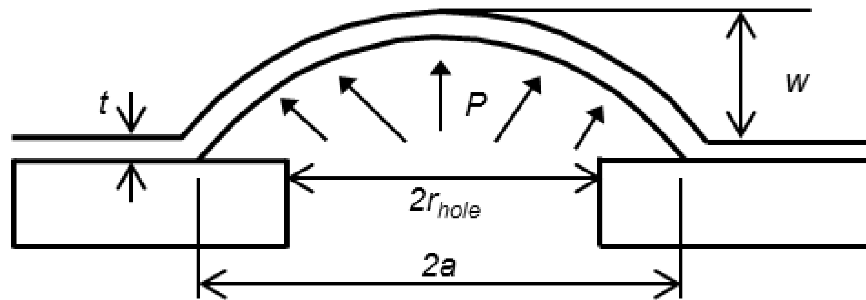

Figure 69. Schematic illustration of a blister test.

Closed-form analytical solutions for the energy release rate exists for particular cases, such as when the polymer film is relatively stiff and under mainly bending loading [66] or very flexible and under mainly stretching [68] loading.

An analytical expressions has previously been developed for the bending dominant case where the film thickness, t, is much smaller the blister deflection, w. This case considers the film as a thin plate undergoing small deformation and derives the pressure-deflection relationship using Timoshenko's beam theory [66]:

$$w = \frac{3Pa^4(1-\upsilon^2)}{16Et^3} \tag{41}$$

Then by applying an energy balance method at the instant the film delaminates from the substrate, the energy release rate, G, is expressed as:

$$G_{bend} = \frac{3\left(1-\nu^2\right)a^4}{32Et^3} \cdot P_{Crit}^2 \tag{42}$$

Similarly, an analytical expression exists for the stretching dominant thin film case. For this case, assumptions are made such that the film is a thin elastic membrane, the blister forms a spherical cap, and the deflection is much smaller than the blister radius, a. Under these assumptions, the pressure-deflection relationship is [68]:

$$w = \left[\frac{3Pa^4(1-\upsilon)}{8Et}\right]^{\frac{1}{3}} \tag{43}$$

and then by applying an energy balance method, the energy release rate, G, is expressed as:

$$G_{stretching} = \left[\frac{5}{4}\left(\frac{3}{8}\right)^{1/3}\right] C_1 \left(\frac{P_{Crit}^4 a^4 \left(1-\nu\right)}{Et}\right)^{\frac{1}{3}} \tag{44}$$

where C_1 is a numerical constant, 0.518, to accommodate the volume difference of the spherical cap due to the clamped end condition of the blister [95].

After testing, the energy release rate can be assessed from the film's material properties and the critical pressure from the experimental test. Alternately, the energy release rate can be expressed just by the critical pressure, the critical blister deflection, and a constant value for both the bending dominant and stretching dominant analytical expressions:

$$G_{bend} = \frac{P_{crit} w_{crit}}{2} \tag{45}$$

and

$$G_{stretching} = \frac{5C_1}{4} P_{crit} w_{crit} \tag{46}$$

For the case of intermediate film thickness and/or larger than expected adhesion strength interfaces, a mixture model was proposed, where a correction factor was prescribed to account for the presence of both modes [66, 70]. This approach is limited to only very specific material interfaces. Others have tried more sophisticated FEA methods (e.g., traction separation models) to describe the delamination at the interface [87, 91, 92], which is very sensitive to the material properties of the film layer.

7.3. Numerical Procedure to Calculate Energy Release Rate

Following a successful blister test, the critical pressure, P_{Crit}, can be obtained from the moment that delamination occurs. Using this critical state from the experiment and the film's structural properties, a numerical model can be developed to recreate the stress/strain state in the film at the point of delamination. Then by using a simple energy balance method, the energy release rate, G, can be extracted from the model.

7.3.1. FEA Model Setup

Due to the simplistic geometry of the blister test, a 2D axisymmetric model is established using commercial FEA software (ANSYS). From the experimental setup, the blister radius, and film thickness are known ahead of time. Material properties of the film and substrate layer should also be known and input into the model. Boundary conditions for this model are shown in Figure 70. For this 2D model, axisymmetric boundary conditions are prescribed at the center of the model. Additionally, the u_x displacement is

constrained at the bottom corner of the substrate; the u_y displacement is fixed at the interface between the film; and substrate is constrained past the blister radius to represent a bonded interface.

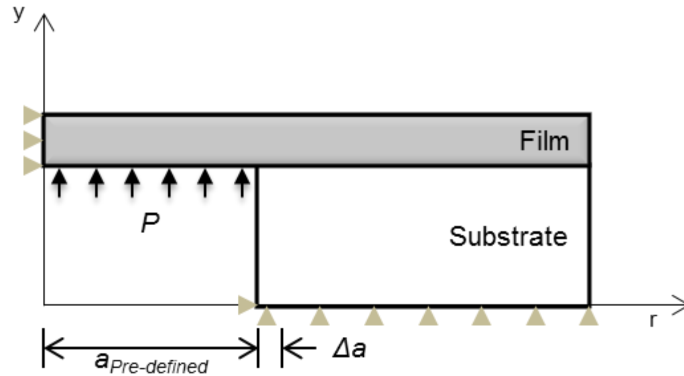

Figure 70. Schematic of boundary conditions applied in axisymmetric 2D model of blister test.

The model must consider large deformations during the analysis due to the nature of the test. The pressure is increased in step to the critical pressure using a constant increment. The pressure and deflection data of the center of the blister are recorded at each step to form a numerical pressure vs. deflection curve.

7.3.2. Energy Release Rate Calculation

To numerically evaluate the energy release rate, G, an energy balance method is employed at the critical moment the blister delaminates. At this state, the critical pressure, P_{crit}, is assumed to be constant and two cases are examined: the moment before delamination when the blister radius is still a, and the moment after an infinitesimal delamination of Δa when the blister radius is $a + \Delta a$. The energy balance of interest is the difference between these two key states at constant pressure, P_{crit}, i.e.,

$$\Delta W = \Delta W_1 + \Delta W_2 \tag{47}$$

where the change in work input into the system, ΔW, is evaluated as:

$$\Delta W = P_{Crit}\Delta V = P_{Crit}\left(V\big|_{a+\Delta a} - V\big|_{a}\right) \tag{48}$$

where V is the volume of the blister.

The energy dissipated when the crack propagates, ΔW_1, is evaluated as:

$$\Delta W_1 = 2\pi G\Delta a \tag{49}$$

and the change in energy stored in the film layer, ΔW_2, is evaluated as:

$$\Delta W_2 = \int \sigma d\varepsilon\Big|_{a+\Delta a} - \int \sigma d\varepsilon\Big|_{a} \tag{50}$$

Combining Equations (48), (49), and (50) into (47), the energy release rate can be expressed as:

$$G = \left(\frac{P_{crit}(V\,|_{a+\Delta a} - V_a) - \left(W_{2_{a+\Delta a}} - W_{2_a}\right)}{2\pi a\Delta a}\right) \tag{51}$$

To demonstrate this procedure, consider blister testing of a polymer film with structural properties of E = 2.5 GPa and ν = 0.4 with a predefined blister radius of 5 mm. Two cases can be considered for the same film: one that falls in a pure bending-only case and another that is pure stretching-only. For the bending only case consider a film thickness of h_{bend} = 500 μm and for the stretching only case consider a film thickness of $h_{stretch}$ = 100 μm. In Figure 71(a) and (b), the deflection vs. pressure curves for the bending only and stretching only cases obtained from the FEA analysis are plotted, respectively. Equations (41) and (43) are also used to plot the analytical bending and stretching relationship. It is clear that there is very good agreement for both cases.

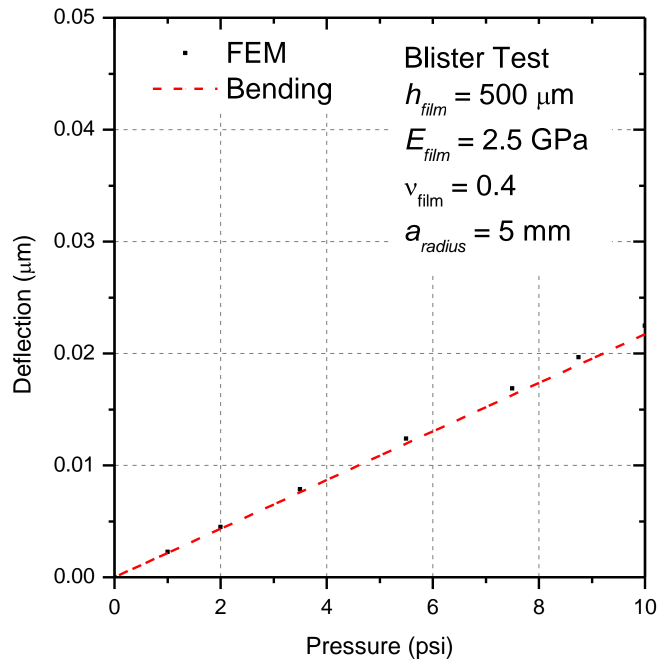

(a)

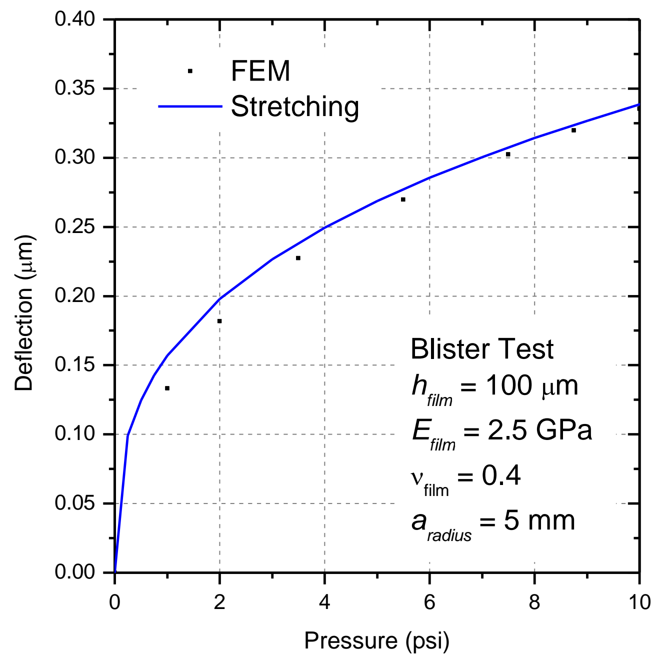

(b)

Figure 71. Deflection v. pressure curve for ideal (a) bending and (b) stretching specimens; FEM results and analytical solutions are compared.

The stored energy in the film can be directly determined from the FEA results. For the volume calculation, a shell integration method can be employed to evaluate the volume as:

$$V = 2\pi \int_0^{a_{radius}} r w(r)\, dr \tag{52}$$

where $w(r)$ is the displacement of the film layer along the radius. For the stretching case, the blister profile from the FEA analysis before and after delamination is illustrated in Figure 72 (P_{crit} = 10 psi). The blister profile is then imported into mathematical software (MATLAB) and the shell integration is carried out using a trapezoidal integration method to obtain the total blister volume for both before, V_a, and after, $V_{a+\Delta a}$, delamination.

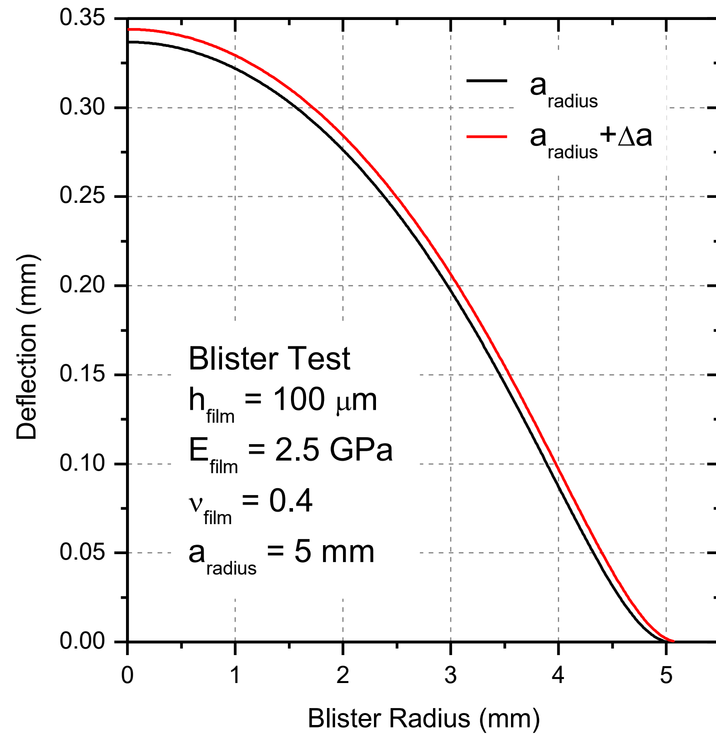

Figure 72. Blister profile before and after a delamination of Δa = 75 μm obtained from the FEA analysis: the case of Figure 71b with P_{crit} = 10 psi.

The procedure continues to calculate the critical energy release rate. Using the stress state at the critical pressure, the stored energy, $W_2\big|_a$, is determined. After all variables are found, the energy release rate is evaluated for a particular Δa using Equation (51). This procedure can be repeated over several Δa step sizes and then by taking the limit of G with respect to Δa the energy release rate can be determined. By evaluating G as Δa approaches zero the error associated with the arbitrary step size is eliminated, thus allowing for an accurate determination of the energy release rate at the instance of delamination.

This step is shown in Figure 73 for the stretching only case. According to the stretching-only analytical Equation (44), $G_{Analytical}$ = 15.1 J/m^2. Following the numerical procedure the energy release rate is evaluated as $G_{Stretch}$ = 14.8 J/m^2. The analytical solution slightly overestimates G since it neglects stress resulting from bending. It is clear from the results that there is good agreement with the numerical method and analytical approaches when within the appropriate domain.

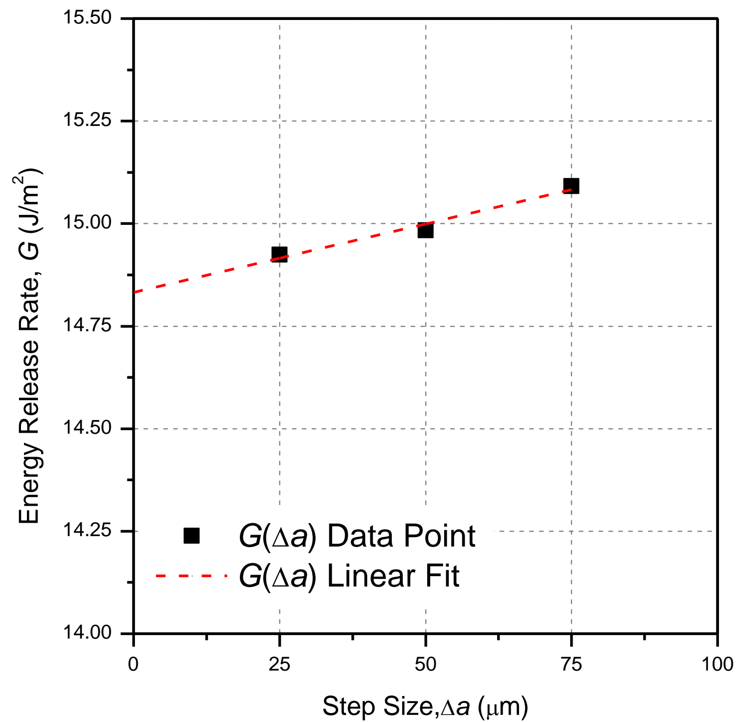

Figure 73. *G* vs. Δa plot for numerically determined energy release rate for the case shown in Figure 72.

7.4. Energy Release Rate with Pseudo-Properties

Consider an intermediate blister testing case where the film thickness is 250 μm. The deflection vs. pressure curve is plotted for this case against both analytical solutions in Figure 74. It is clear that testing of this film falls outside either of the analytical solutions domains. Since this case is no longer in the realm of the analytical solutions, numerical methods must be used to calculate the energy release rate, and thus, the material properties of the film must be known. The concept of pseudo material properties is proposed to cope with the problem.

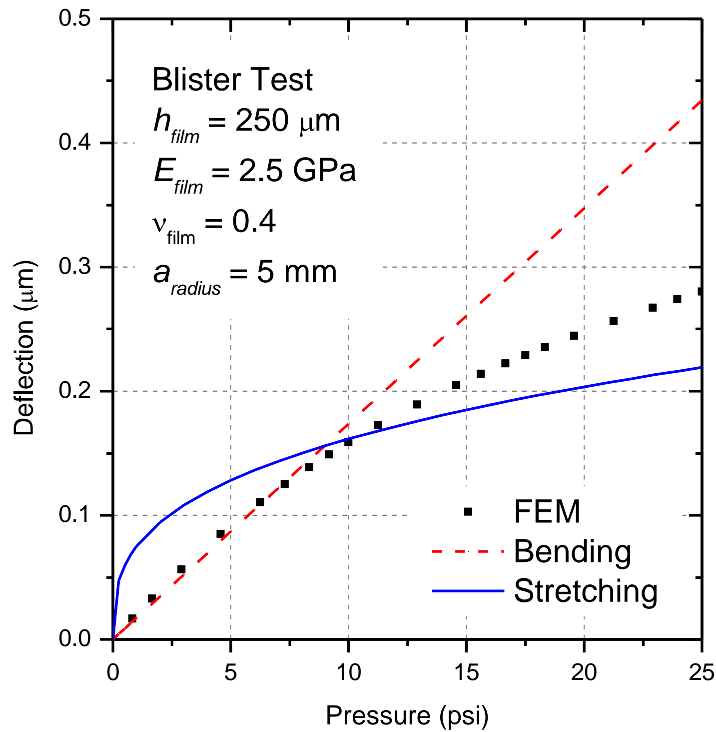

Figure 74. Deflection vs. pressure curve for a blister test specimen with an intermediate thickness.

As mentioned earlier, the load-blister height curve is obtained from a blister experiment. It is important to note that numerous sets of E and ν can produce the same curve. This is illustrated in Figure 75. Each of these curves was created by making an ad-hoc assumption for ν and using a regression analysis to establish the corresponding modulus (this set is referred to as "pseudo-property pair") that produced the deflection vs. pressure curve. The pseudo property pairs used for the analysis are shown in Table 6. It is clear that each of the pseudo property pair (E, ν) recreates the same curve and accurately describes the critical state where delamination occurs.

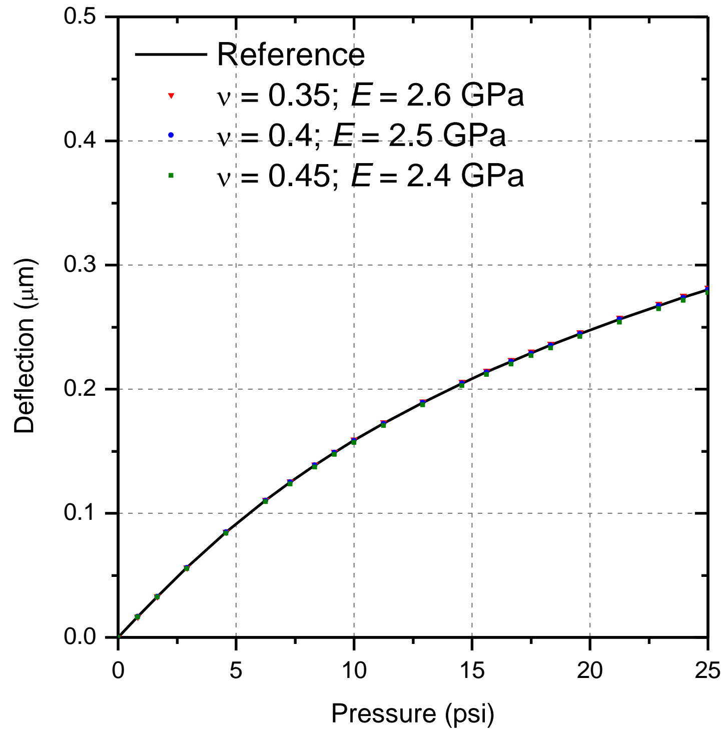

Figure 75. Deflection vs. pressure curve for intermediate case with several pseudo material property pairs to fit experimental curve.

Table 6. Consequence of ad-hoc Poisson's ratio selection.

Poisson's Ratio	Pseudo-*E* (GPa)	Energy Release Rate (J/m^2)	Percent Error
0.35	2.6	48.3	0.4%
0.4	**2.5**	**48.1**	**0.0%**
0.45	2.4	48.1	-0.1%

Using P_{crit} = 25 psi, the energy release rate was calculated from the numerical procedure presented in Section 3. The resulting energy release rate for the reference case (E = 2.5 GPa and v = 0.4) case was G = 48.1 J/m^2. The energy release rates for all pseudo-property pairs were also calculated and the values are summarized in Table 6. It is clear from the table that any pseudo-property pairs that are determined from the deflection vs.

pressure curve by making an ad-hoc assumption of E or v can be used to determine G with virtually no effect on the energy release rate.

This finding is intuitive since as seen in Equations (45) and (46) that the analytical solutions for G can be determined without prior knowledge of the film's material properties. This ability to assess any changes in the material properties in-situ opens up the ability to determine the energy release rate accurately even after environmental conditioning where the structural properties of the polymer are subject to change and degrade between sample sets.

7.5. Application

The adhesion strength was assessed for an interface of a common epoxy used in electronic packages and a copper substrate.

7.5.1. Sample Preparation

For testing, a rigid copper substrate with twelve 3 mm diameter test holes (Figure 76a) was used in this application. Each copper substrate was subjected to successive grinding using a rotational grinding machine set at 150 RPM. The substrates were grinded using 240, 400, 600, and 800 grit paper for five minutes each. This process helped ensure a uniform surface roughness on order of ~6.5 μm while removing any impurities.

(a)

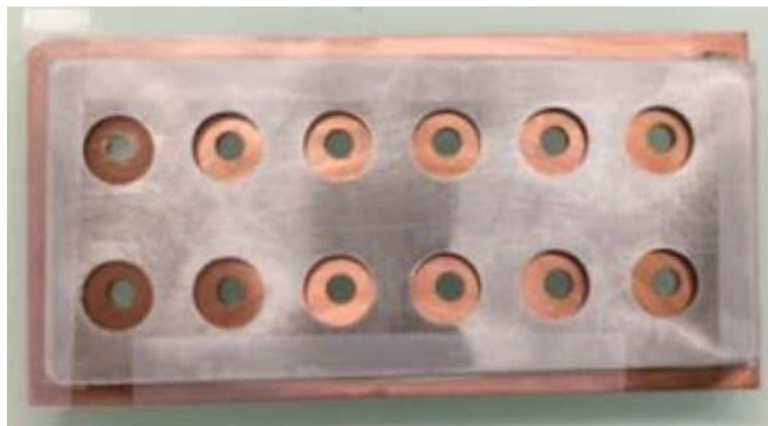

(b)

Figure 76. Copper substrates for blister test samples (a) before and (b) after attaching the stencil.

The radius dependency of the energy release rate is obvious. An accurate well-defined predefined area is critical to the sample repeatability [95]. To establish the extent of the predefined area, a stencil piece composed of flat sheet metal with twelve 3/8" diameter holes was placed on top of the substrate so that the stencil holes were concentric with the pressure holes. Using a residue-free tape, the stencil piece was taped along its edges to the substrate, seen in Figure 76b. The exposed substrate areas will be the predefined areas for 12 blisters. The pressure holes were then temporarily blocked with a

residue-free tape. The stencil prevented the tape contact outside the predefined area. This approach greatly reduced the possibility of introducing impurities to the interface of interest during plug creation.

A schematic of the remaining sample preparation procedure is shown in Figure 77. Before creating the predefined area, the pressure hole must first be temporarily plugged. Silicon rubber was chosen for the temporary plug because of its known low adhesion property, which ensures that it will not adhere to the tape, blister material, or copper. A commercially available silicon rubber (GE RTV615A) was prepared according to the manufacturer's specification and then spun in a centrifuge for 3-5 minutes to remove any gas introduced by mixing. The compound was then carefully poured into each pressure hole, ensuring no gas bubbles form in the process. Meanwhile, twelve 1.5 millimeter diameter dowel pins were allowed to soak in a silicon primer solution (GE SS4120) for five minutes, then allowed to dry for five minutes. By doing so, the dowel pins adhered to silicon rubber. A pin was carefully inserted into each pressure hole, serving as a convenient way to remove the silicon plugs later in the process. The system was allowed to cure for 24 hours at room temperature.

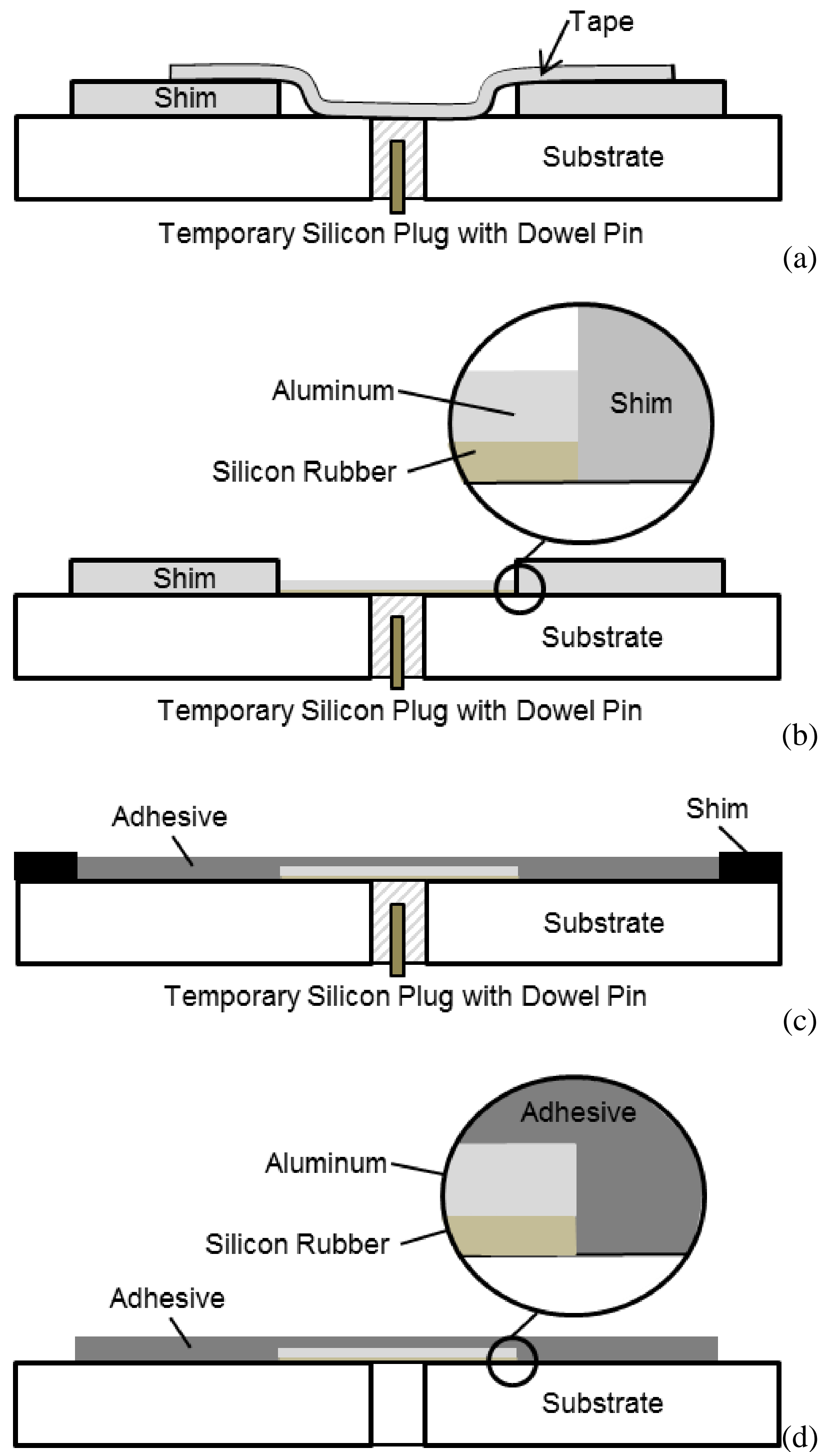

Figure 77. Schematic of sample preparation procedure: a) creating temporary plug, b) creating the predefined area, c) curing the adhesive, and d) the final sample ready for testing.

After a full cure, the tape covering the pressure holes were carefully removed. A small amount of methanol was applied with a cotton swab inside the stencil to remove any possibility of contamination from the tape's adhesive material. A thin coat of a dry film release agent (Sprayon MR311) was then applied inside the stencil, thus defining a low adhesion predefined area for each blister specimen. The use of a wet release agent, such as silicon oil, proved to be unsuccessful due to transport and mixing issues with the blister material.

To further establish the integrity of the predefined area, a ~10 nm thick layer of aluminum was deposited on top of the dry film release agent via the use of a vacuum chamber (Denton DV-502A). The release agent and aluminum layers composed the completed predefined area. While the release agent created the low adhesion surface, the thin aluminum layer provided a clear boundary that prevented the epoxy from adhering directly to the predefined area. The stencil was then removed from the substrate.

To create the film layer, a shim of 300 μm was first created around the edge of the substrate using the tape. The two-part epoxy was prepared according to the manufacturer's recommendation, spun in the centrifuge for roughly two minutes to remove any voids, poured onto the substrate, and allowed to spread evenly via gravity. The samples were then allowed to cure at room temperature for 48 hours. After the full cure was achieved, the silicon plugs were removed by pulling the dowel pins. Finally, the film layer was sectioned into individual specimens on top of the substrate to ensure that delamination from one specimen did not affect the others during testing.

7.5.2. Experimental Setup and Testing Procedure

During testing, the pressure, center blister deflection, and blister profile were captured and integrated into a LabView program to synchronize data collection. A schematic of the experimental setup is shown in Figure 78. Once the specimen is secured over the pressure port, the three-axis translation stage can also be used to ensure accurate alignment of the laser above the center of the blister to capture the maximum deflection during each test.

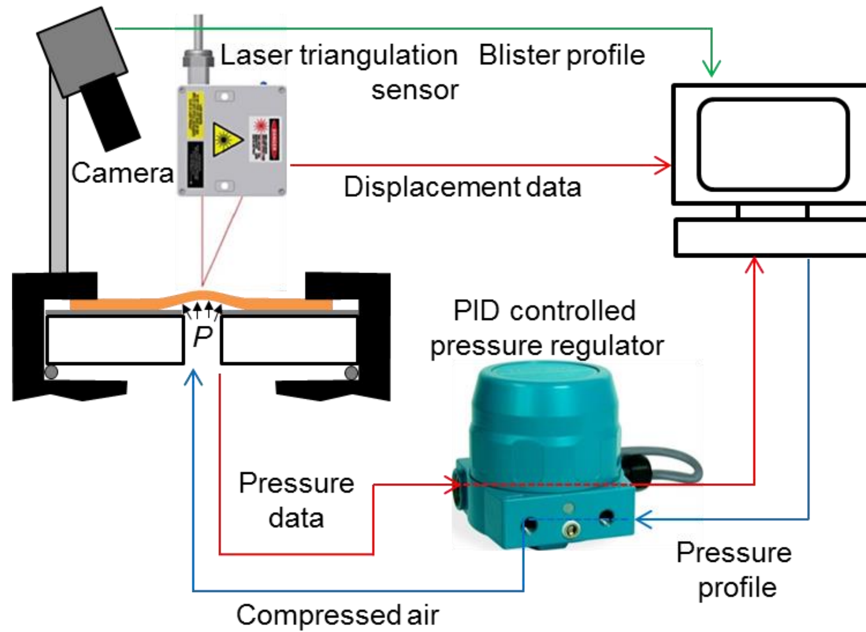

Figure 78. Schematic diagram of the blister test setup.

The pressure regulator (Tescom ER3000) applied pressure at a rate of 1 psi/s while the laser triangulation sensor (MTI MicroTrak II) and camera (Sentech MC133-USB) recorded the center blister height and blister profile, respectively. The pressure regulator allowed for a resolution of 0.1 psi, and the laser displacement sensor had a resolution of 1.25 μm. For each specimen, the pressure was increased monotonically while the blister continued to grow. Once the blister reached a critical pressure, the film delaminated from

the substrate. The critical delamination was captured both in a sudden increase in deflection at P_{Crit} on the deflection vs. pressure curve, and visually through the camera profile.

Several representative deflection vs. pressure curves for the as-is case are shown in Figure 79. An overhead image of the predefined area of a specimen can be seen in in Figure 80a. When the pressure reached a critical pressure, the film delaminated from the substrate and it was recorded with the camera (Figure 80b). This moment of delamination captured in the video matched the critical pressure recorded in the deflection vs. pressure graph for the specimen, which confirmed the validity of the experimental data.

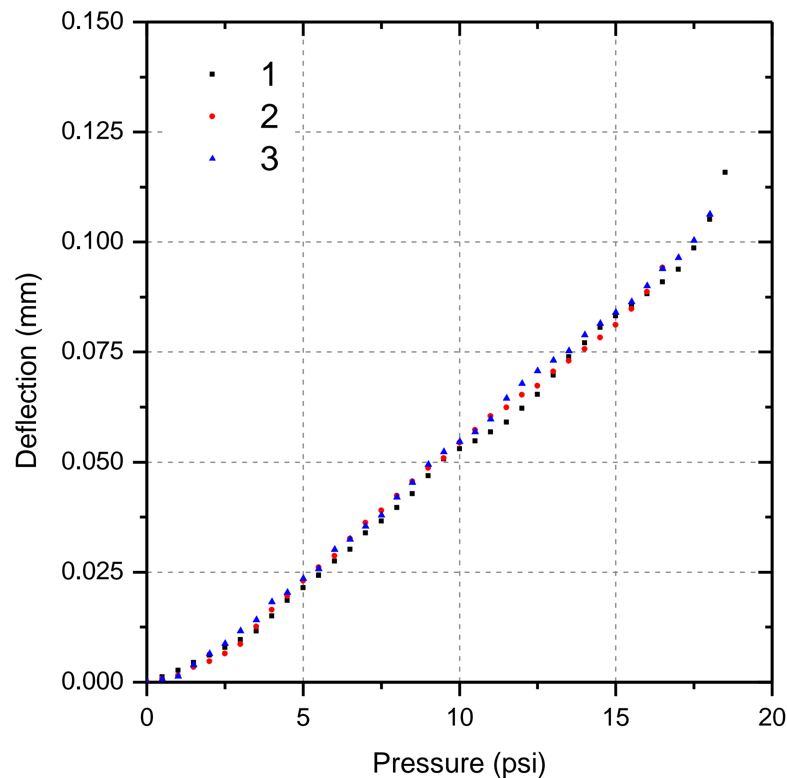

Figure 79. Representative deflection vs. pressure curves for an epoxy/coper interface at as-is testing conditions.

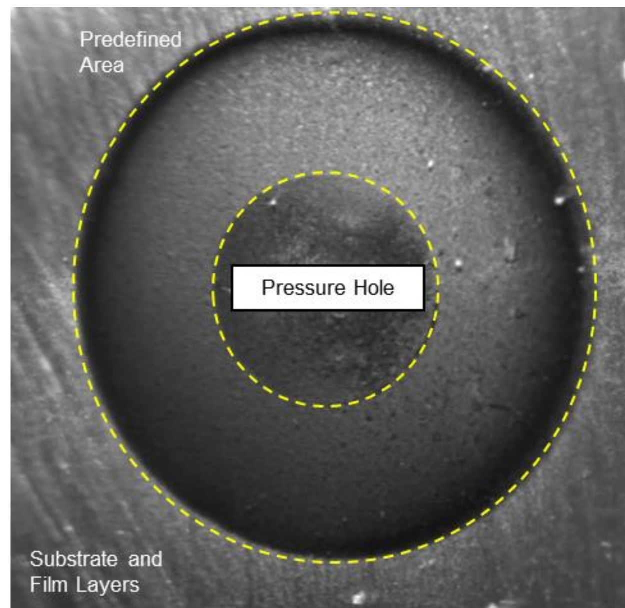

(a)

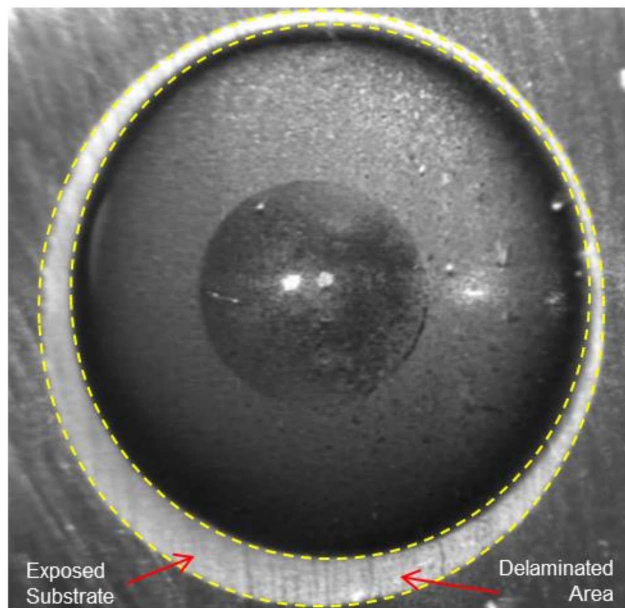

(b)

Figure 80. A typical blister sample a) before and b) after critical delamination event.

Since the typical Poisson's ratio for this type of polymer is 0.4, it was used as an ad hoc assumption for the pseudo-material properties. The twelve as-is samples tested were then modeled in FEA and went through a nonlinear optimization method to determine a corresponding pseudo-modulus for each sample. For as-is samples, the average pseudo modulus was 3.58 GPa with a standard deviation of 1.12 GPa. The average energy release rate was 25.0 J/m^2 with a standard deviation of 4.37 J/m^2.

7.5.3. Results of Environmental Testing

The importance of this approach becomes more apparent when evaluating the effect of environmental conditions. In addition to as-is testing, samples were subjected to two environmental testing conditions: moisture degradation and thermal aging. The moisture degradation sample set consisted of six specimens and was subjecting to a 100% relative humidity environment at room temperature for a duration of seven days. The thermal aging sample set consisted of ten specimens and was subjected to a high temperature storage condition (125°C) over a seven day period.

Figure 79 shows a representative pressure vs. deflection curve and Table 7 lists the statistical information for each sample set tested. Additionally, the average and range of the energy release rate and pseudo-modulus are shown in Figure 82 and Figure 83, respectively, for each sample set.

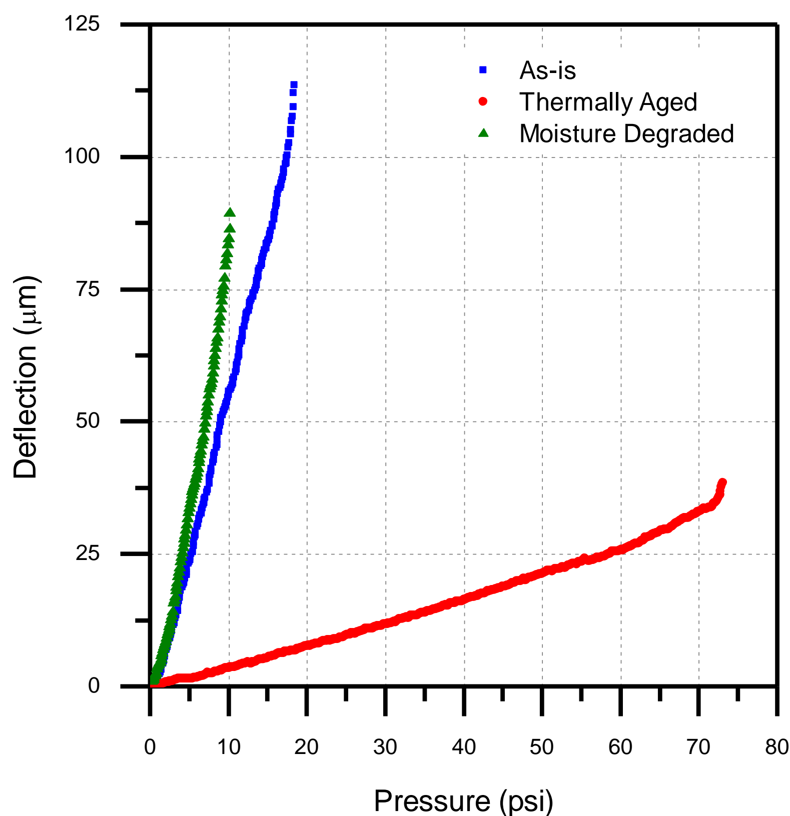

Figure 81. Representative deflection vs. pressure curves for an epoxy/copper sample at three conditions: a) as-is, b) after thermal aging, and c) after moisture degradation.

Table 7. Comparison of testing results.

Parameter	**Mean**	**Standard Deviation**
Pseudo-*E* (as-is)	3.58 GPa	1.12 GPa
G (as-is)	25.0 J/m^2	4.37 J/m^2
Psuedo-*E* (thermally aged)	46.1 GPa	17.1 GPa
G (thermally aged)	28.2 J/m^2	7.32 J/m^2
Psuedo-*E* (moisture degraded)	3.78 GPa	1.36 GPa
G (moisture degraded)	10.7 J/m^2	5.13 J/m^2

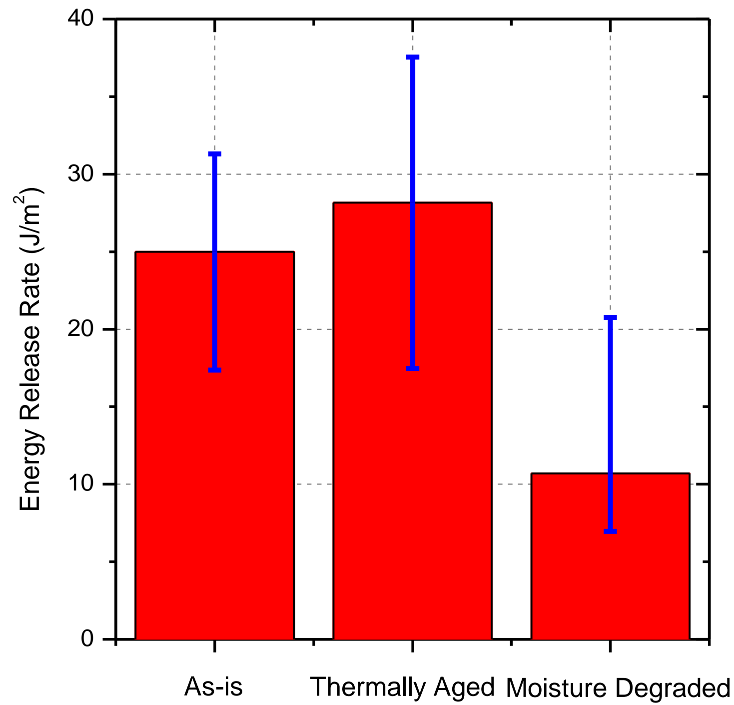

Figure 82. Energy release rate comparison of three conditions: a) as-is, b) after thermal aging, and c) after moisture degradation.

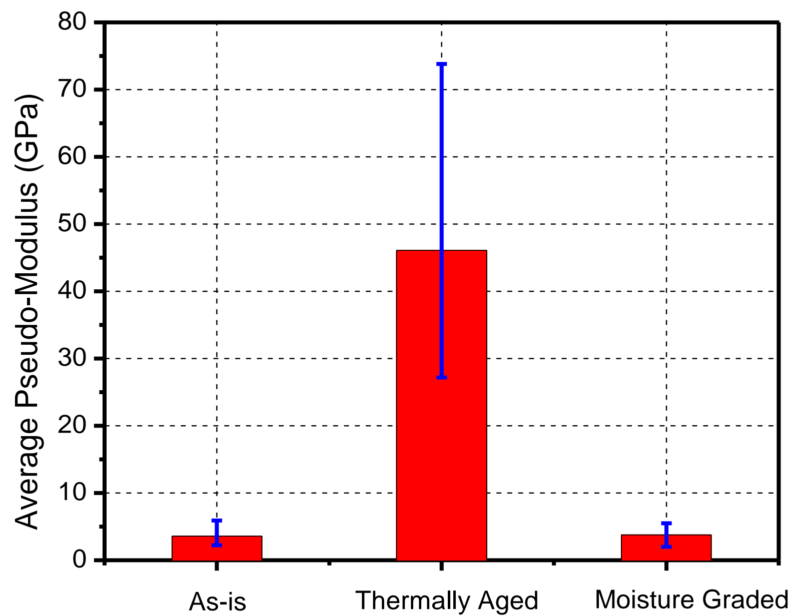

Figure 83. Moduli comparison of three conditions: a) as-is, b) after thermal aging, and c) after moisture degradation.

As expected, the deflection vs. pressure curve showed a reduction in the critical pressure for the moisture degraded case. Compared to the average as-is pseudo-modulus, the average moisture degraded sample pseudo-modulus stayed relatively constant at 3.78 GPa. However, the consequence of subjecting samples to this moisture environment was a 57% reduction in the energy release rate from as-is values.

As seen in the deflection vs. pressure curve for the thermal aging case, there is a drastic change in the film's response to the blister test, which is an indication of changes to the structural material properties of the film layer. While the energy release rate increased by 13% due to additional curing at the higher temperature, the average pseudo-modulus of the thermally aged specimen increased by over an order of magnitude to 46.1 GPa.

Of most importance is how this sudden change in polymer behavior did not greatly affect the energy release rate of the interface (Figure 82). Failure to consider changes in the structural material properties of the film in energy release rate calculations will result in erroneous data. In the thermally aged case if the original as-is material properties were used to evaluate G then there would be a gross over-estimation of the energy release rate that would not capture the actual adhesion strength of the interface. Misuse of environmentally aged data can lead to a misrepresentation of the actual adhesion strength of a critical interface – potentially leading to unintended failure.

7.6. Conclusion

An alternative numerical/experimental blister test method was proposed to characterize the adhesion strength of an interface when the film's structural properties were

unknown. The method was based on the fact that the energy release rate can be calculated from a set of modulus and Poisson's ratio values that can be directly determined from the experimental pressure vs. deflection curve of the blister test. An updated specimen preparation method was presented and implemented, which accurately defined the blister radius without adversely affecting the substrate surface. The proposed approach was carried out for an epoxy/copper interface after subjecting samples to full moisture saturation and a high temperature storage condition. Adhesion strength of the interface for as-is (G = 25.0 J/m^2), thermally aged (G = 28.2 J/m^2), and moisture degraded (G = 10.7 J/m^2) samples were presented. The adhesion strength decreased significantly after moisture degradation, while the thermal aging condition caused only a slight increase of the adhesion strength in spite of a significant change in modulus.

Chapter 8: Contributions and Future Works

8.1. Dissertation Contributions

Adhesion strength testing has been examined with experimental and numerical approaches to enhance and develop specific adhesion strength testing techniques to quantitatively assess the reliability of critical interfaces found in electronic packaging devices. The most significant contributions made in this dissertation are summarized below:

- A theoretical approach for determining if the adhesion strength of a potential material combination in a thin multilayer stack can be evaluated under the four-point bending framework. The approach takes into account the fracture toughness and structural material properties of the interface materials, global loading configurations, and the potential adhesion strength of the interface to analyze the crack kinking competition at the interface of interest. Through a numerical approach it is shown an applicable testing domain for the given test configuration and material set can be established to clearly indicate the limits of the test configuration.
- A novel adhesion test configuration called the "single cantilever adhesion test (SCAT)" that can be employed to determine the adhesion strength at interfaces in thin multilayer semiconductor packages has been developed. The method is optimal for quick and quantitative testing of strong interfaces inside thin multilayer structures. Detailed sample preparation, experimental testing

procedure, and a numerical approach to determine the critical energy release rate and mode mixity are presented. A reliability analysis of two proposed EMC/PSR material sets was then carried out using the SCAT method.

- A modified blister test using a predefined blister area is employed to assess the adhesion strength for a polyurethane conformal coating used to mitigate tin whisker growth. A procedure to prepare blister samples for tin-plated surfaces was created, including a method for creating a well-defined pre-defined area. An elasto-plastic analytical derivation of the adhesion strength from a blister test was developed leading to a more realistic determination of the adhesion strength. After measuring the properties at time zero, the coatings are subjected to accelerated testing conditions (high temperature/humidity storage and temperature cycling) and the degradations of the coating properties are documented. The results indicated that a polyurethane coating would be an effective solution to mitigate the tin whisker growth problem.
- An alternative numerical/experimental blister test method was proposed to characterize the adhesion strength of an interface when the film's structural properties were unknown. The method was based on the fact that the energy release rate can be calculated from a set of modulus and Poisson's ratio values that can be directly determined from the experimental pressure vs. deflection curve of the blister test. An updated specimen preparation method was presented and implemented, which accurately defined the blister radius without adversely affecting the substrate surface. The proposed approach was carried out for an

epoxy/copper interface after subjecting samples to full moisture saturation and a high temperature storage condition.

8.2. Future Work

As new and inventive products are introduced, there will be an increased need for adhesion strength testing methods that can be implemented to quickly and quantitatively assess interface reliability in thin multilayer structures. The contributions by this dissertation can be extended in many directions. Some of them are described below.

Extension to adhesion strength testing at high temperatures

When evaluating the reliability of an interface, testing is typically performed at room temperature to evaluate the adhesion strength of the interface. Additionally, testing is typically performed after subjection to various long term environmental testing conditions in order to assess the degradation of the interface with respect to time. This analysis provides valuable information for design and reliability engineers to make an educated assessment of how long the product will last before failure. However, most ideal would be to evaluate the strength of the interface at the moment when failure is known to occur.

As discussed in this dissertation, interfaces such as the EMC/PSR interface have been known to delaminate under reflow testing environment where temperatures reach 240 °C. Adhesion strength testing at the high temperature condition where failure occurs would be the most direct assessment of the feasibility of a potential material set for a given application. Challenges associate with this approach consist of establishing a test

infrastructure that allows for rapid heating of the specimen up to reflow temperatures followed by rapid testing. Since testing would be occurring at high temperatures, viscoelastic properties of the materials would also need to be taken into consideration.

Extension to testing thinner, stronger interfaces

In this dissertation the SCAT method was developed for testing the EMC/PSR interface in a thin multilayer stack. However, the printed circuit boards and overall form factor of consumer electronics continue to shrink past even the thin structures we have evaluated. The ability to scale the SCAT method for even thinner multilayer stack should be investigated. A critical challenge in doing so will be preventing crack kinking at the edge of the predefined area. The propensity for the crack kinking only increases as the adhesion strength grows and the structure heights are minimized. The ability to reinforce the top layer of the structure to force continued delamination along the interface of interest should be investigated.

Modulus effect in environmental conditioning of EMC/PSR specimens in SCAT testing

In this dissertation the mechanical property degradation of the EMC/PSR sample in SCAT testing was not evaluated during environmental conditioning. If there is a significant chance in the modulus of EMC due to high temperature storage or moisture gain, than the energy release rate calculation could be effected. It is recommended that in future work of the SCAT method the degradation changes to the mechanical properties should be thoroughly investigated.

Mode mixity calculations of EMC/PSR set in SCAT considering nonlinear material properties

In this dissertation linear elastic material properties were considered for both the EMC and PSR materials during SCAT testing. While it was shown that the plasticity was confined to a region around the crack tip, thus allowing for an accurate J-integral calculation under LEFM, this crack tip plasticity may still alter the accuracy of the mode mixity calculation since a VCCT method was used at the crack tip. Because of this, the mode mixity reported in this dissertation is a linear elastic approximation of the mode mixity. It is recommended that in future work, nonlinear behavior of the polymers is investigated for a more accurate determination of the mode mixity.

Advanced constrained blister testing for thin, high adhesion strength interfaces

Conventional adhesion testing struggle to accommodate testing of thin film membranes with very larger adhesion strengths and large compliances. One example of a strong interface in the electronic packaging community is for the Die Attach Film (DAF) to the silicon substrates. DAF layers are on the order of 20 μm thick and as a result have a very large compliance. Blister testing of such membranes experience very large deflections prior to delamination. Analytical equations are insufficient to evaluate this strong adhesion interfaces. This large blister deflection can be several times larger than the blister radius which invalidates spherical cap type assumptions. Furthermore, due to the large compliance of these thin film membranes when testing using a CBT configuration, bulging out occurs at the extent of the membrane which again invalidates assumptions made of the blister volume.

A proposed extension is the advanced constrained blister test (ACBT) method that employs a deformable constrainer instead of the rigid plate constraint found in CBT testing. A schematic of the ACBT setup is seen in Figure 84. The ACBT setup is similar to the blister test setup since the interface of interest is in between the thin film layer and the substrate. There is a pressure hole in the bottom of the substrate for loading, and the predefined area methods previous developed are employed to create a well-defined blister radius, a_{PD} [95]. However in this case, a deformable constraint layer is placed on top of the film layer. A thin layer of grease is applied between the constraint and film layers to minimize contact forces between the two materials. The constraint and film layers are fixed in place by a rigid ring of radius, $a_{constraint}$.

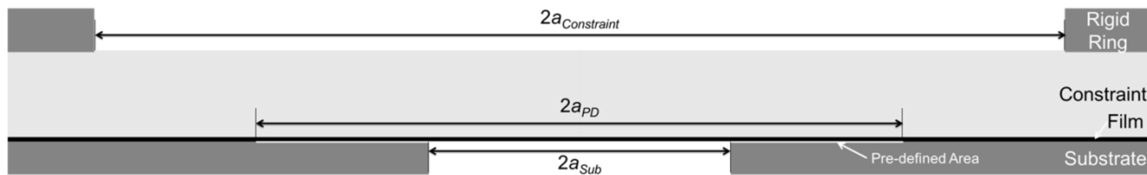

Figure 84. A schematic of the ACBT setup.

The transparent, deformable constraint layer is the key addition to the test method. By using a deformable constrainer, after the film is pressurized the film is free to inflate and conform to the constraint layer. Energy is transferred and stored in the constraint layer while the film layer height is drastically reduced. The reduced blister height allows for a larger pressure to be applied until finally the crack can delaminate along the interface. At this critical pressure the sample can be modeled using FEA and the stored energy in the deformable constraint layer can be extracted to evaluate the energy release rate, G. If a deformable constraint layer that with a significantly larger bending stiffness is used practically all of the energy stored in the system will be stored in the constraint layer. If

the contact area between the constraint layer and the film membrane are also known at the critical pressure, then under this condition it would be possible to assess the energy release rate without prior knowledge of the film's material properties. A transparent constraint layer will allow for detection of the contact area. This capability could also extend to the possibility of rate-dependent testing of film materials. Also, similar to the case of blister testing polymer membranes undergoing environmental conditioning, this test method would allow for evaluating the adhesion strength after environmental conditioning without knowledge of the current material properties.

Full development of the advanced constrained blister test will provide several key contributions, namely, by extending the ability to evaluate the adhesion strength for thinner, more compliant membranes at larger adhesion strengths. The ACBT will be able to fill a gap in the current state of flexible membrane on rigid substrate adhesion testing that currently cannot be evaluated. Additionally, the proposed extension will provide the ability for rate-dependent testing and environmental conditioning of samples without prior knowledge of the material properties, which is very important when in-situ material property measurements are not possible.

References

[1] T. L. Anderson, *Fracture mechanics: fundamentals and applications*: CRC, 2005.

[2] M. L. Williams, "Stress singularities, adhesion, and fracture," in *U.S. National Congress of Applied Mechanics*, Minneapolis, MN, 1966, pp. 451-464.

[3] J. Dundurs, "Elastic interaction of dislocations with inhomogeneities," *Mathematical theory of dislocations,* pp. 70-115, 1969.

[4] A. Agrawal and A. M. Karlsson, "Obtaining mode mixity for a bimaterial interface crack using the virtual crack closure technique," *International Journal of Fracture,* vol. 141, pp. 75-98, 2006.

[5] J. L. Beuth, "Separation of crack extension modes in orthotropic delamination models," *International Journal of Fracture,* vol. 77, pp. 305-321, 1996.

[6] J. W. Hutchinson and Z. Suo, "Mixed mode cracking in layered materials," *Applied mechanics,* p. 63, 1992.

[7] G. Schlottig, "Reliability at the chip interfaces: delaminating the silicon die from molding compound," PhD, Delft University of Technology, The Netherlands, Delft, 2012.

[8] D. Xie and S. B. Biggers, "Progressive crack growth analysis using interface element based on the virtual crack closure technique," *Finite Elements in Analysis and Design,* vol. 42, pp. 977-984, 2006.

[9] J. G. Williams, "Large Displacement and End Block Effects in the 'DCB' Interlaminar Test in Modes I and II," *Journal of Composite Materials,* vol. 21, pp. 330-347, April 1987.

[10] A. G. Evans*, et al.*, "The fracture energy of bimaterial interfaces," *Met. Trans. A,* vol. 21, pp. 2419-2429, 1990.

[11] X. Dai, "Materials study for interfacial adhesion and reliability of microelectronics packaging structures," Doctor of Philosophy, The University of Texas, Austin, 1998.

[12] X. Dai*, et al.*, "Polymer interfacial adhesion in microelectronic assemblies," 1998, pp. 132-137.

[13] X. Dai*, et al.*, "Adhesion measurement for electronic packaging applications using double cantilever beam method," *Components and Packaging Technologies, IEEE Transactions on,* vol. 23, pp. 101-116, 2000.

[14] D. K. Shin*, et al.*, "Chemical and Mechanical Analysis of PCB Surface Treated by Argon Plasma to Enhance Interfacial Adhesion," *Electronics Packaging Manufacturing, IEEE Transactions on,* vol. 32, pp. 281-290, 2009.

[15] D. K. Shin*, et al.*, "Effect of PCB Surface Modifications on the EMC-to-PCB Adhesion in Electronic Packages," *Components and Packaging Technologies, IEEE Transactions on,* vol. 33, pp. 498-508, 2010.

[16] P. G. Charalambides*, et al.*, "A test specimen for determining the fracture resistance of bimaterial interfaces," *Journal of Applied Mechanics,* vol. 56, p. 77, 1989.

[17] R. H. Dauskardt*, et al.*, "Adhesion and debonding of multi-layer thin film structures," *Engineering Fracture Mechanics,* vol. 61, pp. 141-162, 1998.

[18] Z. Huang, *et al.*, "Initiation and arrest of an interfacial crack in a four-point bend test," *Engineering Fracture Mechanics,* vol. 72, pp. 2584-2601, 2005.

[19] H. Tran, *et al.*, "Temperature, moisture and mode-mixity effects on copper leadframe/EMC interfacial fracture toughness," *Int J Fract,* vol. 185, pp. 115-127, 2014.

[20] X. Yan and R. K. Agarwal, "Two test specimens for determining the interfacial fracture toughness in flip-chip assemblies," *Journal of Electronic Packaging,* vol. 120, p. 150, 1998.

[21] J. Rice, "A path independent integral and the approximate analysis of strain concentration by notches and cracks," *Journal of Applied Mechanics,* vol. 35, pp. 379-386, 1968.

[22] J. R. Rice, "Elastic fracture mechanics concepts for interfacial cracks," *J. Appl. Mech.(Trans. ASME),* vol. 55, pp. 98-103, 1988.

[23] D. Xie, *et al.*, "Computation of Energy Release Rates for Kinking Cracks based on Virtual Crack Closure Technique," *CMES,* vol. 6, pp. 515-524, 2004.

[24] D. Xie, *et al.*, "Fracture criterion for kinking cracks in a tri-material adhesively bonded joint under mixed mode loading," *Engineering Fracture Mechanics,* vol. 72, pp. 2487-2504, 2005.

[25] P. Matos, *et al.*, "A method for calculating stress intensities in bimaterial fracture," *International Journal of Fracture,* vol. 40, pp. 235-254, 1989.

[26] H. Krishnamoorthy and H. V. Tippur, "Evaluation of elasto-plastic interfacial fracture parameters in solder-copper bimaterial using moire interferometry," *J. Electronic Packag.,* vol. 120, pp. 267-274, 1998.

[27] X.-K. Zhu and J. A. Joyce, "Review of fracture toughness (G, K, J, CTOD, CTOA) testing and standardization," *Engineering Fracture Mechanics,* vol. 85, pp. 1-46, 2012.

[28] G. R. Irwin, "Onset of fast crack propagation in high strength steel and aluminum alloys," vol. 2, N. R. Laboratory, Ed., ed, 1956, pp. 289-305.

[29] C. T. Sun and X. X. Wu, "On the J-integral in periodically layered composites," *Int Journ of Fracture,* vol. 78, pp. 89-100, 1996.

[30] T. S. Oh, *et al.*, "Cermaic metal interfacial crack-growth - toughening by controlled microcracks and interfacial geometries," *Acta Metallurgica,* vol. 36, pp. 2083-2093, Aug 1988.

[31] J. G. Williams, "On the calculation of energy release rates for cracked laminates," *International Journal of Fracture,* vol. 36, pp. 101-119, 1988.

[32] J. G. Williams, "The fracture mechanics of delamination tests," *The Journal of Strain Analysis for Engineering Design,* vol. 24, pp. 207-214, 1989.

[33] K. L. Ohashi, *et al.*, "Quantitative assessment of interface fracture at bone cement/metal prosthetic interfaces in total hip arthroplasties," *Journal of Orthopedic Research,* vol. 16, pp. 705-714, November 1998 1998.

[34] J. M. Snodgrass, *et al.*, "Adhesion and Subcritical Debonding of Polymer Interfaces for Microelectronic Packaging," *MRS Spring Meeting,* vol. 515, 1998.

[35] S. Zhang, *et al.*, "Influence of surface morphology on the adhesion strength of epoxy-aluminum interfaces," *J. Adhesion Sci. Technol.,* vol. 17, pp. 1685-1711, 2003.

[36] K. H. Lu, *et al.*, "Moisture Transport and its Effects on Fracture Strength and Dielectric Constant of Underfill Materials," in *Electronic Components and Technology Conference*, Reno, NV, 2007, pp. 1040 - 1044.
[37] C. S. Bischof, "Relationship of Adhesion, Delamination, Preconditioning and Preplating Effects at the Plastic to Leadframe Interface," *IEEE,* pp. 827-834, 1995.
[38] L. K. Teh, *et al.*, "Moisture-induced failures of adhesive flip chip interconnects," *IEEE Transactions on components and packaging technologies,* vol. 28, pp. 506-516, 2005.
[39] A. G. Evans, "The mechanical performance of fiber-reinforced ceramic matrix composites," *Materials Science and Engineering a-Structural Materials Properties Microstructure and Processing,* vol. 107, pp. 227-239, Jan 1989.
[40] P. G. Charalambides, *et al.*, "Development of a test method for measuring the mixed-mode fracture-resistance of bimaterial interfaces," *Mechanics of Materials,* vol. 8, pp. 269-283, Feb 1990.
[41] B. Kim, *et al.*, "Interfacial properties of Cu-Cu direct bonds for TSV integration," *Solid State Technology,* vol. 53, pp. 18-21, 2010.
[42] R. Arima, *et al.*, "Control of adhesion strength and TSV filling morphology of electroless barrier layer," *ESC Transactions,* vol. 50, pp. 13-18, 2013.
[43] M. Shirangi, *et al.*, "Determination of Copper/EMC interface fracture toughness during manufacturing, moisture preconditioning and solder reflow process of semiconductor packages," in *ICF12, Ottawa 2009*, 2013.
[44] M. H. Shirangi, "Simulation-based Investigation of Interface Delamination in Plastic IC Packages under Temperature and Moisture Loading," PhD, Verkehrs- und Maschinensysteme, der Technischen Universität Berlin, Berlin, 2010.
[45] M. H. Shirangi and B. Michel, "Mechanism of Moisture Diffusion, Hygroscopic Swelling, and Adhesion Degradation in Epoxy Molding Compounds," pp. 29-69, 2010.
[46] H. C. Cao and A. G. Evans, "An experimental study of the fracture-resistance of bimaterial interfaces," *Mechanics of Materials,* vol. 7, pp. 295-304, Jun 1989.
[47] Z. Suo, "Failure of brittle adhesive joints," *Appl Mech Rev,* vol. 43, pp. S276-S279, 1990.
[48] Z. Suo and J. W. Hutchinson, "Interface crack between two elastic layers," *International Journal of Fracture,* vol. 43, pp. 1-18, 1990.
[49] Q. Ma, *et al.*, "Quantitative measurement of interface fracture energy in multi-layer thin film structures," in *MRS Annual Meeting*, San Francisco, CA, 1995, pp. 91-96.
[50] T. L. Becker, *et al.*, "Limitations on the use of the mixed-mode delaminating beam test specimen: Effects of the size of the region of K-dominance," *Mechanics of Materials,* vol. 25, pp. 291-308, 1997/6// 1997.
[51] M. Lane, *et al.*, "Progressive debonding of multilayer interconnect structures," in *Proceedings of MRS Annual Meeting*, San Francisco, CA, 1997, pp. 21-26.
[52] Q. Ma, "A four-point bending technique for studying subcritical crack growth in thin films and at interfaces," *Journal of Materials Research,* vol. 12, pp. 840-845, 1997.
[53] Q. Ma, *et al.*, "Adhesion measurement of interfaces in multilayer interconnect structures," in *MRS Annual Meeting*, San Francisco, CA, 1997, pp. 3-14.

[54] I. Hofinger, *et al.*, "Modified four-point bending specimen for determining the interface fracture energy for thin, brittle layers," *International Journal of Fracture,* vol. 92, pp. 213-220, 1998.
[55] B. Wang and T. Siegmund, "A modified 4-point bend delamination test," *Microelectronic Engineering,* vol. 85, pp. 477-485, 2008.
[56] S. Roham, *et al.*, "Crack penetration and deflection at a bimaterial interface in a four-point bend test," *Journal of Materials Research,* vol. 19, pp. 3019-3027, 2011.
[57] M. Y. He, *et al.*, "Crack deflection at an interface between dissimilar elastic materials: role of residual stresses," *International Journal of Solids and Structures,* vol. 31, pp. 3443-3456, 1994.
[58] M. Y. He and J. W. Hutchinson, "Kinking of a Crack Out of an Interface," *Journal of Applied Mechanics,* vol. 56, pp. 270-278, 1989.
[59] M. Y. He and J. W. Hutchinson, "Crack deflection at an interface between dissimilar elastic materials," *International Journal of Solids and Structures,* vol. 25, pp. 1053-1067, 1989.
[60] Z. Suo, "Singularities, interfaces and cracks in dissimilar anisotropic media," *Proc. R. Soc. Lond. A,* vol. 427, pp. 331-358, 1990.
[61] Z. Suo, Ed., *Reliability of Interconnect Structures* (Comprehensive Structural Integrity: Interfacial and nanoscale failure. Amsterdam: Elsevier, 2003, p.^pp. Pages.
[62] Z. Suo and J. W. Hutchinson, "Sandwich test specimens for measuring interface crack toughness," *Materials Science and Engineering: A,* vol. 107, pp. 135-143, 1989.
[63] D. Post, *et al.*, *High sensitivity moiré: experimental analysis for mechanics and materials*: Springer, 1997.
[64] H. Hencky, *Zr. Math. PHys.,* vol. 63, pp. 311-317, 1915.
[65] H. Dannenberg, "Measurement of adhesion by a blister method," *Journal of Applied Polymer Science,* vol. 5, pp. 125-134, 1961.
[66] M. L. Williams, "The Continuum Interpretation for Fracture and Adhesion," *J. Appl. Pol. Sci.,* vol. 13, pp. 29-40, 1969.
[67] Hinkley, "A Blister Test for Adhesion of Polymer Films to SiO2," *Adhesion,* vol. 16, pp. 115-126, 1983.
[68] A. N. Gent and L. H. Lewandowski, "Blow-off Pressures for Adhering Layers," *J. Appl. Pol. Sci.,* vol. 33, pp. 1567-1577, 1987.
[69] M. Fernando and A. J. Kinloch, "Use of the 'Iverted-blister' Test to Study the Adhesion of Photopolymers," *In. J. Adhesion and Adhesives,* vol. 10, pp. 69-76, 1990.
[70] B. J. Briscoe and S. S. Penesar, "The Application of the Blister Test to an Elastomeric Adhesive," *Proc. R. Soc. Lond. A,* vol. 433, pp. 23-43, 1991.
[71] H. M. Jensen, "The Blister Test for Interface Toughness Measurement," *Eng. Fract. Mech.,* vol. 40, pp. 475-486, 1991.
[72] H. M. Jensen and M. D. Thouless, "Effects of residual stresses in the blister test," *International Journal of Solids and Structures,* vol. 30, pp. 779-795, 1993.
[73] S. A. Sikorski, "Measurement of Adhesion Using the Island Blister Test," Ph. D. Ph. D. Dissertation, Mechanical Engineering, MIT, 1994.

[74] R. J. Hohlfelder, *et al.*, "Blister test analysis methods," in *Mat. Res. Soc. Symp. Proc.*, 1995, pp. 585-590.
[75] Y.-H. Lai and D. A. Dillard, "A Study of the Fracture Efficiency Parameter of Blister Tests for Films and Coatings," in *Adhesion Measurement of Films and Coatings*, K. L. Mittal, Ed., ed Utrcht, The Netherlands: VSP, 1995.
[76] K.-T. Wan and Y.-W. Mai, "Fracture Mechanics of a New Blister Test with Stable Crack Growth," *Acta Metall. Mater.,* vol. 43, pp. 4109-4115, 1995.
[77] A. Bagchi and A. G. Evans, "The Mechanics and Physics of Thin Film Decohesion and its Measurements," *Interface Scheince,* vol. 3, pp. 169-193, 1996.
[78] M. D. Drory and J. W. Hutchinson, "Measurement of the adhesion of a brittle film on a ductile substrate by indentation," *Proceedings: Mathematical, Physical and Engineering Sciences,* vol. 452, pp. 2319-2341, 1996.
[79] H. J. Moon, "Measurement of Mechanical Properties of a Thermally Evaporated Gold Film Using Blister Test," *Korean Society of Mechanical Engineers,* vol. 20, pp. 882-890, 1996.
[80] B. Cotterell and Z. Chen, "The Blister Test - Transition from Plate to Membrane Behavior for an Elastic Material," *Int. J. Fract.,* vol. 86, pp. 191-198, 1997.
[81] H. S. Yang, *et al.*, "Electrostatic adhesion testing of electronic metallizations," *Review of Scientific Instruments,* vol. 68, p. 2542, 1997.
[82] A. Shirani and K. M. Liechti, "A calibrated fracture process zone model for thin film blistering," *Int Journ of Fracture,* vol. 93, pp. 281-314, 1998.
[83] K.-T. Wan, "A Novel blister Test to Investigate Thin Film Delamination at Elevated Temperature," *Int. J. Adhes. Adhes.,* vol. 20, pp. 141-143, 2000.
[84] Y. C. Zhou, *et al.*, "Determination of Interface Fracture Toughness in Thermal Barrier Coating System by Blister Tests," *J. Eng. Mat. Tech.,* vol. 125, pp. 176-182, 2003.
[85] R. E. Galindo, *et al.*, "A Modified Blister Test to Study the Adhesion of Thin Coatings Based on Local Helium Ion Implantation," *Thn Sold Films,* vol. 471, pp. 170-176, 2005.
[86] S. Guo, *et al.*, "A Bending-to-stretching Analysis of the Blister Test in the Present of Tensile Residual Stress," *Int. J. Solds Struct.,* vol. 42, pp. 2771-2784, 2005.
[87] K. Hbaieb and Y. W. Zhang, "A Parametric Study of a Pressurized Blister Test for an Elastic-plastic Film-rigid Substrate System," *Mat. Sci. Eng. A,* vol. 390, pp. 385-392, 2005.
[88] O. Vallin, *et al.*, "Adhesion Quantification Methods for Wafer Bonding," *Mat. Sci. Eng. R,* vol. 50, pp. 109-165, 2005.
[89] W. D. van Driel, *et al.*, "Characterization of Interface Strength as Function of Temperature and Moisture Conditions," presented at the 6th Int. Conf. Electronic Packaging Technology, 2005.
[90] L. Figiel and B. Lauke, "Interface Fracture of Polymer Films: Blister Test Experiments and Modelling," *Int. J. Fract.,* vol. 139, pp. 71-89, 2006.
[91] L. M. Jiang, *et al.*, "A Pressurized Blister Test Model for the Interface Adhesion of Dissimilar Elastic-plastic Materials," *Mat. Sci. Eng. A,* vol. 487, pp. 228-234, 2008.

[92] L. Jiang*, et al.*, "Characterization of the interface adhesion of elastic–plastic thin film/rigid substrate systems using a pressurized blister test numerical model," *Mechanics of Materials,* vol. 42, pp. 908-915, 2010.
[93] M. Zhao*, et al.*, "Nonlinear elastic mechanics of the ball-loaded blister test," *International Journal of Engineering Science,* vol. 49, pp. 839-855, 2011.
[94] H. Na*, et al.*, "Measurement of Adhesion Work of Electrospun Polymer Membrane by Shaft-Loaded Blister Test," *Langmuir,* vol. 28, pp. 6677-6683, 2012.
[95] K. Mahan*, et al.*, "Adhesion and Puncture Strength of Polyurethane Coating Used to Mitigate Tin Whisker Growth," *Journal of Electronic Packaging,* vol. 136, p. 031004, 2014.
[96] M. J. Napolitano*, et al.*, "The constrained blister test for the energy of interfacial adhesion," *J. Adhesion Sci. Technol.,* vol. 2, pp. 311-323, 1988.
[97] Y. S. Chang*, et al.*, "The constrained blister - a nearly constant strain energy release rate test for adhesives," *Journal of Adhesion,* vol. 27, pp. 197-211, 1989.
[98] A. M. Mousa*, et al.*, "Adhesive strength evaluation via constraint blister test I. SIBS/polystyrene and polypropylene," *Rubber Chemistry and Technology,* vol. 77, pp. 278-292, 2004.
[99] M. J. C. A. M. A. Napolitano, "The Constrained Blister Test for the Energy of Interfacial Adhesion," *Journal of Adhesion Science and Technology Journal of Adhesion Science and Technology,* vol. 2, pp. 311-323, 1988.
[100] S. R. Hartshorn, *Structural Adhesives : Chemistry and Technology*. New York: Plenum Press, 1986.
[101] K. Compton*, et al.*, "Filamentary Growths on Metal Surfaces Whiskers," *Corrosion,* vol. 7, pp. 327-334, 1951.
[102] V. Schroeder*, et al.*, "Tin Whisker Test Method Development," *Electronics Packaging Manufacturing, IEEE Transactions on,* vol. 29, pp. 231-238, 2006.
[103] G. T. Galyon, "Annotated Tin Whisker Bibliography and Anthology," *Electronics Packaging Manufacturing, IEEE Transactions on,* vol. 28, pp. 94-122, 2005.
[104] M. Osterman, "Mitigation Strategies for Tin Whiskers," *Whitepaper CALCE EPSC (www.calce.umd.edu/lead-free/tin-whiskers/),* July 2002.
[105] W. Fox and L. Woody, "Conformal Coatings for Tin Whisker Risk Management," in *IPC APEX EXPO Technical Conference*, Las Vegas, Nevada, 2010, pp. 890-920.
[106] J. S. Kadesch and H. Leidecker, "Effects of conformal coat on tin whisker growth," in *Proceedings of the 37th IMAPS Nordic Annual Conference*, 2000, pp. 108-116.
[107] J. S. Kadesch and J. Brusse, "The Continuing Dangers of Tin Whiskers and Attempts to Control Them with Conformal Coating," *NASA EEE Links Newsletter,* 2001.
[108] T. A. Woodrow and E. A. Ledbury, "Evaluation of Conformal Coatings as a Tin Whisker Mitigation Strategy," in *IPC/JEDEC 8th International Conference on Pb-Free Electronic Components and Assemblies*, San Jose, CA, 2005.
[109] T. A. Woodrow and E. A. Ledbury, "Evaluation of Conformal Coatings as a Tin Whisker Mitigation Strategy, Part 2," in *Proc. of SMTA International Conf.*, Rosemont, IL, 2006.
[110] A. N. Gent and L. H. Lewandowski, "Blow-off pressures for adhering layers," *Journal of Applied Polymer Science,* vol. 33, pp. 1567-1577, 1987.

[111] A. Shirani and K. Liechti, "A calibrated frature process zone model for thin film blistering," *International Journal of Fracture,* vol. 93, pp. 281-314, 1998.
[112] M. Williams, "The continuum interpretation for fracture and adhesion," *Journal of Applied Polymer Science,* vol. 13, pp. 29-40, 1969.
[113] M. Fernando and A. Kinloch, "Use of the 'inverted-blister' test to study the adhesion of photopolymers," *International journal of adhesion and adhesives,* vol. 10, pp. 69-76, 1990.
[114] J. A. Hinkley, "A Blister Test for Adhesion of Polymer Films to SiO2," *The Journal of Adhesion,* vol. 16, pp. 115-126, 1983.
[115] K. Mahan*, et al.*, "PoF Model of Conformal Coating against Tin Whisker Growth: Performance Evaluation under Operating and Storage Conditions," Center for Advanced Life Cycle Engineering (CALCE), College Park, MD C11-06, 2011.
[116] C. Nguyen and T. Vu-Khanh, "Mechanics and mechanisms of puncture of elastomer membranes," *Journal of materials science,* vol. 39, pp. 7361-7364, 2004.
[117] JESD201, "Environmental Acceptance Requirements for Tin Whisker Susceptibility of Tin and Tin Alloy Surface Finishes " in *JEDEC Solid State Technology Association*, ed, 2006.
[118] IPC-CC-830B, "Qualification and Performance of Electrical Insulating Compound for Printed Wiring Assemblies," 2008.
[119] E. K. L. Chan*, et al.*, "Effect of Interfacial Adhesion of Copper/Epoxy under Different Moisture Level," presented at the 7th. Int. Conf: on Thermal, Mechanical and Multiphysics Simulation and Experiments in Micro-Electronics and Micro-Systems, EuroSimE, 2006.
[120] T. P. Ferguson, "Moisture and Interfacial Adhesion in Microelectronic Assemblies," PhD, Mechanical Engineering, Georgia Institute of Technology, Atlanta, Georgia, 2004.
[121] T. P. Ferguson and J. Qu, "The Effect of Moisture on the Adhesion and Fracture of Interfaces in Microelectronic Packaging," in *Micro- and Opto-Electronic Materials and Structures: Physics, Mechanics, Design, Reliability, Packaging*, E. Suhir*, et al.*, Eds., ed: Springer US, 2007.
[122] Y. B. Park and J. Yu, "A fracture mechancis analysis of the popcorn cracking in the plastic IC packages," in *IEEE/CPMT Int'l Electronics Manufacturing Technology Symposium*, 1997, pp. 12-19.
[123] C. Lin*, et al.*, "Isothermal aging induced evolution of the material behavior of underfill encapsulants," in *Electronic Components and Technology Conference*, 2009, pp. 134-149.
[124] S. Noijen*, et al.*, "On the epoxy moulding compound aging effect on package reliability," presented at the Thermal, Mechanical and Multi-Physics simulation and Experiments in Microelectronics and Microsystems, 2009.
[125] I. Emri, "Rheology of solid polymers," *Rheology Reviews,* vol. 2005, p. 49, 2005.
[126] X. Q. Shi*, et al.*, "Investigation of effect of temperature and strain rate on mechanical properties of underfill material by use of microtensile specimens," *Polymer Testing,* vol. 21, pp. 725-733, 2002.

[127] Y. Sun, *et al.*, "Generalized hybrid modeling to determine chemical shrinkage and modulus evolutions at arbitrary temperatures," *Experimental Mechanics,* vol. 53, pp. 1783-1790, 2013.